SISSA

Scuola Internazionale Superiore di Studi Avanzati
International School for Advanced Studies

Statistical Physics Group

Academic year 2013/2014

Fluctuations effects in population genetics and in protein translation

November 5th, 2014

Thesis submitted for the degree of
Philosophiae Doctor
in statistical physics

candidate
Pierangelo Lombardo

supervisor
Dr. Andrea Gambassi

co-supervisor
Dr. Luca Dall'Asta

Acknowledgements

I am deeply grateful to Andrea Gambassi and to Luca Dall'Asta for their advice, and for the many helpful discussions which were invaluable lessons in how to conduct scientific research.

I acknowledge the profitable and stimulating collaboration with L. Caniparoli, who introduced me to the fascinating world of protein translation.

I would like to warmly thank the present and former members of the Statistical Physics group in SISSA, in particular L. Caniparoli, G. Menegoz, P. Smacchia, and G. Gori, for the many useful discussions. I also would like to thank the colleagues and friends in Molecular and Statistical Biophysics group and in Condensed Matter group, in particular S. Saccani and E. Sarti, for the interesting discussions which helped me in developing my scientific mindset.

Finally, I would like to deeply thank my family and all my friends, who sustained me during these hard but wonderful four years.

Contents

Introduction

Physics has been traditionally associated with the quest for the fundamental laws governing the nature; in this direction there have been astonishing progresses, and currently we have elegant mathematical theories, such as the well-established standard model of particle physics, which are potentially able to explain "almost all" the fundamental laws governing the universe, or the promising string theory and m-theory, which may complete that task (see, for instance, Refs. [1, 2, 3, 4]). On the other hand, physicists have realised that these *ab initio* theories alone are not sufficient to give an accessible description of the behavior of many common real systems (including examples which may appear trivial, but are in fact complex from the physical point of view, such as a pot of boiling water or the steam in a steam engine), due to the large number of interacting microscopic entities involved. With the aim of finding an *effective* description for these macroscopic systems, new branches of physics appeared. Thermodynamics, dating back to the 17th century and vigorously developed during the industrial revolution, is probably the oldest attempt to give a quantitative description of the behavior of a large complex physical system, and, by considering macroscopic average quantities such as the internal energy, the work, and the heat transfer, it provided valuable insight, in particular in the physics of equilibrium systems (i.e., when the dynamical condition of detailed balance is satisfied) and their transformations, see for instance Refs. [5, 6, 7, 8, 9, 10].

Statistical physics was initially developed in the 19th century in order to describe the same systems considered in thermodynamics but from the microscopic point of view, i.e., in terms of the interactions between their constituent atoms and molecules. Its original purpose was, in fact, to build a bridge between the physics of fundamental interactions (at that time, primarily mechanics) and thermodynamics, in order to provide a microscopic justification of the empirical laws which ruled the latter (see for instance Refs. [11, 12, 13, 14]). During the last century however, statistical physics has become a stand-alone discipline which has been successfully applied for describing various physical systems composed by a collection of entities (e.g., atoms, colloids, spins, etc.): see, for instance, Refs. [7, 15, 10, 16]. In the statistical physics approach, a system at equilibrium (i.e., the dynamics of which satisfies detailed balance) is described in terms of a possibly reduced number of relevant degrees of freedom x, selected from its microscopic configuration space. The system is then characterized by the equilibrium probability $P_{\rm eq}(x)$ to find it in the state x, where, as far as the dynamics is concerned, the remaining non-relevant microscopic degrees of freedom result in an effective noise for the evolution of x.

For systems at equilibrium, the stationary Gibbs ensemble allows us to determine the

equilibrium probability distribution $P_{\rm eq}(x)$ in terms of the microscopic Hamiltonian $H(x)$ which rules the interaction between the microscopic degrees of freedom. Using this Gibbs distribution, it is formally possible to evaluate the expectation value $\langle O\rangle = \sum_{\{x\}} O(x)P_{\rm eq}(x)$ of any quantity of interest $O(x)$ by summing over all the possible configurations of the system; in some cases (see for instance Refs. [17, 16]) the summation can be done exactly, while, in general, statistical physicists have developed a set of toolboxes (e.g., mean-field approximation, series expansion, and renormalization group) which provide approximate solutions (see, e.g., Refs. [18, 10, 15]).

A phenomenon which challenges the applicability of most of the simplest approximation schemes and which therefore greatly attracted the attention of statistical physicists is the so-called *criticality*, i.e., the emergence of long-range correlations and collective behaviours typically associated with continuous (i.e., second order) phase transitions. A crucial role in the appearance of these phenomena is played by fluctuations, which are then typically relevant, at least in low spatial dimensionality, and cannot be neglected in studying critical systems. The behavior near critical points turns out to depend only on the gross features but not on the details of the system, and this theoretical and experimental fact allowed for a robust classification of the equilibrium continuous phase transitions into universality classes, each one being characterised by a set of critical exponents; in particular, in two spatial dimensions, conformal field theory, provides a complete classification (see, e.g., Refs. [19, 20]).

Nonequilibrium statistical physics and absorbing phase transitions

Despite the theoretical interest in equilibrium systems, nonequilibrium ones are much more common in nature, and for understanding the latter no general principles such as those leading to the Boltzmann-Gibbs distribution are available. In fact nonequilibrium properties cannot be directly inferred without solving the dynamics, and in fact the probability $P(x;t)$ to find a nonequilibrium system in the state x at time t has to be derived case-by-case from the solution of the so-called *master equation*, which describes the evolution of $P(x,t)$; this remarkably difficult challenge led to the development of a variety of (exact or approximate) methods, suited to deal with particular cases and situations (see for instance Refs. [21, 22, 10]). Since the constraint of detailed balance, which characterises equilibrium systems, is released, nonequilibrium statistical physics presents a much richer variety of possible dynamics, compared with the equilibrium case. For instance, the classification of nonequilibrium phase transitions is still seeking for a guiding principle, even if some progress has been made, in particular concerning the so-called absorbing phase transitions, i.e., transitions occurring between an absorbing phase, in which the system collapses into a certain which cannot be left state, and an active phase in which several states are explored. Descriptions based on the generalised Langevin equations (or stochastic differential equations), which play a primary role in chapters 1 and 2, have been of crucial importance in the identification of these classes.

One of the first universality classes to be recognised among the large variety of absorbing phase transitions is the one associated with directed percolation (DP), or, equivalently to the so-called Reggeon field theory (see, e.g., Refs. [23, 24, 25]). Directed percolation takes

its name from the process of percolation of a liquid in porous media, but it actually models a number of systems which share the same transitions, as directed random connectivity, epidemic spreading, forest fires, certain catalytic reactions, synchronisation of maps, surface growth, intermittent turbulence, and even certain hadronic interactions, and it can be alternatively viewed as a reaction-diffusion model, i.e., as a system of interacting particles which diffuse in space and which might react according to certain rules (see for instance Refs. [24, 25]).

A phenomenological Langevin equation can be derived from the master equation of the microscopic model of DP (see Ref. [26]) and it reads, in the Stratonovich convention (see App. A.1 for a brief description of Itō and Stratonovich conventions)

$$\dot{x}(\vec{r},t) = -ax(\vec{r},t) - bx^2(\vec{r},t) + D\nabla^2 x(\vec{r},t) + \sigma\sqrt{x(\vec{r},t)}\,\eta(\vec{r},t), \tag{1}$$

where x is a positive-valued real field; in the case of DP interpreted as a reaction-diffusion model, x represents the coarse-grained density of particles in the point $\vec{r}$ at time t, while a, b, D, and σ are real-valued coefficients and $\eta(\vec{r},t)$ is a normalized white Gaussian noise characterized by $\langle\eta(\vec{r},t)\eta(\vec{r}',t')\rangle = \delta^d(\vec{r}-\vec{r}')\delta(t-t')$ in d spatial dimensions. It can be noticed that Eq. (1) is characterized by the so-called multiplicative noise, as the noise amplitude is proportional to the square root of the field x; this feature is crucial in order to ensure that the state $x = 0$ is absorbing (although, as we shall see in Chap. 1, sometimes this requirement might not be sufficient). Heuristically, in fact, once the state $x = 0$ is reached, the stochastic contribution to $\dot{x}$ vanishes as well as the deterministic one, and therefore the system cannot leave this state. In chapter 1 we will describe the character of the absorbing state $x = 0$ for a Langevin equation similar to Eq. (1) (interpreted à la Itō), but with a generic power y of the variable x in the noise amplitude, in the zero dimensional case; we will see that systems with different powers y displays significantly different behaviours and that apparently absorbing states might not be so because of the strong effect of fluctuations.

Another relevant and well-established universality class is the so-called voter class.The classical voter model is a lattice model in which each site i represents a voter with opinion described by the variable x_i which takes two possible values (e.g., $0, 1$). The process evolves by randomly selecting a voter who then adopts the opinion of a randomly chosen nearest neighbour; the model is characterized by the presence of two competing absorbing states, associated respectively with the convergence of all voters to the opinion 0 or 1. The introduction of interfacial noise in the voter model generates a phase transition whose universality class can be described in terms of a phenomenological Langevin equation which reads (see Ref. [27])

$$\dot{x} = \left[a + b(1-2x)^2\right] x(1-x)(1-2x) + D\nabla^2 x + \sigma\sqrt{x(1-x)}\,\eta(\vec{r},t), \tag{2}$$

where the real field $x(\vec{r},t)$, representing a sort of coarse-grained "density" of opinion, varies within the interval $[0,1]$, while a, D, σ and η are analogous to the corresponding quantities in Eq. (1), and $b \geq 0$. Beyond the issue of the nature and features of the possible phase transition, another relevant problem concerns the so-called *fixation*, which leads a system to an absorbing state, and its time scale. It turns out that this issue can be effectively addressed

within the framework of Langevin equations, as we shall see in Chap. 2, where we consider a system in the context of population genetics which can be described by an equation formally equivalent to Eq. (2), interpreted within the Itō convention, with $b = 0$.

Statistical physics applied to biological processes

In the past decades, together with the rise of statistical physics to a prominent role in physical research, there has been an increasing interest towards its application to other disciplines, such as biology, ecology, economics, genetics, etc. (see, e.g., Refs. [28, 29]). On the one hand, this is due to the versatility of the statistical physics approach, which has proven to be very effective in providing insights and in answering many questions which arise within these interdisciplinary application, particularly when the number of basic components involved (e.g., individuals of a population, molecules, etc.) is large and/or when the incomplete knowledge of the processes at shorter time and length scales can be modeled by an effective stochastic noise; a paradigmatic example of this approach is provided by the Brownian motion, i.e., by the motion of a mesoscopic particle (e.g., a micrometer-sized colloid) in a fluid composed by microscopic molecules, which is described in terms of the position of the mesoscopic particle alone, while the interaction of the molecules with the particle is modeled by a stochastic noise which produces random changes in the velocity of the latter (see for instance Refs. [30, 31]). On the other hand, many biological problems have attracted the attention of physicists because they are characterised by the formation of spatial or temporal, highly regular patterns , (non-equilibrium) phase transitions or other features which are intriguing from the point of view of statistical physics, where they have been studied at length in the past decades (see, e.g., Ref. [32, 33]).

Fluctuations, known to become relevant near a critical point in equilibrium systems, have highly non-trivial effects also on the dynamics out of equilibrium (see, e.g., Refs. [34, 35, 24]); their accurate analysis is therefore of the outmost importance in stochastic systems, and this is one of the main reasons for the success of statistical physics in the modelling of living systems, which are generally out of equilibrium and characterized by fluctuating quantities. In this thesis we focus on the effects of stochastic fluctuations on two relevant paradigmatic problems in biology, namely *population genetics* and *protein translation*; these problems are strictly related for the following reason. Every living organism is characterized by a genetic code (the so-called *genotype*) encoded in the DNA, which, through a process called gene expression strongly influences the *phenotype*, i.e., the set of all observable characteristics and traits (such as the morphology, the biochemical properties, the behavior). Depending on its phenotype and on the contingent environment in which it is living, each individual has a certain probability to survive and to reproduce; this determines the Darwinian natural selection, which favours some genotypes and depresses others, contributing to the (highly non-trivial) evolutionary rules for the genotypes present in a living population, which are the object of interest in population genetics. Protein translation, besides being one of the most common biochemical reaction happening in the living cells, is a fundamental step in gene expression, and therefore its understanding can help in the explanation of the microscopic processes by which the genotype of an individual influences its phenotype; in population

genetics, these processes affect the form of the "forces" which model the Darwinian natural selection in the effective "macroscopic" equations for the evolution of the genetic composition of a population, and therefore their knowledge is of primary importance in order to develop accurate effective equations.

Summary of the thesis

This presentation consists of three main chapters. In the first one we introduce Langevin equations with multiplicative noise, which are useful tools for describing many stochastic systems, among which the paradigmatic example in population genetics discussed in Chap. 2; in particular, we focus here on the generalization of the zero-dimensional version of Eq. (1) to a generic power-law amplitude of the noise. This equation is characterized by the presence of a stationary point in $x = 0$ (i.e., a point in which both the deterministic force and the amplitude of the noise vanish), whose actual effect on the dynamics of the system depends on the exponent of the noise amplitude, and which does not necessarily constitutes a separatrix for the dynamics. This effect is described with the aid of the so-called *boundary classification*, which is based on the analysis of three functionals depending on both the deterministic and the stochastic forces in the Langevin equation, and it allows us to understand the conditions under which the system is expected to collapse into the stationary state, i.e., to *fix*.

The second chapter, based on Refs. [36, 37] deals with population genetics, which describes how the biodiversity and the composition of a population evolve in time due to the action of evolutionary forces. The simplest models of population genetics focus on one gene of the genotype (i.e., on one locus in the DNA sequence), and describe the time evolution of the fractions of the population which carry the various alleles, i.e., the possible different values of the considered gene. The dynamics of these fractions can be described via an effective Langevin equation (with multiplicative noise) in the space of allele frequencies, which, as we anticipated above, closely resemble Eq. (2). In the absence of mutations the dynamics is characterized by the presence of two absorbing states because, once extinct, an allele cannot appear again (at least in the absence of mutations); moreover, in a population constituted by a finite number of individuals, all alleles except one will eventually get extinct due to stochastic fluctuations, leading to fixation. The mean time needed by a finite population to reach fixation (mean fixation time) depends on the number of individuals in the population, on the presence of selective advantage for an allele and on the initial configuration. Actual populations are typically subdivided and fragmented in space, with the consequence that migration occurring among subpopulations affects their collective evolution: genetic traits get locally extinct and recolonized by migration from neighbouring subpopulations. In this case, fixation happens only when the same allele fixes in all the sub-populations, and the determination of the mean fixation time becomes a non-trivial problem. With these motivations in mind, we considered the paradigmatic Island model, which is the simplest possible setting to study the evolution of a subdivided population: N sub-populations (demes) of fixed size are located at the sites of a fully connected graph, i.e., every sub-population interacts with all the others, by exchanging individuals. When the selection is constant or absent, the mean fixation time in the Island model is known to decrease monotonically upon

increasing the migration rate. In Refs. [36, 37], we considered evolutionary forces that favour the coexistence of different alleles (e.g., balancing selection, which is common in the evolution of many natural populations), showing that the mean fixation time can actually display a nonmonotonic dependence on the migration rate. Beyond the nonmonotonicity in the mean fixation time, our analysis predicts, in the large N limit, a transition between a phase characterized by coexistence of the two alleles and a phase characterized by fixation of one of them. The analysis of the metastable dynamics of this subdivided population has been carried out by combining a self-consistent theoretical analysis of the fluctuations, inspired by common problems of statistical mechanics, with a numerical analysis of the corresponding discrete models. Stochastic fluctuations in the microscopic model appear to have non-trivial effects — qualitatively different depending on the range of parameters — on the macroscopic behavior of the population, and it would be interesting to investigate the extent to which this remains true in populations with more realistic and more complex spatial structures.

The third chapter, based on Ref. [38], deals with protein translation, a crucial and only partly understood step in gene expression and one of the most common biochemical reactions occurring in the cell: the individual triplets of nucleotides (the codons) composing a messenger RNA (mRNA) are translated into amino acids (the units composing the proteins) by the ribosomes. This process is biologically and chemically well understood, but the implications of its intrinsic stochastic nature have not yet been fully elucidated. In particular, we focus on understanding the effect of fluctuations on protein translation, basing our analysis on methods which are typically employed in statistical physics in order to describe the stochastic evolution of physical systems. More in detail we address an intriguing question concerning the ribosome dwell time distribution, i.e., the distribution of the time intervals between two subsequent codon translation events. The form of this distribution heavily influences the ribosome traffic along the mRNA sequences and affects the efficiency, accuracy and regulation of the translation process. The translation of a codon involves several subsequent biochemical steps and one among them (the binding step) requires that the ribosome binds to an additional molecular species, the transcript RNA (tRNA), which has an internal stochastic dynamics. The dwell time distribution we are concerned with depends therefore on the binding time distribution, i.e., on the distribution of the time intervals needed by the ribosome to bind to a tRNA. The tRNA molecules carry the corresponding amino acid to the ribosome, and physically recognise the codons, effectively decoding the genetic code. After translation has occurred and the tRNA molecule has left the ribosome, it must be recharged with the correct amino acid before it can be used to perform the same task again. The interplay between these two mechanisms, consumption and recharge, determines the fluctuations of the fraction of charged tRNAs, which effect combines with the fluctuations (due to diffusion in the cell) in the number of tRNAs in the neighbourhood of the ribosome. In Ref. [38], we introduced a stochastic model which mimics the tRNA charging-discharging and diffusive dynamics and we studied its nonequilibrium steady state by solving the corresponding master equation. This stationary solution allowed us to provide an analytic estimate for the binding time distribution, which deviates from the exponential distribution expected in the absence of fluctuations in the number of charged tRNAs around the ribosome. Moreover, we quantified the way in which the stochasticity in the tRNA dynamics increases the fluctu-

ations in the binding time distribution and therefore in the dwell time distribution. In our study we established a relationships between the parameters of the model and measurable quantities. Since we have considered a simplified case with only one kind of amino acid and one kind of tRNA in the cell, our model needs to be generalised in order to predict the dwell time distribution in an actual cell (*in vivo*); on the other hand, it would be in principle already possible to test our predictions by experimentally reconstructing *in vitro* the simplified situation described by our model.

Chapter 1

Power-law noise and absorbing states

1.1 A paradigmatic equation from finance

In many fields (ranging from game theory to ecology) one encounters non-equilibrium systems, characterized by the presence of stochastic fluctuations, which can be effectively modeled by Langevin equations with a so-called multiplicative noise, i.e., a noise the amplitude of which depends on the state x of the system; x can be, depending on the specific case, a concentration, a frequency, a velocity, etc. . Very often the quantity x is non-negative and the state $x = 0$ is a stationary state of the dynamics, i.e., a state in which the velocity $\dot{x}$ of the system in the configuration space vanishes. If the state $x = 0$ cannot be left, it is said to be *absorbing*, and, as it will be clarified in what follows, the stationarity condition is not sufficient to ensure that a state is absorbing. With the terminology of population genetics, we will call *fixation* the evolution of a system that leads it into an absorbing point. In particular, close to $x = 0$, one can have a noise with a power-law amplitude:

$$\dot{x} = \mu(x) + \sigma\, x^y\, \eta(t), \tag{1.1}$$

where $\mu(x)$ is the deterministic force driving the dynamics, which vanishes at $x = 0$, η is a normalized Gaussian noise characterized by $\langle \eta(t)\eta(t')\rangle = \delta(t - t')$, and σ and y are positive parameters; in writing this equation we use the Itō interpretation of the Langevin equation (see App. A.1). The value $y = 1/2$ appears very frequently in systems with internal fluctuations, where, because of the central limit theorem, the total amplitude of the noise ($\propto \sigma x^y$) is proportional to the square root of the number ($\propto x$) of individuals the fluctuations of which constitute the source of the noise for the evolution of x.

Equation (1.1) is known in finance as the *constant elasticity of variance* (CEV) model, which provides an effective description of the evolution of the price of an option in the financial market [39, 40]. In this model the exponent y has to be fitted from the data, and, depending on the option considered and on the historical period, it ranges from $y \simeq 3$ to $y \simeq 0$, or even to negative values (see Refs. [41, 42]).

Although in the CEV model the exponent y is not *a priori* constrained to any particular value, some possible values deserve particular attention, as they naturally appear in the description of a variety of statistical physics models. For instance, as anticipated above,

the value $y = 1/2$ appears very frequently, the most celebrated examples being directed percolation (see for instance Refs. [26, 43, 25]) and population genetics models with the so-called genetic drift (an example of which will be studied in detail in Chapter 2).

Another value which is quite common in statistical models is $y = 1$, as it can be related to the so-called "external fluctuations", where the system is coupled to a fluctuating environment and the coupling is modelled by a term linear in x, with a randomly evolving parameter. Paradigmatic examples for this case are the KPZ equation[1], directed polymers in random media and population genetics models with fluctuating selection coefficient (see for instance Refs. [44, 43, 45]).

Other noteworthy values for the noise exponent y are $y = 0$, which corresponds to the standard diffusion for the variable x (i.e., to a Langevin equation with constant noise) and for which $x = 0$ is no longer a stationary point of the dynamics (although $\mu(x = 0) = 0$), and $y = 2$, which has been found in the evolution of the number ($\propto x$) of parasites in an ecosystem (see Ref. [46]).

In the following part of the chapter we will see that the values 1/2 and 1 for the noise exponent y are peculiar also from the strictly mathematical point of view, since they represent the boundaries between regions in the parameter space in which the addition of the noise changes *qualitatively* the behavior of the system close to $x = 0$ compared to the one dictated by the deterministic part (i.e., in the absence of noise).

We consider here the simplest deterministic force $\mu(x)$ which ensures the stationarity of the point $x = 0$, i.e., a linear force $\mu(x) = -ax$ and, in order to avoid a possible escape to $x = \infty$ in the case of $a < 0$, we add a confining quadratic term $-bx^2$ with $b > 0$. The deterministic force $\mu(x)$ can be written in terms of a "potential" $V(x)$ such that $\mu(x) = -V'(x)$, with

$$V(x) = ax^2/2 + bx^3/3. \tag{1.2}$$

In the absence of noise, with this potential, the point $x = 0$ is absorbing for the dynamics described by Eq. (1.1) because $\mu(x = 0) = 0$, and there are two qualitatively different regimes:

- if $a > 0$ the potential $V(x)$ has one minimum at $x = 0$ (red solid curve in Fig. 1.1), which is reached asymptotically by the dynamics for $t \to \infty$. This is the absorbing phase, characterized by a vanishing value $x = 0$.

- If $a < 0$ the potential has one minimum at $x = -a/b$ (green dashed curve in Fig. 1.1), which is reached asymptotically for $t \to \infty$, unless $x(0) = 0$. This is the active phase, characterized by a positive value $x = -a/b > 0$.

If we consider the probability $P(x, t)$ to find the system in the configuration x at time t, in the absence of noise, it relaxes asymptotically to a stationary probability $P_{\rm s}(x)$, which,

[1]The KPZ equation is usually written in the form of a Langevin equation describing the evolution of a height h of an interface, in which the noise is additive (i.e., independent of h) and a deterministic term exponentially dependent on h is present; however, by means of the inverse of the so-called Cole-Hopf transformation $x = \exp[h]$, one obtains an equation describing the evolution of x, which is analogous to Eq. (1.1) with $y = 1$.

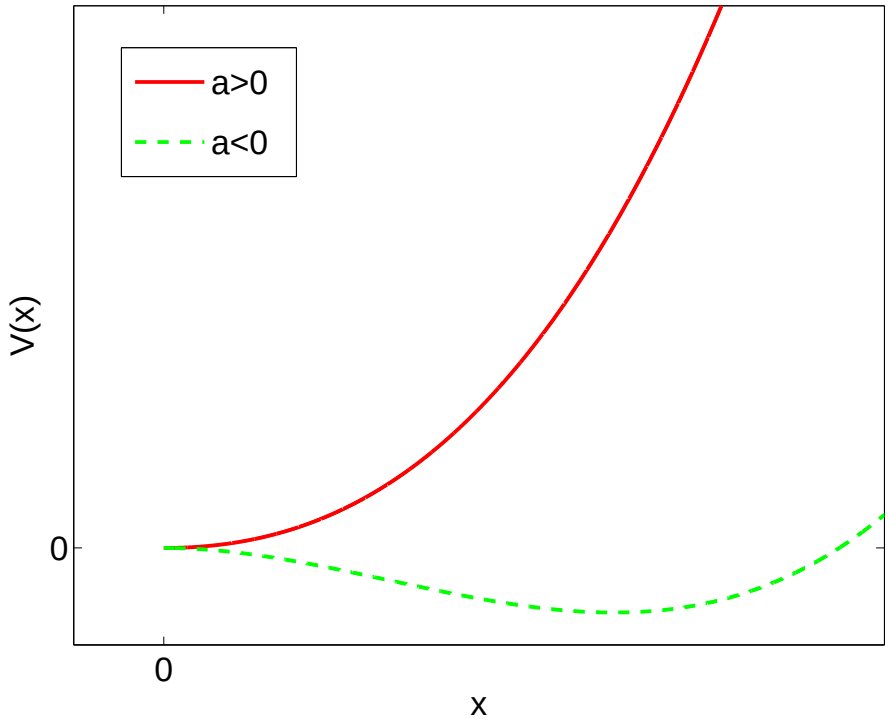

Figure 1.1: The potential $V(x)$ for a positive (red, solid line) and negative (green, dashed line) value of the parameter a.

for any positive initial condition $x(0)$ reads

$$P_{\rm s}(x) = \begin{cases} \delta(x) & \text{for} \quad a > 0, \\ \delta(x + \frac{a}{b}) & \text{for} \quad a < 0. \end{cases} \tag{1.3}$$

The introduction of the noise term in Eq. (1.1) changes qualitatively the behavior of the system and in particular, for some values of the exponent y, it becomes necessary to introduce proper boundary conditions in $x = 0$ in order to preserve the non-negativity of x, because the deterministic stationarity of $x = 0$ in Eq. (1.1) is not sufficient to exclude that the point $x = 0$ is crossed under the effect of the noise, although the amplitude of the noise itself (since we assume $y > 0$) vanishes for $x = 0$ (see Ref. [42, 47]).

In view of the fact that, contrary to the heuristic expectation, the point $x = 0$ can be actually crossed by the dynamics in the presence of the noise (unless suitable boundary conditions are added), we consider below a symmetric version of Eq. (1.1), in which negative values for the configuration x are allowed, i.e.,

$$\dot{x} = \mu_{\rm s}(x) + \sigma\, |x|^y\, \eta(t). \tag{1.4}$$

The stochastic part in Eq. (1.4) is symmetric under $x \to -x$ and the deterministic part $\mu_{\rm s}(x) = -V_{\rm s}(x)$ is the derivative of the symmetric version $V_{\rm s}(x) = ax^2/2 + b|x^3|/3$ of the

potential $V(x)$ in Eq. (1.2). Alternatively, the cubic term in the potential could be replaced by a quartic one, but this would be inconsequential for the properties discussed below.

1.2 Heuristic analysis of the point $x = 0$

As anticipated in the previous section, for some values of the parameters (y, a, σ), Eq. (1.4) allows the system to reach negative values of x, i.e., to cross the point $x = 0$. In this section we provide a heuristic explanation of this fact.

The first step is to approximate Eq. (1.4) with a simpler expression. First of all, we rewrite Eq. (1.4) in its differential form, i.e., $\mathrm{d}x = \mu_{\mathrm{s}}(x)\,\mathrm{d}t + \sigma\,|x|^y\,\mathrm{d}W$, where $\mathrm{d}W$ is the infinitesimal Wiener process (see for instance Ref. [22]). This equation is in turn defined as the $\delta t \to 0$ limit of a discrete-time process, with time steps of duration δt and characterized by an increment

$$\delta x = \mu_{\mathrm{s}}(x)\,\delta t + \sigma\,|x|^y \sqrt{\delta t}\,\tilde{\eta}, \tag{1.5}$$

where $\tilde{\eta}$ is a Gaussian-distributed random variable with zero mean and unit variance (see, e.g., Ref. [22]). For $x \ll |a|/b$, we can neglect the quadratic term in $\mu_{\mathrm{s}}(x)$, so that Eq. (1.5) reduces to

$$\delta x = -a\,x\,\delta t + \sigma |x|^y \sqrt{\delta t}\,\tilde{\eta}. \tag{1.6}$$

For a finite small value of δt, depending on the parameter y and on the configuration x, the largest contribution to the one-step increment δx in Eq. (1.6) can be either due to the deterministic term or to the stochastic one. More precisely, we can identify a length scale

$$\ell = \left(\frac{|a|}{\sigma}\right)^{\frac{1}{y-1}} \delta t^{\frac{1}{2(y-1)}}, \tag{1.7}$$

at which the deterministic and the stochastic term in Eq. (1.6) give equivalent contributions to the mean square increment $\langle \delta x^2 \rangle$ within the time step δt. If $y > 1$, the noise amplitude $\sigma|x|^y$ vanishes for $x \to 0$ faster than the deterministic term, and we can identify a region $|x| \ll \ell$ in which the one-step increment δx is typically dominated by the deterministic term (i.e., $\delta x \simeq -a\,x\,\delta t$), while in the region $|x| \gg \ell$ it is typically dominated by the stochastic one (i.e., $\delta x \simeq \sigma |x|^y \sqrt{\delta t}\,\tilde{\eta}$). Viceversa, if $y < 1$, the noise amplitude $\sigma|x|^y$ vanishes for $x \to 0$ more slowly than the deterministic term, and therefore the two regions are interchanged. The length scale ℓ represents thus, for $y > 1$ ($y < 1$), the minimum (maximum) distance from $x = 0$ at which the stochastic force is relevant for a single jump.

1.2.1 Superlinear noise ($y > 1$)

As anticipated above, for $y > 1$, in the region $|x| \ll \ell$, i.e., close to the origin, the one-step increment δx is dominated by the deterministic contribution. If $a < 0$, the deterministic contribution pushes the system away from the origin because $\mu_{\mathrm{s}}(x)$ is positive for $x > 0$ and negative for $x < 0$, therefore, once x is close to the origin ($|x| \ll \ell$), the system can neither cross nor reach the point $x = 0$. As we argue below, the probability that, due to the

contribution of a fluctuation, the system crosses the origin $x = 0$ starting from the region $|x| \gtrsim \ell$ vanishes for $\delta t \to 0$, so we expect that the origin is a boundary for the dynamics without the need of introducing additional boundary conditions and that the system will remain in the active phase (characterized by $\langle x \rangle \neq 0$). If $a > 0$, on the other hand, the deterministic part pushes the system towards the origin, so we expect that not only the origin is a boundary for the dynamics without the need for the introduction of boundary conditions, but it is also an absorbing state into which the system will eventually collapse (i.e., the system undergoes a *fixation* process to the state $x = 0$).

In order to heuristically investigate the possible crossing of the point $x = 0$, we consider the discrete-time process in Eq. (1.6). If a trajectory, solution of Eq. (1.6), crosses $x = 0$, it has to contain (at least) one step which crosses the origin. Since every step in the region $|x| \ll \ell$ is dominated by the deterministic force, which does not allow the crossing of $x = 0$, this crossing may happen only during a step with initial configuration in the region $x \gtrsim \ell$, and its probability can be heuristically estimated with the probability $P_{\rm j}$ that the system crosses the origin with a single jump starting from $x = \ell$. The probability $P(x + \delta x, \delta t | x, 0)$ to find the system in the configuration $x + \delta x$ at time δt, provided that it was in the state x at time 0, can be obtained by considering Eq. (1.6) as a change of variable from the random variable $\tilde{\eta}$ to the variable δx, and it reads

$$P(x + \delta x, \delta t | x, 0) = \frac{1}{\sqrt{2\pi s^2(x)}} \, \mathrm{e}^{-\frac{(\delta x - m(x))^2}{2 s^2(x)}} \, , \tag{1.8}$$

where $m(x) = -a\, x\, \delta t$, $s(x) = \sigma\, |x|^y \sqrt{\delta t}$, and the prefactor $1/\sqrt{s^2(x)}$ comes from the Jacobian of the change of variable. Accordingly, the probability $P_{\rm j}$ to jump from $x = \ell$ to $x < 0$ in the small time δt, reads

$$P_{\rm j}(\delta t) = \int_{-\infty}^{0} \mathrm{d}x' \, P(x', \delta t | \ell, 0) = \frac{1}{\sqrt{2\pi}} \int_{\frac{\ell - m(\ell)}{s(\ell)}}^{\infty} \mathrm{d}z \, \mathrm{e}^{-z^2/2}. \tag{1.9}$$

The probability $P_{\rm j}$ in Eq. (1.9) depends, as expected, on the duration δt of the discrete time interval (because the length scale ℓ is a function of δt); therefore, in order to understand the behavior of the system described by Eq. (1.4), we have to consider the limit $\delta t \to 0$. For $y > 1$, the lower integration extreme $[\ell - m(\ell)]/s(\ell)$ on the r.h.s. of Eq. (1.9) diverges in this limit, so we heuristically expect that the probability that the system crosses the origin vanishes, as anticipated.

1.2.2 Sublinear noise ($y < 1$)

Unlike the case considered in the previous section, for $y < 1$ the stochastic force vanishes more slowly then the deterministic one for $x \to 0$, and thus, in the region $|x| \ll \ell$ (i.e., close to the origin), the one-step increment δx is dominated by the stochastic contribution. Due to this fact, the heuristic argument used for discussing the case $y > 1$ cannot be straightforwardly applied.

In order to recover a situation in which the deterministic force dominates near the origin, we perform here the change of variable[2] $z = x|x|^{1-2y}/[\sigma^2(1-y)^2]$ in Eq. (1.4), obtaining

$$\dot{z} = -Az - Bz|z|^{1-d/2} + d\, z/|z| + 2|z|^{1/2}\,\eta, \tag{1.10}$$

with coefficients $A = 2a(1-y)$, $B = 2b(1-y)[\sigma(1-y)]^{\frac{1}{1-y}}$ and $d = (1-2y)/(1-y)$, which depend on the parameters a, b and y of Eq. (1.4). Note that in the range of values of y considered here, i.e., for $y < 1$, the point $x = 0$ is mapped to $z = 0$ and the term proportional to B (which prevents the escape of the system to $|z| = \infty$) in Eq. (1.10) is negligible for $z \ll (b/a)^{2/(d-2)}$. Within this region Eq. (1.10) reduces therefore to the so-called square d-dimensional Bessel process (see Ref. [48])

$$\dot{z} = -Az + d\, z/|z| + 2|z|^{1/2}\,\eta, \tag{1.11}$$

which, for $z \ll d/A$, can be further simplified to

$$\dot{z} = d\, z/|z| + 2|z|^{1/2}\,\eta. \tag{1.12}$$

Analogously to Eq. (1.4), also Eq. (1.12) is defined as the limit $\delta t \to 0$ of a discrete-time process with time steps of duration δt and characterized by an increment

$$\delta z = d\, z/|z|\delta t + 2|z|^{1/2}\delta t\,\tilde{\eta}, \tag{1.13}$$

where $\tilde{\eta}$ is again a Gaussian-distributed random variable with zero mean and unit variance. As for Eq. (1.6), we can define a length scale $\tilde{\ell} = d^2\delta t/4$ at which the deterministic and the stochastic term in Eq. (1.13) give equivalent contributions to the mean square displacement $\langle \delta z^2 \rangle$. It can be noticed that the deterministic term dominates Eq. (1.13) for $|z| \ll \tilde{\ell}$ (i.e., near the origin), and viceversa it is negligible for $|z| \gg \tilde{\ell}$.

Depending on the sign[3] of the parameter d (i.e., on the fact that the exponent y in Eq. (1.4) is larger or smaller than $1/2$), the system has a completely different evolution. For $d < 0$ (i.e., for $1/2 < y < 1$), the deterministic term in Eq. (1.13) pushes the system towards the point $z = 0$ (i.e., towards $x = 0$), so we heuristically expect that the system will eventually fix to that value.

On the other hand, for $d > 0$ (i.e., for $y < 1/2$), the deterministic term in Eq. (1.13) pushes the system away from the point $z = 0$, and the probability $\tilde{P}_{\rm j}(\delta t)$ to jump from $z = \tilde{\ell}$ to $z < 0$, evaluated as in Eq. (1.9), does not vanish for $\delta t \to 0$. This means that in this regime we heuristically expect a non-vanishing crossing probability for the point $z = 0$ (i.e., for $x = 0$).

Summarizing, we heuristically expect qualitatively different scenarios depending on the exponent y of the noise amplitude. For $y < 1/2$ the system can cross the point $x = 0$, which does not appear to be absorbing, independently of the value of the deterministic force,

[2] See App. A.1 for details on the change of variables in a Langevin equation.

[3] In the definition of the Bessel process, d is the dimension of the space in which the process takes place, so it is constrained to positive integer values. However Eq. (1.11) can be generalized to non-integer and even to negative values of the "dimension" d (see, e.g., Ref. [48]).

i.e., of the deterministic "attractive" or "repulsive" character of $x = 0$. On the contrary, for $1/2 < y < 1$, we expect that $x = 0$ is absorbing, and the system reaches fixation independently of the value of a. For $y > 1$ instead, as argued in the previous subsection, the system is expected to remain in the active phase if the deterministic force makes $x = 0$ repulsive (i.e., if $a < 0$) and to fix to $x = 0$ in the opposite case. In the following section, we will study the problem with the well-established boundary classification, which confirms these heuristic results.

1.3 Boundary classification

The process associated with Eq. (1.1) can be analyzed by means of the relative *boundary classification* (see Refs. [49, 50, 51, 28]). This is a method to determine the character of a point x_0 (typically a boundary of the process, hence the name) when the evolution of the state $x \in (x_\mathrm{l}, x_\mathrm{r})$ of a system is described by a Langevin equation of the form (see Ref. [28])

$$\dot{x} = f(x) + \sqrt{v(x)}\,\eta, \tag{1.14}$$

with suitable smooth functions $f(x)$ and $v(x)$, and a delta-correlated and Gaussian-distributed noise $\eta(t)$. More precisely the classification is based on answering the following three questions:

i) Starting from an initial configuration $x \neq x_0$, can the system reach x_0 before all the rest of the configuration space is visited?

ii) If the answer to the previous question is yes, is x_0 reached in a finite expected time?

iii) For $t \to \infty$, is the system stuck at $x = x_0$? (i.e., does the system undergo *fixation*?)

The answers to the questions (i), (ii), and (iii) can be obtained via the analysis of three functionals L_1, L_2, and L_3, which will be described in the following part of the section and depend on the behaviour of the functions $f(x)$ and $v(x)$ near the point $x = x_0$.

1.3.1 Attractiveness of the point x_0

If the answer to the question (i) is positive, the point x_0 is said to be *attracting*. In order to investigate the attractiveness of x_0, we consider here the probability $u(x; x_0, x_1)$ that the system, starting from the initial configuration x, reaches the point $x_1 \neq x_0$ before x_0. This probability satisfies the homogeneous backward Fokker-Planck equation (see, e.g., Ref. [51])

$$f(x)\partial_x u(x; x_0, x_1) + v(x)\partial_x^2 u(x; x_0, x_1)/2 = 0 \tag{1.15}$$

with the boundary conditions $u(x_0; x_0, x_1) = 1$ and $u(x_1; x_0, x_1) = 0$. The solution of Eq. (1.15) is rather straightforward [51]

$$u(x; x_0, x_1) = \frac{L_1(x_0, x)}{L_1(x_0, x_1)}, \tag{1.16}$$

where

$$L_1(x_0, x_1) = \int_{x_0}^{x^1} \mathrm{d}\xi \exp[-g(\xi)], \tag{1.17a}$$

$$g(\xi) = \int_{\xi_\mathrm{a}}^{\xi} \mathrm{d}\xi' \, 2f(\xi')/v(\xi'), \tag{1.17b}$$

while ξ_a is an arbitrary value of x which does not affect the result in Eq. (1.16). The state x_0 is attracting if $u(x; x_0, x_1) < 1$ for at least one value of the initial condition x and one value of the point x_1; the latter can therefore be chosen, for $x > x_0$ ($x < x_0$), as the right (left) boundary of the process, There are two possible scenarios: either $u(x; x_0, x_1) = 1$ for any choice of the initial condition x, or $u(x; x_0, x_1) < 1$ for at least some choice of the initial condition x. In the latter case the point x_0 is attracting, and this happens if and only if the functional $L_1(x_0, x)$, defined in Eq. (1.17a), takes a finite value for some x.

1.3.2 Attainability of the point x_0

If the answer to both questions (i) and (ii) above is positive, i.e., if the system, starting from an initial configuration $x_1 \neq x_0$, can reach x_0 in a finite expected time, the point x_0 is said to be *attainable*. In order to investigate the attainability of x_0, we consider here the mean time $T(x; x_0, x_1)$ to reach either x_0 or x_1 starting from the initial condition x, where x_1 is the boundary which is on the same side of x with respect to x_0. T satisfies the differential equation (see, e.g., Ref. [51])

$$f(x)\partial_x T(x; x_0, x_1) + v(x)\partial_x^2 T(x; x_0, x_1)/2 = -1 \tag{1.18}$$

with the boundary conditions $T(x_0; x_0, x_1) = T(x_1; x_0, x_1) = 0$. The solution of Eq. (1.18) is (see Ref. [51])

$$T(x; x_0, x_1) = 2\left\{u(x; x_0, x_1)L_2(x_1, x) + [1 - u(x; x_0, x_1)]\, L_2(x_0, x)\right\}, \tag{1.19}$$

where

$$L_2(x_0, x) = \int_{x_0}^{x} \mathrm{d}\xi \, L_1(x_0, \xi) m(\xi), \tag{1.20a}$$

$$m(x) = \exp[g(x)]/v(x), \tag{1.20b}$$

while $u(x; x_0, x_1)$, $L_1(x_0, x_1)$, and $g(x)$ have been defined in Eqs (1.16), (1.17a), and (1.17b) respectively. According to the previous subsection, the point x_0 is attracting if $u(x; x_0, x_1) < 1$ for some values of x, x_1. In this case, the expected time $T(x; x_0, x_1)$ in Eq. (1.19) is finite if and only if the functional $L_2(x_0, x)$ in Eq. (1.20a) is finite (see Ref. [51]).

1.3.3 Fixation and stationary distribution

In order to investigate whether the system undergoes fixation, i.e., whether it localizes into an absorbing state, we consider here the probability $P(x, t|x', 0)$ to find the system at the

configuration x at time t conditioned to the fact that at time 0 it was at the configuration x'. This probability satisfies the forward Fokker-Plank equation associated with Eq. (1.14), which reads (see, e.g., Ref. [22])

$$\partial_t P(x,t|x',0) = -\partial_x \left[f(x)P(x,t|x',0)\right] + \frac{1}{2}\partial_x^2 \left[v(x)P(x,t|x',0)\right]. \tag{1.21}$$

The long-time behaviour of P can be understood by studying the stationary version of Eq. (1.21), whose solution does not depend on the initial condition (unless the initial state is an absorbing one) and can be formally written as

$$P_{\rm s}(x) = m(x)/Z \tag{1.22}$$

where the function $m(x)$ has been defined in Eq. (1.20b), while Z is a normalization constant. If the function $m(x)$ is well-defined and normalizable on the whole configuration space, Eq. (1.22) defines the asymptotic probability distribution of the system, which therefore does not fix to an absorbing boundary. On the other hand, when the system undergoes fixation to an absorbing point x_0, the function $m(x)$ has a non-normalizable singularity at that point, and we can introduce the so-called fixation probability $p(x_0|x)$, i.e., the probability that the system reaches the absorbing point x_0, starting from the configuration x.

A point x_0 is called *regular* if the function $m(x)$ is normalizable for $x \to x_0$, i.e., if the functional

$$L_3(x_0,x) = \int_{x_0}^{x} {\rm d}\xi\, m(\xi) \tag{1.23}$$

is finite for some x. As explained in the next subsection, a regular point is not absorbing.

Relation between fixation probability and stationary distribution

For any stochastic process with an absorbing state x_0, the fixation probability $p(x_0|x)$ to that point and the stationary distribution $P_{\rm s}(x)$ have disjoint support on $x \neq x_0$, i.e., at any point $x \neq x_0$, either the fixation probability $p(x_0|x)$ or the stationary distribution $P_{\rm s}(x)$ vanishes.

In fact, let us consider a stochastic process with an absorbing state x_0 and with a stationary distribution $P_{\rm s}(x)$ which does not vanish on a set I (with $x_0 \notin I$). If we take an ensemble of $\mathcal{N} \to \infty$ systems distributed according to $P_{\rm s}$ and we let them evolve according to the dynamics, the ensemble is still described by the same stationary distribution $P_{\rm s}$ (because $P_{\rm s}$ is by definition invariant under the dynamics); in particular there cannot be a probability current from the set I to x_0, because, being x_0 absorbing, it could not be compensated by a flow from x_0 to I, as required by the condition of stationarity. Therefore the fixation probability $p(x_0|x)$ has to vanish on the whole set I.

To our knowledge, this simple argument has never been presented in the literature.

1.3.4 Boundary classification for the point $x = 0$ in Eq. (1.4)

The general classification described in the previous sections 1.3.1, 1.3.2, and 1.3.3, can be straightforwardly applied to Eq. (1.4). We simply use the expressions $f(x) = \mu_{\rm s}(x)$ and

$v(x) = \sigma^2|x|^{2y}$ characterizing, respectively, the deterministic part and the variance of the noise in Eq. (1.4) into the Eqs. (1.17a), (1.20a), and (1.23), defining the functionals $L_1(x_0, x)$, $L_2(x_0, x)$, and $L_3(x_0, x)$ respectively, the values of which depend on the parameters y, a, and σ. We summarize here the results of the boundary classification.

(*i*) *Attractivity* — The functional $L_1(0, x)$ is finite and therefore the point $x = 0$ is attracting (i.e., it can be reached before all the rest of the configuration space is visited) for

- $y < 1$, or
- $y = 1$ and $a > -\sigma^2/2$, or
- $y > 1$ and $a > 0$.

(*ii*) *Attainability* — The functional $L_2(0, x)$ is finite and therefore the point $x = 0$ is attainable (i.e., it is reached in a finite expected time) if and only if $y < 1$. This means in particular that, (I) for $y = 1$ and $a > -\sigma^2/2$ or (II) for $y > 1$ and $a > 0$, the point $x = 0$ is attracting but not attainable, i.e., it can be reached, but with an infinite expected time.

(*iii*) *Regularity* — The functional $L_3(0, x)$ is finite and therefore the point $x = 0$ is regular (i.e., it is not absorbing), for

- $y < 1/2$, or
- $y = 1$ and $a < -\sigma^2/2$, or
- $y > 1$ and $a < 0$.

It can be noticed that for $y \geq 1$ the point $x = 0$ is regular for the same values of a for which it is not attractive, i.e., for which it can not be reached by the system. For $y < 1/2$, instead, the point $x = 0$ is attainable (i.e., it can be reached in a finite expected time), but nevertheless it is regular, meaning that it can be left (or crossed), as expected from the heuristic argument is Sec. 1.2.2. This means that, in order to have a process constrained to involve only positive values of the variable x, we have to enforce auxiliary boundary conditions in the point $x = 0$. In Sec. 1.4.1 we will describe this fact from the perspective of the probability $P(x, t)$ to find the system in the configuration x at time t.

1.4 Probability distribution

In order to describe more in detail the potential crossing of the point $x = 0$ by a system described by Eq. (1.4), we consider now the probability $P(x, t|x', 0)$ to find the system in the configuration x at time t, conditioned to the fact that at time 0 it was in the configuration x'. We focus here on the case $y < 1$, i.e., on the case in which the noise vanishes sublinearly for $x \to 0$. From the boundary classification, we already know that the character of the

point $x = 0$ depends on the value of the noise exponent y, but not on the parameters a and b. We can therefore set $a = b = 0$ without changing significantly the properties of the point $x = 0$. In this case the Fokker-Planck equation describing the evolution of the probability $P(x, t|x', 0)$ reduces to

$$\dot{P}(x, t|x', 0) = \frac{\sigma^2}{2}\partial_x^2 \left[|x|^{2y} P(x, t|x', 0)\right], \tag{1.24}$$

where the initial condition is $P(x, 0|x', 0) = \delta(x - x')$. The solution of Eq. (1.24) can be written in terms of the modified Bessel functions $K_\nu(z)$ and $I_\nu(z)$ of order $\nu = 1/[2(1 - y)]$ and depends, as expected, on the value of y (see App. A.3 for more details).

1.4.1 Noise exponent $0 < y < 1/2$

For $0 < y < 1/2$ (i.e., for $1/2 < \nu < 1$), the solution of Eq. (1.24) with a positive initial condition x' reads (see App. .A.3 for the derivation)

$$\begin{aligned} P(x, t|x', 0) =& \frac{\sigma^2 \nu x'^{1/2}}{2t} |x|^{\frac{1}{\nu}-\frac{3}{2}} \exp\left[-\frac{\sigma^2 \nu^2 (x'^{1/\nu} + |x|^{1/\nu})}{2t}\right] \\ & \times \left[\sin(\pi\nu) K_\nu\left(\frac{\sigma^2 \nu^2 x'^{\frac{1}{2\nu}} |x|^{\frac{1}{2\nu}}}{t}\right) + \theta(x) I_\nu\left(\frac{\sigma^2 \nu^2 x'^{\frac{1}{2\nu}} x^{\frac{1}{2\nu}}}{t}\right)\right]. \end{aligned} \tag{1.25}$$

The probability distribution $P(x, t|x', 0)$ in Eq. (1.25) is plotted in Fig 1.2 with initial condition $x' = 1$, for $\sigma = 1$, $\nu = 0.25$, and for various times t. It can be noticed that the probability is localized around the initial condition 1 at short times, while it spreads to both negative and positive values of x at longer times. Note that in the original equation (1.4), the escape to $|x| = \infty$ of the two pronounced peaks, which move to the right for $x > 0$ and to the left for $x < 0$, would be prevented by the presence of the cubic confining term $b|x^3|/3$ in the deterministic potential V_s, in which case the probability $P(x, t|x', 0)$ relaxes to the stationary probability

$$P_s(x) \propto \frac{1}{|x|^2 y} \exp\left[-\frac{a}{1-y}|x|^{2-2y} - \frac{2b}{3-2y}|x|^{3-2y}\right]. \tag{1.26}$$

The result of Eq. (1.25), despite the fact that it does not capture the correct long time behavior of the (confined) solution of Eq. (1.4), is interesting as it shows, in agreement with the results of Secs. 1.2.2 and 1.3.4, that (i) the point $x = 0$ can be crossed and (ii) there is not fixation to $x = 0$.

1.4.2 Noise exponent $1/2 \leq y < 1$

For $1/2 \leq y < 1$ (i.e., for $\nu \geq 1$), the solution of Eq. (1.24) with a positive initial condition x' reads (see App. A.3)

$$\begin{aligned} P(x, t|x', 0) =& \frac{\sigma^2 \nu x'^{1/2}}{2t} |x|^{\frac{1}{\nu}-\frac{3}{2}} \exp\left[-\frac{\sigma^2 \nu^2 (x'^{1/\nu} + |x|^{1/\nu})}{2t}\right] \theta(x) I_\nu\left(\frac{\sigma^2 \nu^2 (x'x)^{\frac{1}{2\nu}}}{t}\right) \\ & + p(0, t|x', 0)\delta(x), \end{aligned} \tag{1.27}$$

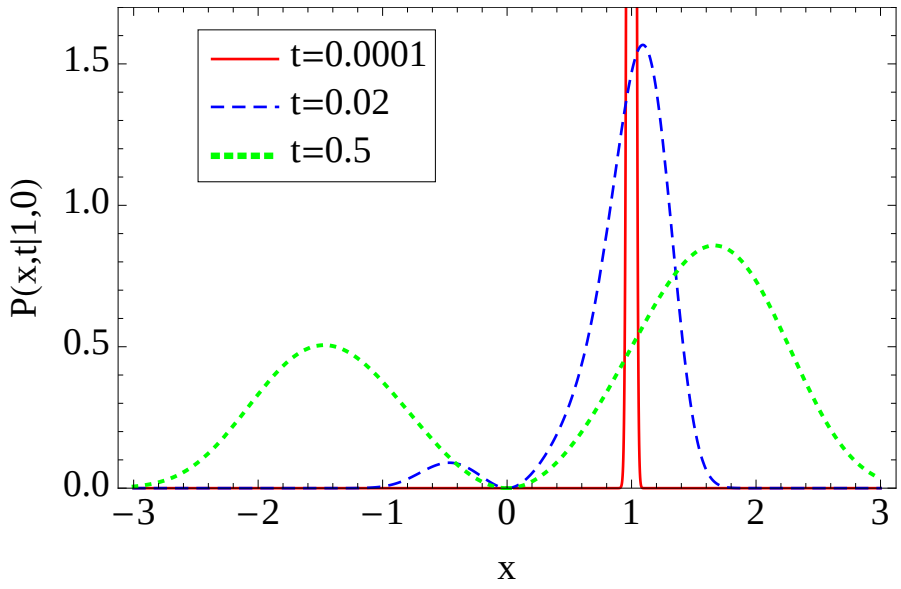

Figure 1.2: Plot of the probability distribution $P(x,t|1,0)$ to find the system in the configuration x at time t, with the assumption that $x = 1$ at time $t = 0$, for various values of t; $P(x,t|x',0)$ is reported in Eq. (1.25) and it has been derived for $0 < y < 1/2$ and $a = b = 0$. At short times $P(x,t|1,0)$ is localized around the initial condition 1 and, upon increasing time, it spreads to both negative and positive values of x, trespassing the point $x = 0$.

where $p(0,t|x',0) = 1 - \gamma(\nu, \sigma^2\nu^2 x'^{\frac{1}{\nu}}/(2t))/\Gamma(\nu)$ is the time-dependent fixation probability to the state $x = 0$ and $\gamma(\nu,z) = \int_0^z \mathrm{d}t\, \mathrm{e}^{-t} t^{\nu-1}$ is the (upper) incomplete gamma function. It can be noticed that the probability $p(0,t|x,0)$ is an increasing function of time, as depicted in Fig. 1.4, indicating the presence of an absorbing state in $x = 0$ and the eventual fixation of the system. The probability distribution $P(x,t|x',0)$ in Eq. (1.27) is plotted in Fig 1.3 with initial condition $x' = 1$, for $\sigma = 1$, $\nu = 0.75$ and for various values of the time t. At short times the probability is localized around the initial condition 1, while it spreads to every positive value of x at longer times. It can be noticed however that the area subtended by $P(x,t|x',0)$ decreases for increasing time, indicating an increasing probability to find the system in the absorbing state $x = 0$. This is confirmed by Fig. 1.4, in which we report the probability $p(0,t|1,0)$ to find the system in the absorbing state $x = 0$ at time t, conditioned to the fact that at the initial time it was in the configuration 1.

1.4.3 Noise exponent $y = 1$

If the noise decreases linearly as x approaches 0, the solution of the stationary Fokker-Planck equation (1.24) can be formally written as

$$P_{\mathrm{s}}(x) \propto \frac{1}{|x|^{2a/\sigma^2+2}} \exp[-2b|x|/\sigma^2]. \tag{1.28}$$

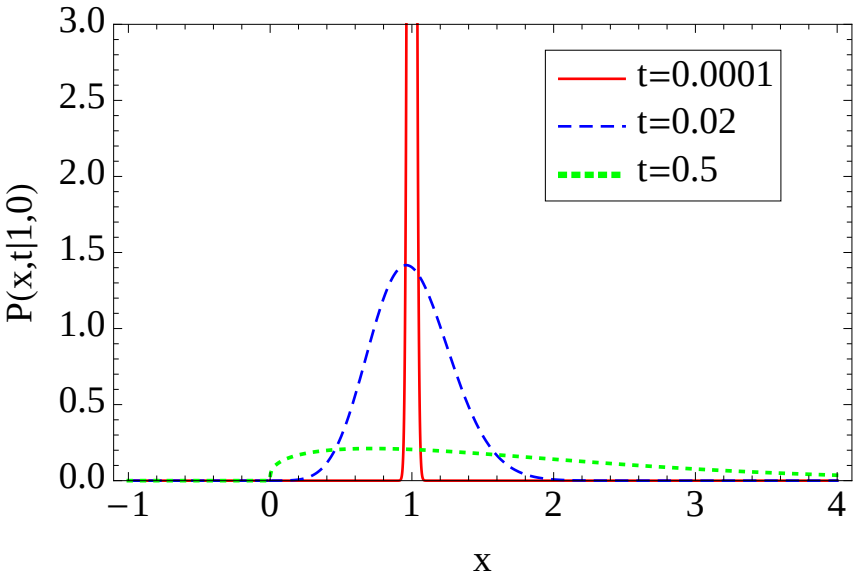

Figure 1.3: Plot of the probability distribution $P(x,t|1,0)$ to find the system in the configuration x at time t, with the assumption that $x = 1$ at time $t = 0$, for various values of t; $P(x,t|x',0)$ is reported in Eq. (1.27) and it has been derived for $1/2 < y < 1$ and $a = b = 0$. The area subtended by $P(x,t|x',0)$ decreases by increasing the time t, indicating that the probability to find the system in the absorbing state $x = 0$ is an increasing function of time, as Fig. 1.4 clearly shows.

The expression reported in Eq. (1.28) is normalizable and represents thus a well-defined stationary distribution only for $a < a_c$, where $a_c = -\sigma^2/2$ represents a critical value above which the "order parameter"[4] $\langle x \rangle$ asymptotically[5] relaxes to the value $\langle x \rangle = 0$, which identifies the absorbing state, and above which the system is in an active phase characterized by a stationary value $\langle x \rangle > 0$([6]). This is an example of a noise-induced ordering transition (see, e.g., Refs. [43, 52, 28]), which is controlled by the noise amplitude σ determining whether, for a certain value $a < 0$, the system is in an ordered (i.e., active) or disordered (i.e., absorbing) phase.

[4] In analogy with equilibrium phase transitions, the expectation value $\langle x \rangle$ can be considered as a sort of order parameter.

[5] Note that the point $x = 0$ is not attainable for $y \geq 1$, i.e., it cannot be reached in a finite expected time (see Sec. 1.3.4). In population genetics, the behavior of a system which reaches asymptotically an absorbing state is called *quasi-fixation* (see Ref. [45]).

[6] If we assume a positive initial condition $x(0) > 0$.

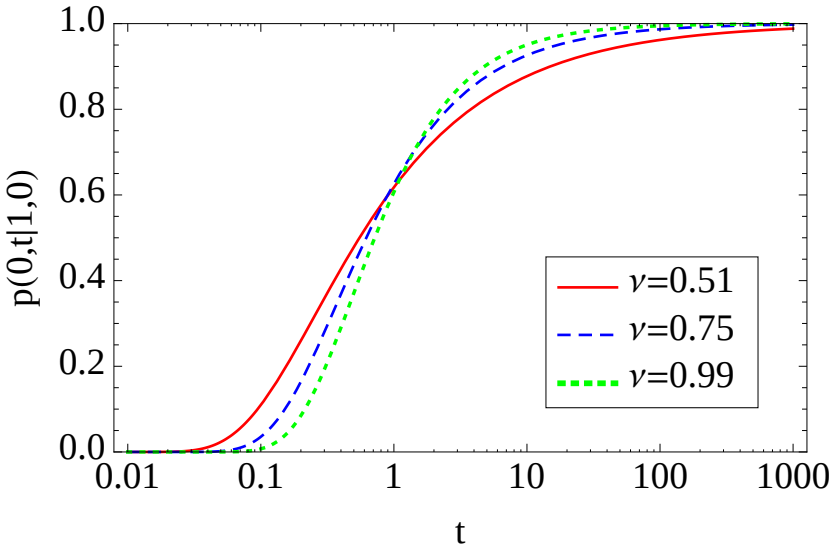

Figure 1.4: Time-dependent fixation probability $p(0,t|1,0)$ to the absorbing state $x = 0$, with the assumption that $x = 1$ at time $t = 0$; $p(0,t|1,0)$ has been evaluated for $a = b = 0$ and for various values if the parameter $\nu = 1/[2(1-y)]$.

1.4.4 Noise exponent $y > 1$

For a noise exponent $y > 1$ (i.e., when the noise decreases faster than linearly as x approaches 0), the solution of the stationary Fokker-Planck equation (1.24) can be formally written as

$$P_{\rm s}(x) \propto \begin{cases} \dfrac{1}{|x|^{2y}} \exp\left[\dfrac{a}{y-1}|x|^{2-2y} - \dfrac{2b}{3-2y}|x|^{3-2y}\right], & y \neq 3/2, \\ \dfrac{1}{|x|^{3+2b}} \exp\left[2a|x|^{-1}\right], & y = 3/2. \end{cases} \tag{1.29}$$

As in the case $y = 1$, also for $y > 1$ there is a critical value a_c of the parameter a — which in this case is $a_c = 0$ — above which the formal solution reported in Eq. (1.29) is not normalizable, the system asymptotically[7] fixes to the point $x = 0$, and the order parameter $\langle x \rangle$ asymptotically relaxes to 0.

1.5 Summary of results

We have shown that a system described by Eq. (1.4) displays qualitatively different behaviors depending on the value of the exponent y of the noise. In particular, $y = 1/2$ and $y = 1$ — which, as discussed in Sec. 1.1, are by far the most common in physical systems — represent the boundaries between the different regions in the phase portrait which are depicted in Fig. 1.5 and summarized below.

[7] See footnote 5

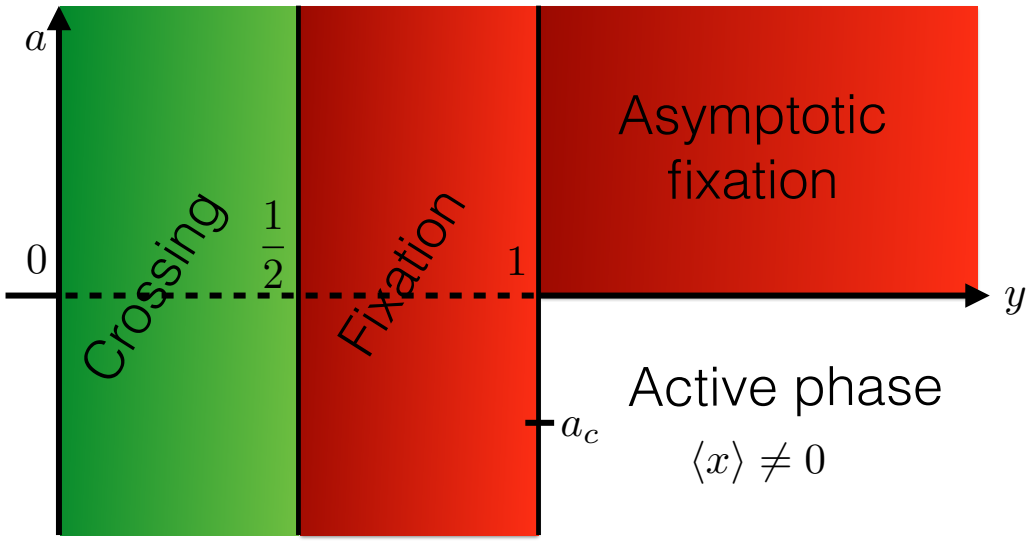

Figure 1.5: "Phase diagram" which summarizes the behavior of the point $x = 0$ in Eq. (1.4) in the space of the relevant parameters y and a.

If $y > 1$, i.e., if the noise vanishes superlinearly for $x \to 0$, the fate of the system depends on the value of the coefficient a of the linear term in the deterministic force: similarly to the solution of the purely deterministic case described in Eq. (1.3), for $a > 0$ there is asymptotic fixation to $x = 0$, while for $a < 0$ the system remains in the active phase characterized by $\langle x \rangle > 0$. Compared to the deterministic solution in Eq. (1.3), the noise widens the stationary distribution $P_{\rm s}(x)$, but it does not allow the system to cross the state $x = 0$, and this can be heuristically understood by analyzing the probability for a system, described by the discrete-time version of Eq. (1.4) (with time step δt), to cross $x = 0$: this probability turns out to vanish as $\delta t \to 0$.

The value $y = 1$ for the noise exponent, as anticipated in Sec. 1.1, is associated to a number of statistical physics systems, as KPZ equation, directed polymers in random media and population genetics models with fluctuating selection coefficient (see for instance Refs. [44, 43, 45]). For this particular value of y, the behavior of the system is still qualitatively similar to the previous (superlinear) case, but with the crucial difference that the critical value a_c of the coefficient a which separates the "active" from the "absorbing" phase is now $a_c = -\sigma^2/2$; this produces a so-called noise-induced ordering transition (see, e.g., Ref. [43, 52, 28]), because, for a certain value $a < 0$, the amplitude σ of the noise determines whether the system is in an ordered (i.e., active) or disordered (i.e., absorbing) phase.

The sublinear noise (i.e., the noise with an exponent $y < 1$) introduces, instead, significant changes compared to the deterministic behavior. For $1/2 \leq y < 1$, the state $x = 0$ is absorbing and attainable (i.e., the system is expected to fix to this state in finite time), independently of the value of the coefficient a of the deterministic part, i.e., of the deterministic

"attractive" or "repulsive" character of $x = 0$. It can be noticed that the smallest exponent y falling in this class is $y = 1/2$, which, as anticipated in Sec. 1.1, appears very frequently in systems with internal fluctuations, as directed percolation (see for instance Refs. [26, 43, 25]) and population genetics models with the so-called genetic drift (an example of which will be studied in detail in Chapter 2). For $y < 1/2$ instead, the state $x = 0$ is a regular point, i.e., it is not absorbing. Since we know from the boundary classification that it is also attainable (i.e., that it can be reached in a finite expected time), this means that it can be leaved and crossed. In a sense, the separatrix nature of the state $x = 0$ for Eq. (1.4) — with vanishing deterministic part and vanishing noise amplitude — is only apparent, and fluctuations close to $x = 0$ turn it into a regular point. This is confirmed by the solution of the Fokker-Planck equation for the probability $P(x, t)$ to find the system in the state x at time t in a simplified version of Eq. (1.4), i.e., with $a = b = 0$, which however retains the same behavior for $x \simeq 0$. This means that, in order to describe a system in which the state x is constrained to be non-negative (as in the case of the CEV model for the price of options on the financial market), Eq. (1.1) has to be supplemented with proper boundary conditions (see, e.g., Ref. [42]).

The behavior of the system in the presence of sublinear noise can be heuristically understood with the change of variable $z = x|x|^{1-2y}/[\sigma^2(1-y)^2]$ in Eq. (1.4), which renders an equation of motion for the variable z with a constant term proportional to $(1-2y)z/|z|$, which strongly pushes the system towards the point $z = 0$ (i.e., $x = 0$) for $y > 1/2$ and away from this point for $y < 1/2$. In the latter case, the probability for a system described by the discrete-time version of Eq. (1.4) to cross the state $x = 0$ turns out to remain finite as $\delta t \to 0$, and this explains heuristically the crossing of the point $x = 0$.

Chapter 2

Population genetics in a subdivided population

This chapter is primarily based on the results originally presented in Refs. [36, 37].

2.1 Introduction

Among the fields in which the approach of statistical physics turns out to be particularly useful and effective, there is *population genetics*, which is at the core of a quantitative theory of evolution. Population genetics can help, for instance, in understanding the origin and history of species, the migration behavior of animals and microbial, in predicting and control epidemics or in contrasting diseases with an evolutionary character. An additional reason of interest lies in the fact that the same mathematical models used in population genetics can be often applied to other contexts such as ecology, evolutionary game theory, language competition, learning dynamics, and epidemics (see, for instance, Refs. [53, 54, 55, 56]).

The simplest models of population genetics focus on one gene of the genotype (i.e., on one locus in the DNA sequence), and describe the time evolution of the fractions $\{x^{(i)}\}$ of individual in a population carrying the various alleles, i.e., the different possible "values" $i = 1, ..., N_{\text{allele}}$ of the gene considered; due to their simplicity, particular attention is devoted to the diallelic models, in which $N_{\text{allele}} = 2$ and, if the total number of individuals is constant, one fraction x is sufficient to describe the state of the population. In asexual populations (e.g., in bacteria) the dynamics can then be interpreted as a sort of random walk in the space of the allele frequency x, with state-dependent jump rates.

In a natural population with no structure or subdivision — usually referred to as a *well-mixed* population — the temporal evolution of the gene content results from the competition between the deterministic evolutionary force (*selection*) which favors "stronger" genotypes and the stochastic effects generated by the death and reproduction of individuals (*genetic drift*). Due to the possibility of errors in the microscopic process involved in the DNA replication, an allele may occasionally be substituted by a different one during its reproduction (*mutation*); however, mutations typically occur on a time scale ($\tau_{\text{mutation}} \simeq 10^8$ generations, see, e.g., Ref. [57]) much longer than the other forces mentioned above ($\tau_{\text{migration}} \simeq \tau_{\text{selection}} \simeq$

$\tau_{\text{genetic drift}} \simeq (10^1 \div 10^4)$ generations, see, e.g., Ref. [58]), and they can be neglected on shorter time scales.

Because of genetic drift, every finite population in the absence of mutations eventually reaches an absorbing state (*fixation*) in which all individuals have the same value of the allele we are focusing on. Accordingly, biodiversity, defined as the coexistence of various traits, is lost. When a population presents an internal structure, e.g., it is subdivided in subpopulations, the individuals can move between different subpopulations and this migration acts together with selection and genetic drift, determining local extinction and recolonization of genetic traits and influencing relevant long-time properties of the dynamics, such as the *mean fixation time* (MFT). The fixation time — which by itself is a stochastic variable — is defined as the time it takes to a certain population to reach the absorbing state of the dynamics. It is widely observed that habitat fragmentation and population subdivision play a major role in the process of ecological change and biodiversity loss. Understanding and predicting the effects of migration on the collective behavior of a subdivided population is therefore of primary importance in order to preserve ecosystems and species abundance.

Depending on the specific landscape into which the natural population is embedded, its spatial structure can be conveniently modeled by means of either one-, two-, three-dimensional regular lattices or, more generally, by a network with certain connections. Figure 2.1 schematically depicts two opposite cases of spatial arrangement for a subdivided population with (a) high and (b) small connectivity. Subpopulations are represented by green circles, while the possible migration paths are represented by arrows. If the degree of connec-

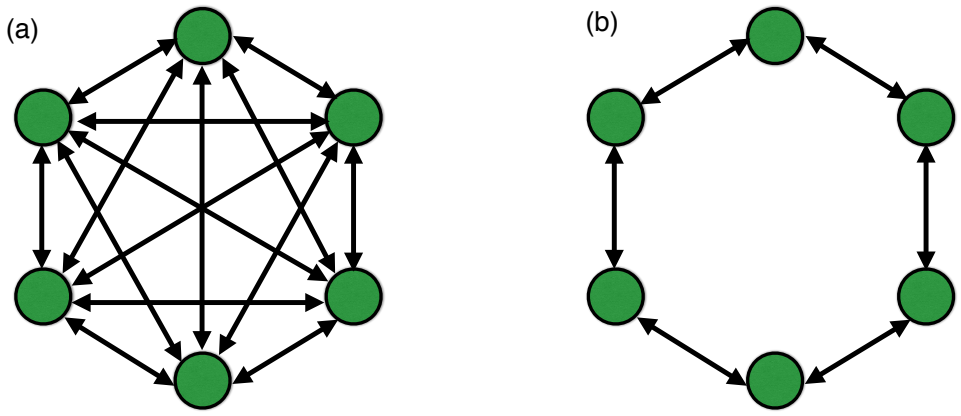

Figure 2.1: Two different spatial arrangements of subdivided populations considered in this chapter: the fully-connected graph (a) represents the network underlying the island model described in Sec. 2.2.2, while the one-dimensional regular lattice with periodic boundary conditions (b) underlies the stepping stone model presented in Sec. 2.6.1. Each node (green circle) of the graph represents a subpopulation (*deme*), while the links (arrows) represent the possible migration paths.

tivity of each node of this network is sufficiently large and the connected subpopulations have constant and equal sizes, the effects of subdivision typically amounts to a rescaling of the relevant parameters of the population, such as the effective population size N_{e} and the effec-

tive strength s_e of selection [59, 60]. However, both N_e and s_e are functions of the rate with which individuals migrate between subpopulations, therefore both the fixation probability and the MFT depend on it. For constant or absent selection, the MFT is known to decrease monotonically upon increasing the migration rate [61, 62, 58, 56]. When evolutionary forces which favor biodiversity are present, instead, as we will show in the present chapter, the MFT can surprisingly display a nonmonotonic dependence on the migration rate [36]. Even in the absence of mutation, this kind of evolutionary forces are common to natural populations. In particular the *balancing selection* [63, 64, 65] introduces a selective advantage for the "weakest" allele, encompassing mechanisms such as over-dominance or heterozygote advantage, which act in several contexts, most notably mammalian [66, 67] and plants [68, 69]. For example, it has been proposed that some genetic diseases in humans, such as sickle-cell anemia [70], cystic fibrosis [71], and thalassemia [72] actually persist as a consequence of balancing selection. Analogous mechanisms are responsible for the emergence of bilingualism in language competition [73] or for cooperative behaviors in ecology and coevolutionary dynamics [74, 75], such as those recently observed in microbial communities [76].

In this chapter, based primarily on Refs. [36, 37], we consider a group of N equally sized subpopulations (i.e., forming a *metapopulation*) which evolve under the effect of balancing selection, while migration takes place between any pair of subpopulations, such as to form a fully connected graph with each subpopulation occupying one of its vertices, as schematically depicted in see Fig. 2.1(a). While balancing selection tends to drive the frequency x_i of each subpopulation towards a certain (common) allele frequency x_*, the random genetic drift introduces fluctuations around it which possibly lead x_i to 0 or 1, corresponding to a uniform subpopulation composition, and to the absorbing states of the dynamics of the corresponding isolated subpopulation (no mutation is considered here). However, migration might cause the introduction of an individual with a different genetic trait compared to the majority of this subpopulation and therefore renders $x_i = 0$ and 1 no longer absorbing states, unless all the subpopulations coherently reach the state 0 or 1 under the effect of fluctuations. The interplay between the time scales which characterize the various processes involved is at the origin of the rich dynamical behavior we explore in the present chapter, both numerically and analytically.

In Sec. 2.2.3 we present the approximate description of the dynamics of the system proposed in Ref. [36], which hinges on the emergence of a separation between the time scale of the local dynamics occurring at each vertex of the network and that of the global dynamics at the level of the whole network. The resulting approximation allows us to obtain an analytic estimate for the MFT of the whole population, and it highlights a nonmonotonicity of the MFT as a function of the migration rate. This nonmonotonicity is related with a similar nonmonotonicity in the biodiversity, already observed in the literature, and it appears to be a quite general feature for subdivided populations with balancing selection, as it is also present in space embedded populations (discussed in Sec. 2.6). The approximation described in Sec. 2.2.3 turns out to be accurate when the effective selection strength is sufficiently small and the number N of subpopulations is sufficiently large. In Sec. 2.3 we show that in the limit $N \to \infty$, a phase transition takes place between species coexistence and biodiversity loss. In order to be able to investigate the fixation properties of the system for larger values

of the selection strength — which are not immediately accessible with the previous approach — we propose in Sec. 2.5.1 an effective description of the metapopulation in terms of a voter model, which is generically accurate for small values of the migration rate. This coarser description applies to a generic metapopulation model, independently of the specific form of the natural selection; in addition, in the presence of balancing selection, the effective voter model can be conveniently generalized by introducing an additional intermediate state in its dynamics, as we discuss in Sec. 2.5.2. This amended model turns out to reproduce accurately the fixation time of the original metapopulation up to larger values of the migration rate compared to the standard voter model. In contrast to the latter, the one with the additional state is actually able to reproduce the distinctive nonmonotonic dependence of the MFT on the migration rate found in Sec. 2.2.3. Moreover, it provides a semi-quantitative explanation of a nonmonotonic behavior observed in the MFT as a function of the selection coefficient s, which appears for small migration rate m in addition to the one discussed above. In Sec. 2.6 we consider a population embedded in one spatial dimension, i.e., arranged along a line with periodic boundary conditions, as schematically depicted in Fig. 2.1(b): we show that also in this case the MFT can develop a nonmonotonic behavior as a function of the migration rate, similarly to the fully-connected case discussed in Sec. 2.2.3.

2.2 The microscopic model

2.2.1 Dynamics of an isolated population

The evolution of finite diallelic (i.e., with $N_{\text{allele}} = 2$) well-mixed populations is conveniently described at the microscopic level by the Wright-Fisher model [77, 78], which consists of a (haploid) population of Ω individuals, each one carrying one of two possible alleles A or B. At each time step of the dynamics the original population is substituted by a new generation obtained by a binomial random sampling determined by the features of the previous one: the allele of each new individual is randomly drawn with a probability which depends on the frequency of occurrence of A (or, equivalently B) in the older generation. The time interval τ_g between two consecutive steps of this dynamics represents the duration of a generation. In a neutral model, i.e., in the absence of selection, each new individual carries allele A (respectively B) with probability $x = \Omega_A/\Omega$ (respectively $1 - x$), where Ω_A is the number of individuals carrying allele A in the previous generation. In order to mimic the effects of natural selection, which favors one of the alleles compared to the other, one introduces different allele fitnesses $w_A = 1+\tilde{s}$ and $w_B = 1$ for alleles A and B, respectively, which affect the probability $p_{\text{r}}(x)$ that a new individual carries allele A after reproduction as

$$p_{\text{r}}(x) = \frac{w_A\Omega_A}{w_A\Omega_A + w_B\Omega_B} = \frac{(1+\tilde{s})x}{1+\tilde{s}x}. \tag{2.1}$$

Alternatively, the dynamics of the same population can be described by the Moran model [79]. At each time step of the dynamics two individuals (not necessarily distinct) are randomly selected in the population. In the absence of selection, an exact copy of the first one is introduced in order to replace the second one, which is therefore removed from the population.

Since individuals are randomly chosen, the probability $d_A = \Omega_A/\Omega = x$ of removing an individual with allele A from the population equals the probability r_A of reproducing one of them. Analogously, for an individual carrying allele B these probabilities are $d_B = r_B = 1-x$. Within the Moran model, a selective advantage can be accounted for by modifying the reproduction probability $r_{A,B}$ of the alleles with the fitnesses w_A and w_B specified above, according to $r_A(x) = (1+\tilde{s})x/(1+\tilde{s}x)$ and $r_B(x) = x/(1+\tilde{s}x)$. With these probabilities, the number of individuals carrying allele A increases/decreases by one at each step of the dynamics with rates W_{+1}/W_{-1}, respectively, given by

$$\begin{aligned} W_{+1}\delta t &= r_A d_B = (1+\tilde{s})x(1-x)/(1+\tilde{s}x), \\ W_{-1}\delta t &= r_B d_A = x(1-x)/(1+\tilde{s}x), \end{aligned} \tag{2.2}$$

where δt is the duration of the time step[1].

Although the Wright-Fisher and Moran models are implemented with different rules at the microscopic level, for a wide range of values of the parameters and sufficiently large populations, they turn out to be effectively described by the same Langevin equation (with Itō prescription, see App. B.1)

$$\dot{x} = \mu(x) + \sqrt{v(x)}\,\eta(t), \tag{2.3}$$

where the evolution of the frequency x of allele A in the population is driven by the sum of a deterministic force $\mu(x) = \tilde{s}x(1-x)$ generated by selection and of a stochastic term — referred to as *genetic drift* in the literature — which is a delta-correlated Gaussian noise with zero mean and variance $v(x) = x(1-x)/(\Omega\tau_g)$. This noise is conveniently expressed as $\sqrt{v(x)}\,\eta(t)$ in terms of the normalized Gaussian noise η with $\langle\eta\rangle = 0$ and $\langle\eta(t)\eta(t')\rangle = \delta(t-t')$. Note that Eq. (2.3) provides an approximate description of the dynamics in terms of an effective diffusion process. While this approximation turns out to be accurate for the Wright-Fisher and Moran models, at least within a certain range of parameters (see Refs. [80, 81, 82]), it is known to fail in other cases, e.g., in the susceptible-infected-susceptible (SIS) model of epidemiology [83].

Note also that, differently from Eq. (1.1) considered in Chap. 1, Eq. (2.3) has two stationary states, i.e., two states (namely the two boundaries 0 and 1 of the range of the allowed values of x) characterized by the vanishing of both the deterministic term $\mu(x)$ and the variance $v(x)$ of the noise. According to the boundary classification introduced in Sec. 1.3, these boundaries are *absorbing* (i.e., if the system reaches one of them, it cannot escape) and *attainable* (i.e., they can be reached in a finite expected time, namely, the MFT described further below in this section), as long as the size Ω of the population is finite. For finite Ω indeed, the absorbing properties of each boundary of the system described by Eq. (2.3) are the same as those of the system described by Eq. (1.1) with noise exponent $y = 1/2$.

[1]The Moran and Wright-Fisher models are different microscopic implementations of a dynamics which is expected to be the same at the mesoscopic level, i.e., for large enough populations ($\Omega \gg 1$) and at least within some range of their parameters. In order to recover the same behavior as the Wright-Fisher model, one has to choose, in the Moran model, a duration $\delta t = 2\tau_g/\Omega$ for the Moran time step and to replace the rates m and s with $2m$ and $2s$ respectively (see App. B.1).

Without loss of generality, time can be measured in units of generations, so that $\tau_g = 1$ and the rates become dimensionless quantities. Balancing selection is characterized by a selective advantage $\tilde{s}$ which favors the evolution towards a state of the population characterized by an optimal frequency x_* of allele A; in the simplest case one can assume a linear dependence

$$\tilde{s} = s(x_* - x), \tag{2.4}$$

with a constant $s > 0$. Note that in an infinitely large population (with $\Omega \to \infty$), the fluctuation effects represented by η in Eq. (2.3) are suppressed, and the resulting deterministic dynamics due to the selection term μ drives the population towards the optimal frequency x_* of allele A. In a finite population, instead, the presence of fluctuations due to the random genetic drift eventually drives x towards one of the two possible absorbing states $x = 0$ and 1, corresponding to the fixation of allele B and A, respectively.

The time required in order to reach fixation with an initial frequency x is a stochastic variable; its mean, i.e., the MFT[2] $T_{\text{fix1}}(x)$ is determined within the diffusion approximation by $v(\bar{x})T''_{\text{fix1}}(x)/2+\mu(x)T'_{\text{fix1}}(x) = -1$ (see Sec. 1.3.2 and Ref. [84]), and it reads (see App. A.2 for a detailed derivation)

$$\frac{T_{\text{fix1}}(x)}{\Omega} = \frac{2\left[S(x,1)F(0,x) - S(0,x)F(x,1)\right]}{S(0,1)}, \tag{2.5}$$

where x is the initial condition, while the functions $S(a,b)$ and $F(a,b)$ are defined by

$$\begin{aligned} S(a,b) &= \int_a^b \mathrm{d}x \exp\left[-s'x(2x_* - x)\right], \\ F(a,b) &= \int_a^b \mathrm{d}z \int_z^1 \mathrm{d}y \frac{\exp\left\{s'\left[y(2x_* - y) - z(2x_* - z)\right]\right\}}{y(1-y)}, \end{aligned} \tag{2.6}$$

where we conveniently introduced the rescaled selection coefficient $s' = \Omega s$([3]).

In the symmetric case $x_* = 1/2$, Eq. (2.5) reduces to

$$\frac{T_{\text{fix1}}(x)}{\Omega} = \int_{(1-2x)^2}^1 \mathrm{d}u \int_0^1 \mathrm{d}z \frac{\mathrm{e}^{s'u(1-z^2)/4}}{1-uz^2}. \tag{2.7}$$

As expected, $T_{\text{fix1}}(x)$ vanishes if the initial condition x corresponds to one of the two absorbing states, $x = 0$ or 1, while it reaches smoothly its maximum value as the initial condition moves towards $x = 1/2$. In the following we focus on the initial condition $x = 1/2$, which, for $x_* \simeq 1/2$ and s large enough, corresponds to a long-lived metastable state promoted by balancing selection.

Note that starting from an initial value x_0, the frequency x does not typically visit the whole interval of possible values $x \in (0,1)$ during its evolution because of the presence of

[2]The label 1 in the subscript of T_{fix1} is meant to distinguish this MFT, associated with a single well-mixed population, from the MFT T_{fix} which will be introduced in Sec. 2.4, associated with the whole subdivided population.

[3]In what follows the prime indicates that the corresponding quantity has been rescaled by the population size Ω.

absorbing states which cause fixation: in fact, the probability $p(x_1|x_0)$ that the population reaches the value x_1 during the evolution which precedes fixation can be evaluated via the procedure described in Sec. 1.3.3 (see also Ref. [85]) and it reads

$$p(x_1|x_0) = \begin{cases} \dfrac{\int_0^{x_0} \mathrm{d}y \exp\left[-s'y(2x_* - y)\right]}{\int_0^{x_1} \mathrm{d}y \exp\left[-s'y(2x_* - y)\right]} & \text{for } x_1 > x_0, \\ \dfrac{\int_{x_0}^{1} \mathrm{d}y \exp\left[-s'y(2x_* - y)\right]}{\int_{x_1}^{1} \mathrm{d}y \exp\left[-s'y(2x_* - y)\right]} & \text{for } x_1 < x_0. \end{cases} \tag{2.8}$$

These expressions turn out to be useful when discussing the voter model approximation in Sec. 2.5.

Based on Eq. (2.8) one can read in particular the *fixation probability* $p(1|x)$, i.e., the probability that allele A fixes in the whole population starting from the initial frequency x. In Fig. 2.2 we report the fixation probability evaluated for a population characterized by $\Omega = 100$, $x_* = 1/2$, and by various values of the selection strength s'; it can be noticed that, as expected, $p(1|x)$ is an increasing function of the initial frequency x. While in the limit of vanishingly small selection strength the fixation probability coincides with the initial frequency ($p(1|x) \simeq x$ for $s' \lesssim 1$), for large selection strength it develops, in the region around $x = 1/2$, a plateau characterized by a probability $p(1|x) \simeq 1/2$; this is due to the fact that the population, for strong balancing selection, and unless it starts very closed to an absorbing state, reaches almost certainly the state $x = x_* = 1/2$, from which it will eventually relax to the $x = 0$ or $x = 1$ absorbing state, with equal probabilities.

2.2.2 Metapopulation models

In the absence of spatial embedding, a celebrated prototypical model of subdivided populations is the so-called island model, originally proposed by Wright [78] for neutral evolution. It consists of N interacting subpopulations (called *demes*) of identical size Ω, labeled by an integer $i = 1, \ldots, N$ and characterized by the frequencies $\{x_1, x_2, \ldots, x_N\}$ for the occurrence of allele A, with $x_i \in [0, 1]$. Within each deme, the internal dynamics (assumed to be the same for all demes in the absence of migration) proceeds as in either Moran's or Wright-Fisher's stochastic models, while different demes interact by exchanging randomly picked individuals, such that the sizes Ω of the demes involved in the exchange are not affected. As schematically depicted in Fig. 2.1(a), migration occurs between any possible pair (i, j) of demes, and its rate m is defined as $m = n_{i \leftrightarrow j} N/\Omega$, where $n_{i \leftrightarrow j}$ is the mean number of individuals exchanged between the demes i and j in one generation.

Within the Wright-Fisher model the effect of migration is typically accounted for by modifying the probability with which a new generation is sampled. In particular, due to migration, the probability $p_r(x_i, \bar{x})$ that a new individual in deme i carries allele A acquires a dependence on the mean frequency

$$\bar{x} = \sum_{i=1}^{N} x_i / N \tag{2.9}$$

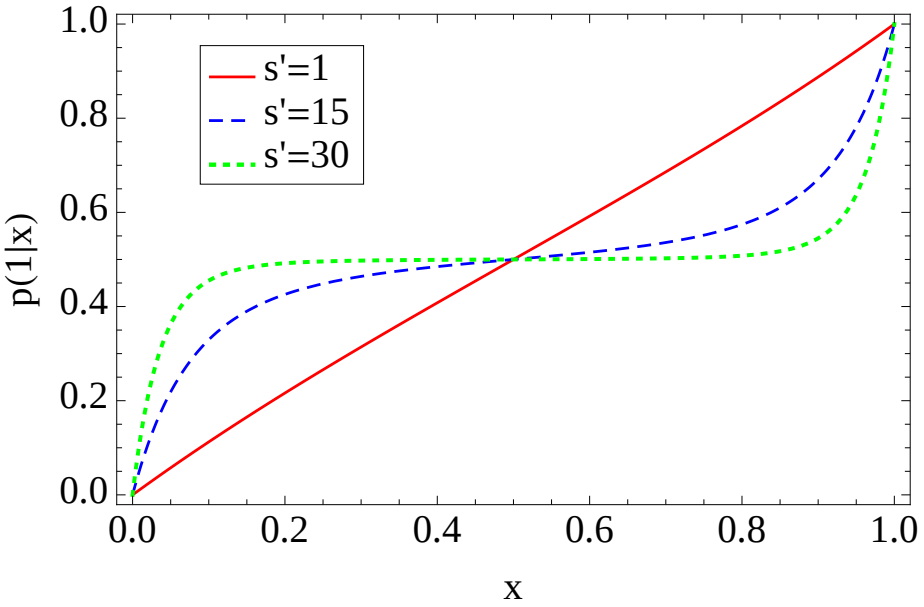

Figure 2.2: Fixation probability $p(1|x)$ as a function of the initial frequency x for a well-mixed population with $\Omega = 100$ individuals the evolution of which is characterized by balancing selection with optimal frequency $x_* = 1/2$ and by various values of the selection strength s'.

(hereafter the bar over a quantity refers to its inter-deme average), and it has the form (see App. B.2.1)

$$p_{\rm r}(x_i, \bar{x}) = \frac{(1+\tilde{s}_i)[m\bar{x} + (1-m)x_i]}{1 + \tilde{s}_i[m\bar{x} + (1-m)x_i]}, \tag{2.10}$$

where $\tilde{s}_i = \tilde{s}(x = m\bar{x} + (1-m)x_i)$ is the value of the function $\tilde{s}(x)$, defined in Eq. (2.4), evaluated at the point $x = m\bar{x} + (1-m)x_i$.

In the Moran model, the migration process affects the rate of increase/decrease of the fraction x_i of A-type individuals in the i-th deme. For $\Omega \gg 1$ the evolution turns out to be described by the rates (see App. B.2.2)

$$\begin{aligned} W_{+1} &= (1+\tilde{s})x_i(1-x_i)/(1+\tilde{s}x_i) + m\bar{x}(1-x_i), \\ W_{-1} &= x_i(1-x_i)/(1+\tilde{s}x_i) + m(1-\bar{x})x_i. \end{aligned} \tag{2.11}$$

Migration is expected to affect the level of biodiversity (i.e., the level of coexistence of the various alleles) of a population. In diallelic models, this effect is usually studied in terms of (i) the *global heterozygosity*

$$H = 2\bar{x}(1-\bar{x}), \tag{2.12}$$

which quantifies the diversification of the global population but neglects the possible subdivision in demes, and of (ii) the *intra-deme heterozygosity*

$$h = (2/N)\sum_{i=1}^{N} x_i(1-x_i) = 2\overline{x(1-x)}, \tag{2.13}$$

which measures the average level of diversification inside each deme. Note that $0 \leq h \leq H \leq 1/2$. $H = 0$ corresponds to the loss of global biodiversity, namely all individuals within the population have the same genotype; $H = 1/2$, instead, corresponds to the maximal possible global biodiversity in which the two genotypes are equally present within the whole population. Analogous interpretation holds for $h = 0$ and $h = 1/2$ at the intra-deme level. Fig. 2.3 shows the time evolution of the allele frequencies $x_i(t)$ in the various demes of a

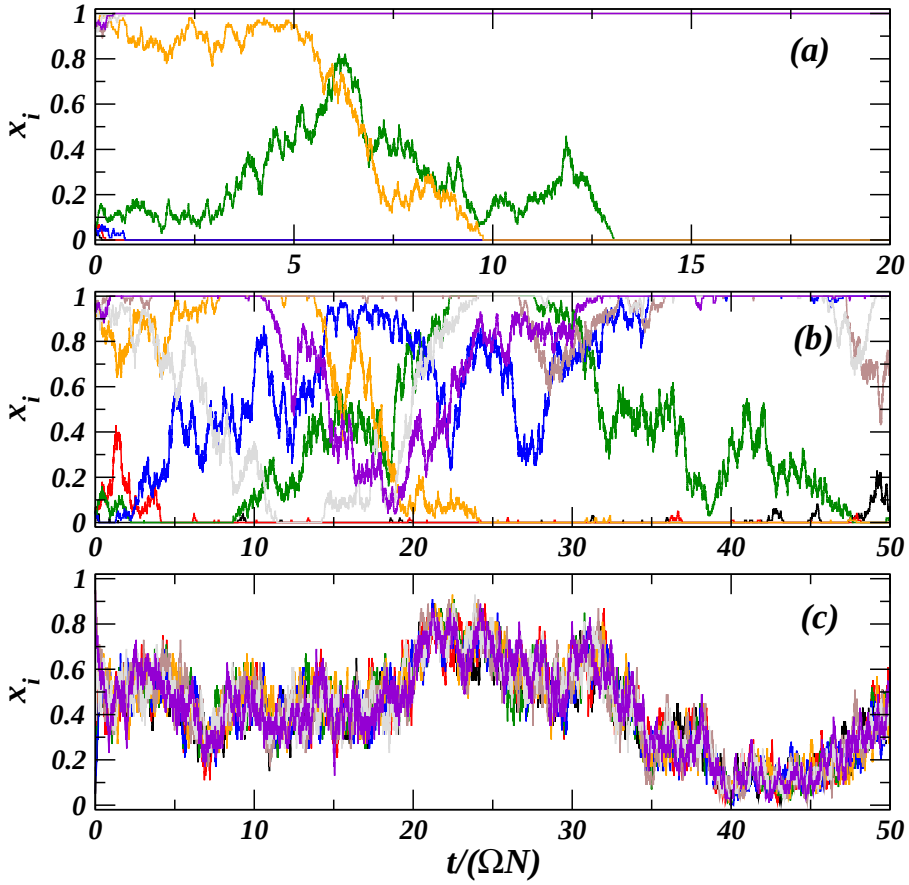

Figure 2.3: Time evolution of the frequency x_i of allele A in the various demes (represented by different colors) of a fully-connected population consisting of $N = 8$ demes with $\Omega = 100$ individuals each (a) in the absence of migration ($m = 0$) or (b) for small ($m' = 0.05$) and (c) large ($m' = 50$) migration rate. The balancing selection is characterized here by $x_* = 0.5$ and $s' = 5$. At time $t = 0$, half of the demes have $x_i = 0.05$, while the remaining ones $x_i = 0.95$. Upon increasing N, the fluctuations of $\bar{x}$ around x_* reduce significantly in panel (c).

population with $x_i(t = 0)$ either equal to 0.05 or 0.95, (a) in the absence of migration ($m' = 0$) or for (b) small ($m' = 0.05$) and (c) large ($m' = 50$) migration rate. The balancing selction is characterized here by $x_* = 0.5$ and $s' = 5$. It can be noticed that for large m' (panel (c)) the local allele frequencies $\{x_i\}$ approach each other for $\Omega m \gg 1$, with $x_i \simeq x_j$ and therefore $h \simeq H$. In the case of moderate migration rate $\Omega m \lesssim 1$ of panel (b), instead, different demes

fix different alleles, causing $h \simeq 0$, while H is maintained positive by migration which acts as a constant source of biodiversity.

2.2.3 Time scale separation

For $\Omega \gg 1$ and $m, s \ll 1$, the evolution of the allele frequency $x_i \in [0,1]$ in the i-th deme can be described, both within the Moran and Wright-Fisher models, by the following Langevin equation with Itō prescription (see App. B.1)

$$\dot{x}_i = \mu(x_i) + m(\bar{x} - x_i) + \sqrt{v(x_i)}\ \eta_i, \tag{2.14}$$

where η_i are the independent Gaussian noises which characterize each single deme, with $\langle \eta_i(t)\eta_j(t')\rangle = \delta_{i,j}\delta(t-t')$, while the term $m(\bar{x} - x_i)$ [see Eq. (2.9) for the definition of $\bar{x}$] accounts for the migration of individuals between the demes. In fact, the effect of an exchange between the i-th and a j-th deme ($j \neq i$) is to increase the fraction x_i of allele A by the amount $m(x_j - x_i)$ per unit time, which leads to the previous expression upon summing the contributions coming from the exchanges with all possible demes. In turn, this term contributes in an approximately additive way to the variation of the single-deme frequency x_i, the dynamics of which is otherwise described by Eq. (2.3).

The mean fixation time $T_{\text{fix}}(m)$ of the population as a whole depends on the initial state x_i of each single deme but, as we argue below and in Sec. 2.5, the mean frequency $\bar{x}$ provides an effective description of the state of the system at any time. For simplicity, in the following we focus primarily on an initial state with $\bar{x} = 1/2$: for $x_* \simeq 1/2$ and migration rate m large enough, it actually corresponds to a metastable state onto which the population quickly relaxes from its initial state (see Sec. 2.3). $T_{\text{fix}}(m)$ differs from the one of a single deme T_{fix1} also in the absence of migration, i.e., for $m = 0$, when each deme evolves independently of the others. In this case, the average time $T_{\text{fix}}(m=0)$ required by the overall population to reach one of the two absorbing states is given by the average time necessary for all demes to reach it, after which no evolution occurs within the metapopulation. This is given by the maximum of the single-deme fixation times calculated over N demes, and it turns out to be $T_{\text{fix}}(m=0) \simeq T_{\text{fix1}} \log N$ (see App. B.6).

In the presence of migration, instead, each deme exchanges individuals with the others, a process that effectively acts as a source of biodiversity inside each deme, preventing them from achieving independent fixation. In fact, the single-deme states $x_i = 0$ and 1 are no longer *per se* absorbing for $m \neq 0$ and global fixation requires a coordinate evolution towards the two global absorbing states $X_0 \equiv \{x_i = 0\}_{i=1,\dots,N}$ or $X_1 \equiv \{x_i = 1\}_{i=1,\dots,N}$ in which all demes fix the same allele. In this case, the dynamics of the population can be conveniently described via the evolution equation for the mean frequency $\bar{x}$, which can be obtained from Eq. (2.14) by considering the infinitesimal increment of $\bar{x}$

$$\mathrm{d}\bar{x} = \sum_{i=1}^{N} \frac{\partial \bar{x}}{\partial x_i}\mathrm{d}x_i = \frac{s}{N}\sum_{i=1}^{N} x_i(1-x_i)(x_* - x_i)\mathrm{d}t + \frac{1}{N}\sum_{i=1}^{N}\sqrt{\frac{x_i(1-x_i)}{\Omega}}\mathrm{d}w_i, \tag{2.15}$$

where $\mathrm{d}w_i$ indicate the increments of the independent Wiener processes driving the dynamics of each single deme. Since the individual stochastic increments $[x_i(1-x_i)/\Omega]^{1/2}\mathrm{d}w_i/N$ are

independent and Gaussian random variables with variance $x_i(1-x_i)/(\Omega N^2)\mathrm{d}t$, their sum is a Gaussian random variable with variance $\sum_{i=1}^{N} x_i(1-x_i)\mathrm{d}t/(\Omega N^2) = (\overline{x} - \overline{x^2})/(\Omega N)\mathrm{d}t$, where the overbar indicates the mean over the demes. Accordingly, we obtain

$$\dot{\overline{x}} = s[x_*\overline{x} - (1+x_*)\overline{x^2} + \overline{x^3}] + \sqrt{\frac{\overline{x} - \overline{x^2}}{\Omega N}}\,\eta, \tag{2.16}$$

where η is a Gaussian noise with $\langle \eta(t)\eta(t')\rangle = \delta(t-t')$ and $\overline{x^k} = \sum_{i=1}^{N} x_i^k/N$. Due to the nonlinear nature of Eq. (2.14), the evolution equation for $\bar{x}$ involves higher-order moments $\overline{x^2}$ and $\overline{x^3}$ which in principle could be determined by solving a whole hierarchy of coupled differential equations. For a large number of demes N and small selection strength s however, as we argue below, a time scale separation emerges between the local dynamics and the global one, which allows one to express these higher-order moments in terms of $\bar{x}$.

Indeed, since the global variable $\bar{x}$ is the average of N local frequencies, it is heuristically expected to have a dynamics much slower than that of the individual frequencies $\{x_i\}$. Being coupled only via the slowly varying quantity $\bar{x}$, $\{x_i\}$ can be considered as almost independent random variables, each one described by a conditional quasi-stationary distribution $P_{\mathrm{qs}}(x_i|\bar{x})$. The latter can be obtained by solving the stationary Fokker-Planck equation associated with Eq. (2.14), in which $\bar{x}$ is treated as a constant parameter. Under these assumptions the population average $\overline{x^k}(t)$ can be approximated, for $N \gg 1$, by the corresponding mean $\int \mathrm{d}x_i\, x_i^k\, P_{\mathrm{qs}}(x_i|\bar{x})$, leading to the effective Langevin equation

$$\dot{\bar{x}} = M(\bar{x}) + \sqrt{V(\bar{x})}\,\eta(t), \tag{2.17}$$

where the deterministic term and the variance of the noise are respectively given by

$$M(\bar{x}) = s\int_0^1 \mathrm{d}x\, x(1-x)(x_*-x)P_{\mathrm{qs}}(x|\bar{x}) \tag{2.18a}$$

and

$$V(\bar{x}) = (\Omega N)^{-1}\int_0^1 \mathrm{d}x\, x(1-x)P_{\mathrm{qs}}(x|\bar{x}). \tag{2.18b}$$

Small selection limit

For $s = 0$ one obtains the Beta distribution [62, 58]

$$P_{\mathrm{qs}}^{(0)}(x_i|\bar{x}) = \frac{x_i^{2m'\bar{x}-1}(1-x_i)^{2m'(1-\bar{x})-1}}{B(2m'\bar{x}, 2m'(1-\bar{x}))}, \tag{2.19}$$

where $B(u,v)$ in the normalization is the Beta function, which can be expressed in terms of Euler's gamma function $\Gamma(u)$ as $B(u,v) = \Gamma(u)\Gamma(v)/\Gamma(u+v)$. This distribution $P_{\mathrm{qs}}^{(0)}(x|\bar{x})$ satisfies the consistency condition $\bar{x} = \int_0^1 \mathrm{d}x\, x\, P_{\mathrm{qs}}^{(0)}(x|\bar{x})$ and it can then be used for evaluating

$\overline{x^2}$ and $\overline{x^3}$ in Eq. (2.16) and for calculating the mean drift $M(\bar{x})$ and variance $V(\bar{x})$ in Eq. (2.18a) and in Eq. (2.18b) respectively (see Refs. [62, 58]):

$$M^{(0)}(\bar{x}) = s_{\rm e}\bar{x}(1-\bar{x})(x_*^{\rm e}-\bar{x}), \tag{2.20a}$$

$$V^{(0)}(\bar{x}) = \bar{x}(1-\bar{x})/N_{\rm e}, \tag{2.20b}$$

This implies that at the lowest, nonvanishing order in s, in agreement with the results of Refs. [59, 60, 62, 58], the subdivided population behaves like a well-mixed one with an *effective selection coefficient* $s_{\rm e}$, an *effective population size* $N_{\rm e}$, and an *effective optimal frequency* $x_*^{\rm e}$ respectively given by [62, 58]

$$s_{\rm e} = s/\left[\left(1+\frac{1}{m'}\right)\left(1+\frac{1}{2m'}\right)\right], \tag{2.21a}$$

$$N_{\rm e} = N\Omega\left(1+\frac{1}{2m'}\right), \tag{2.21b}$$

$$x_*^{\rm e} = x_* + (x_*-1/2)/m'. \tag{2.21c}$$

It is worth noting that as the migration rate m' increases, the effective parameters $s_{\rm e}$ and $x_{\rm e}^*$ approach the values they have for the isolated demes, while the effective size $N_{\rm e}$ tends to the total number $N\Omega$ of individuals in the metapopulation; accordingly, in the limit $m' \to \infty$, the internal structure of the metapopulation does not affect its dynamics and subdivision plays no actual role.

For later convenience, let us point out that the time scale $T_{\rm migr}$ associated with the local response of x_i to a variation of $\bar{x}$ can be read from Eq. (2.14) and it is $T_{\rm migr} \simeq 1/m$. The typical time scale of the global dynamics of $\bar{x}$ is determined, instead, either by the time scale $T_{\rm rel} \simeq 1/s_{\rm e}$ of the drift (see Eq. (2.20a)) or by the time scale $T_{\rm fluct} \simeq N_{\rm e}$ of the stochastic term (see Eq. (2.20b)). When $T_{\rm rel} < T_{\rm fluct}$, i.e., $N\Omega s > 1 + 1/m'$, our approximation requires $T_{\rm rel} \gg T_{\rm migr}$, i.e., $s_{\rm e} \ll m$, while in the opposite case, it is accurate whenever $N \gg 1$ (see App. B.5 for a detailed discussion).

Higher order corrections in $\alpha = s_{\rm e}/m$

The approximation in Eqs. (2.20a) and (2.20b) can be generalized to small but nonvanishing values of $\alpha = s_{\rm e}/m$ by accounting (a) for $s \neq 0$ in the quasi-stationary distribution $P_{\rm qs}$ and (b) for the fact that $\bar{x}$ slowly changes during the fast evolution of x_i, which results in a distribution $P_{\rm qs}(x_i|y(t))$ where the *effective field* $y(t) \simeq \bar{x}(t)$ has to be determined self-consistently in order to obtain a distribution consistent with the first order average $\bar{x}$ (i.e., such that $\langle x\rangle_{P_{\rm qs}} = \bar{x}$). The single-deme quasi-stationary distribution for $s' \equiv \Omega s \neq 0$ is

$$P_{\rm qs}(x|y) \propto x^{2m'y-1}(1-x)^{2m'(1-y)-1}{\rm e}^{s'x(2x_*-x)}. \tag{2.22}$$

Note that in the presence of selection an additional factor ${\rm e}^{s'x_i(2x_*-x_i)}$ appears on the r.h.s. of Eq. (2.22) compared to Eq. (2.19)and the associated normalization constant changes accordingly. For $x_* = 1/2$, the $O(\alpha)$ correction to the quasi-stationary distribution $P_{\rm qs}^{(0)}$ in

Eq. (2.19) reads

$$P_{\rm qs}^{(1)}(x|y) = \frac{x^{2m'y-1}(1-x)^{2m'(1-y)-1}}{B(2m'y, 2m'(1-y))}\left\{1+\alpha(m'+1)\left[\frac{2m'+1}{2m'}x(1-x)-y(1-y)\right]\right\}+O(\alpha^2), \tag{2.23}$$

while the consistency condition

$$\bar{x} = \int_0^1 {\rm d}x\, x\, P_{\rm qs}(x|y) \tag{2.24}$$

can in principle be solved numerically. However, in order to obtain analytical approximations for the effective drift and variance in Eqs. (2.18a) and (2.18b), we proceed to an expansion in the small parameter α, which gives $y = \bar{x} - \alpha\bar{x}(1-\bar{x})(x_*^{\rm e} - \bar{x}) + O(\alpha^2)$. This value can be substituted into Eq. (2.23), which, in turns, allows one to approximate the effective drift and variance in Eqs. (2.18a) and (2.18b). Neglecting terms of order $O(\alpha^2)$, the latters become

$$M^{(1)}(\bar{x}) = s_e\bar{x}(1-\bar{x})\left(\frac{1}{2}-\bar{x}\right)\Big\{1+\alpha[A+B\bar{x}(1-\bar{x})]\Big\} \tag{2.25}$$

and

$$V^{(1)}(\bar{x}) = \frac{\bar{x}(1-\bar{x})\left\{1+\alpha[C+D\bar{x}(1-\bar{x})]\right\}}{N_e}, \tag{2.26}$$

with coefficients

$$A = \frac{1-7m'-6m'^2}{4m'(m'+1)(2m'+3)}, \quad B = \frac{3(4+3m')}{(m'+2)(2m'+3)}, \quad C = \frac{1-2m'}{4m'(2m'+3)}, \quad D = \frac{3}{2m'+3}. \tag{2.27}$$

Note that, in order to extend this analysis to larger values of the parameter α, one could either carry on with the perturbative expansion, or rely on the numerical solution of Eqs. (2.24), (2.18a), and (2.18b).

In Fig. 2.5 we report the corresponding functions $M^{(1)}(\overline{x})/s_{\rm e}$ (panel (a)) and $N_{\rm e}V^{(1)}(\overline{x})$ (panel (b)) as functions of $\bar{x}$ for $m' = 1$ and various values of α. By comparing with the case $\alpha = 0$ (solid line) one clearly sees that the first-order correction in α does not introduce new qualitative features in M and V but is merely responsible for some quantitative changes.

2.3 Phase transition in the infinite island model ($N = \infty$)

In this section we show that balancing selection slows down fixation only if the optimal frequency x_* is sufficiently close to the symmetric value 1/2, while it facilitates fixation in the opposite case. In addition, in the limit $N \to \infty$ this results into a phase transition between species coexistence and biodiversity loss.

If balancing selection is not symmetric, i.e., $x_* \neq 1/2$, the effective drift $M^{(0)}(\bar{x})$ in Eq. (2.20a) can be written as the sum of a symmetric term

$$M_{\rm symm}^{(0)}(\bar{x}) = s_{\rm e}\bar{x}(1-\bar{x})(1/2-\bar{x}) \tag{2.28}$$

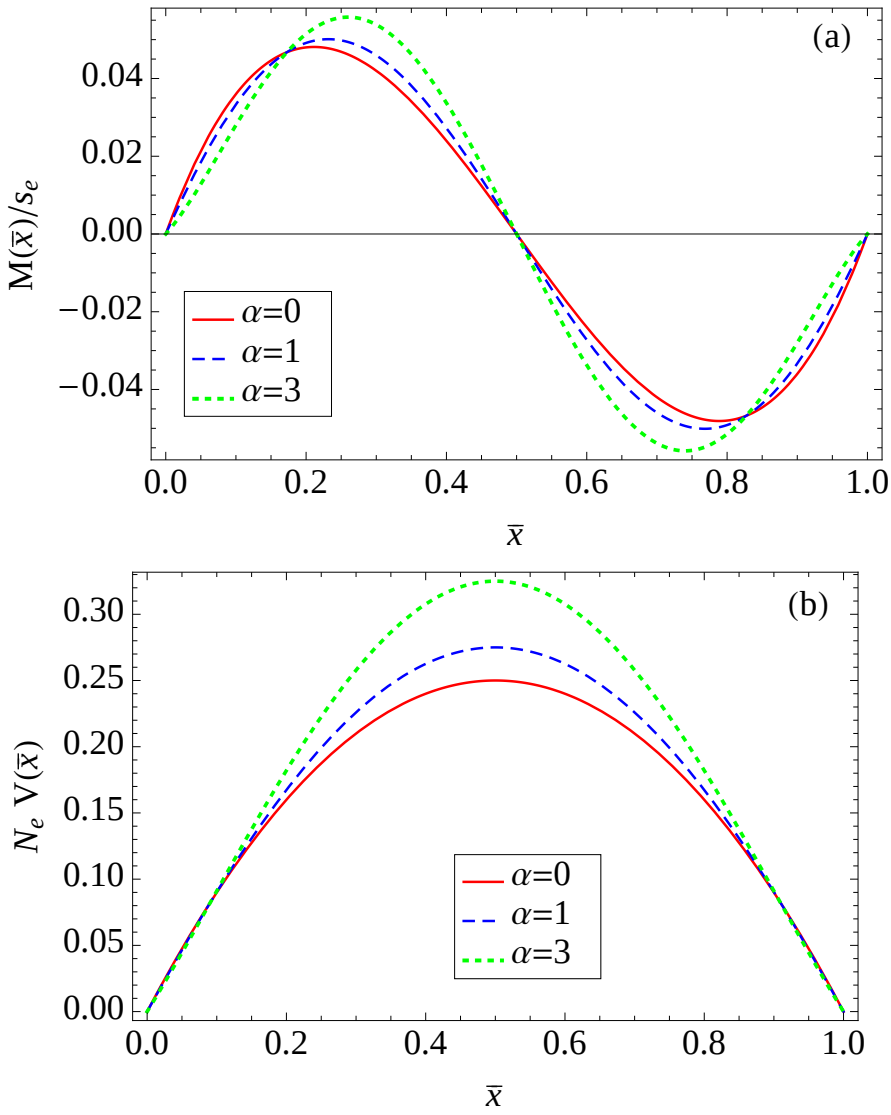

Figure 2.4: (a) Mean variation $M^{(1)}(\overline{x})$ and (b) variance $V^{(1)}(\overline{x})$, reported in Eq. (2.25) and in Eq. (2.26) respectively, as functions of $\bar{x}$, for $m' = 1$ and for various values of α.

and a directional selection term[4]

$$M^{(0)}_{\rm dir}(\bar{x}) = \sigma_{\rm e}\bar{x}(1-\bar{x}), \tag{2.29}$$

where

$$\sigma_{\rm e} = s_{\rm e}(x^{\rm e}_* - 1/2) \tag{2.30}$$

is an *effective directional selection coefficient*. $M^{(0)}_{\rm symm}$ promotes coexistence of the two alleles and therefore it increases the biodiversity of the system, slowing down fixation; $M^{(0)}_{\rm dir}$, instead,

[4]The term in Eq. (2.29) is often referred to as *selection term* in the literature, since it corresponds to the simplest possible form of selection, characterized by having a constant $\tilde{s}$ in Eqs. (2.1) and (2.2).

favors fixation of one of the alleles (depending on the sign of σ_e). The competition between these two terms determines whether balancing selection actually slows down or speeds up fixation of the population as a whole. One can therefore expect that, depending on the ratio $|\sigma_e/s_e|$ being larger than some threshold θ, $M^{(0)}_{\rm dir}$ prevails over $M^{(0)}_{\rm symm}$, so that balancing selection eventually accelerates fixation. According to Eqs. (2.30) and (2.21c), this occurs for

$$|x_* - 1/2| > \frac{m'\theta}{m'+1}, \tag{2.31}$$

which provides a heuristic estimate of the region of the parameter space within which balancing selection should facilitate fixation. The fact that balancing selection slows down fixation only if the optimal frequency x_* is far enough from the absorbing boundaries (i.e., if it is close enough to $x_* = 1/2$) was first noticed in Ref. [64] for the case of balancing selection in well-mixed populations, by analyzing the eigenvalues of the transition matrix of the Moran-like dynamics. In the following, we argue that this change of behavior becomes an actual phase transition in the limit $N \to \infty$ of subdivided populations.

In the limit of an infinite number of demes, Eq. (2.17) becomes deterministic because the variance $V(\bar{x})$ of the noise vanishes; this is not the case for the noise in the single-deme equation (2.14), which does not vanish as long as Ω is finite and therefore determines a nontrivial quasi-stationary distribution $P_{\rm qs}(x|y(\bar{x}))$ which, in turn, affects Eq. (2.17). Depending on the values of the parameters s', m', and x_*, the internal stochasticity of the demes might be sufficiently strong to drive the metapopulation to fixation even in the infinite-size limit $N \to \infty$. In fact, the deterministic part of Eq. (2.17) might drive $\bar{x}$ towards one of the two absorbing states X_0 and X_1 corresponding to $\bar{x} = 0$ and $\bar{x} = 1$, respectively. In addition to these latter solutions, Eq. (2.17) admits also a stationary state with $\bar{x} = x_\infty$, which can be determined by requiring that $M(x_\infty)$ vanishes, i.e., by solving the corresponding condition [see Eq. (2.18a)]

$$\int_0^1 {\rm d}x\, x(1-x)(x_* - x)P_{\rm qs}(x|y) = 0, \tag{2.32}$$

where $y = y(x_\infty)$ is defined by the consistency condition in Eq. (2.24). Figure 2.5 shows the numerical determination of $M(\bar{x})$ as a function of $\bar{x}$ for various values of x_* in a population characterized by the parameters reported in the caption. The nontrivial zero x_∞ of M corresponds to an attracting stable state for the deterministic part of Eq. (2.17), which is asymptotically reached for $t \to \infty$ unless the initial conditions are exactly on a boundary. The stability of the point x_∞ follows from the fact that $M'(x_\infty) < 0$. When $x_\infty \in (0, 1)$, it represents a stable "active" state for the infinite population and it corresponds to the infinite-size limit ($N \to \infty$) of the metastable state in which a finite system ($N < \infty$) would spend a long time before fixating [36]. However x_∞ might coincide with one of the two boundaries 0 and 1, depending on the values of the parameters x_*, m', and s', and correspondingly $M(\bar{x})$ has the same sign within the whole interval $(0, 1)$: when this happens, the deterministic part of the dynamics drives the system towards fixation. Note that this fixation process is deterministic in nature and the system always reaches (asymptotically in time) the absorbing state determined by x_∞, differently from the case with finite N in which fixation is a stochastic process and both boundaries are attainable.

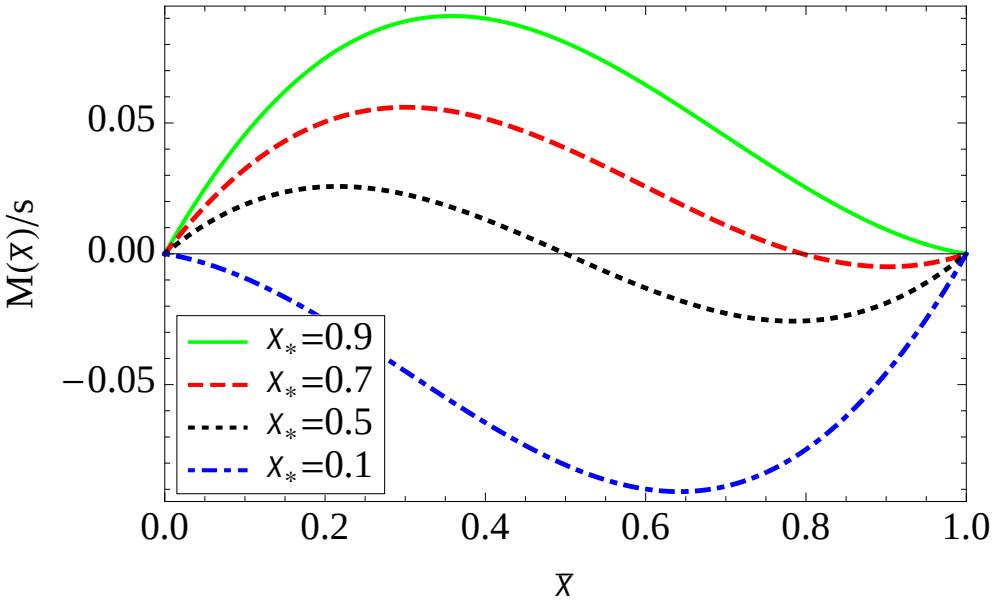

Figure 2.5: Drift $M(\bar{x})$ as a function of $\bar{x}$, as obtained from the numerical solution of Eq. (2.32) for $m' = 2$, $s' = 1$, and for various values of x_*. It can be noticed that, depending on the value of x_*, a nontrivial zero x_∞ of $M(\bar{x})$ emerges, which is always an attractive state for the deterministic evolution of $\bar{x}$.

When computing the stationary value x_∞ as a function of the optimal frequency x_* for fixed s' and m', there exists a critical value $x_*^{\rm c}(s', m')$, such that for $x_* \in (x_*^{\rm c}, 1 - x_*^{\rm c})$ the infinite population is in the active phase, i.e., $x_\infty \in (0, 1)$, while it otherwise reaches one of the two absorbing states $x_\infty = 0$ or 1. Figure 2.6 shows the dependence of the critical value x_*^c on the migration rate m' for several values of selection strength s'. Analytic estimates for the stationary value x_∞ and for the critical value $x_*^{\rm c}$ can be easily obtained for small α, in which case the condition (2.32) reduces to $M^{(0)}(\bar{x}) = 0$. Using Eq. (2.20a) one gets

$$x_\infty^{(0)} = \begin{cases} x_*^{\rm e} & \text{if } x_*^{\rm e} \in [0, 1], \\ 0 & \text{if } x_*^{\rm e} < 0, \\ 1 & \text{if } x_*^{\rm e} > 1, \end{cases} \tag{2.33}$$

where $x_*^{\rm e}$ is given in Eq. (2.21c), while

$$x_*^{\rm c(0)} = \frac{1}{2(m'+1)}. \tag{2.34}$$

Here the superscript (0) denotes that the corresponding quantity has been calculated on the basis of the zeroth-order approximation $M^{(0)}(\bar{x})$ for $M(\bar{x})$ in Eq. (2.17). This expression agrees with the heuristic estimate of Eq. (2.31) if one sets the numerical threshold θ to $\theta = 1/2$. The analytic determination of $x_*^{\rm c(0)}$ in Eq. (2.34) is reported in Fig. 2.6 as a solid line and it coincides, as expected, with the estimate based on the numerical solution of

Eq. (2.32) for small s' (uppermost dashed line). Within the same approximation, the mean frequency $\bar{x}$ evolves according to $\partial_t \bar{x}(t) = M^{(0)}(\bar{x}(t))$; in the active phase, $\bar{x}$ approaches the effective optimal frequency $x_*^{\rm e}$ exponentially fast in time, i.e., $\bar{x}(t) - x_*^{\rm e} \propto \exp[-s_{\rm e} x_*^{\rm e}(1-x_*^{\rm e})t]$. In the absorbing phase, instead, an equally rapid evolution drives the system to fixation: for example $\bar{x}(t) \propto \exp[-s_{\rm e}|x_*^{\rm e}|t]$ if the deterministic evolution drives the system towards $\bar{x} = 0$ (i.e., for $x_*^{\rm e} < 0$), with an analogous expression holding when the evolution is towards $\bar{x} = 1$.

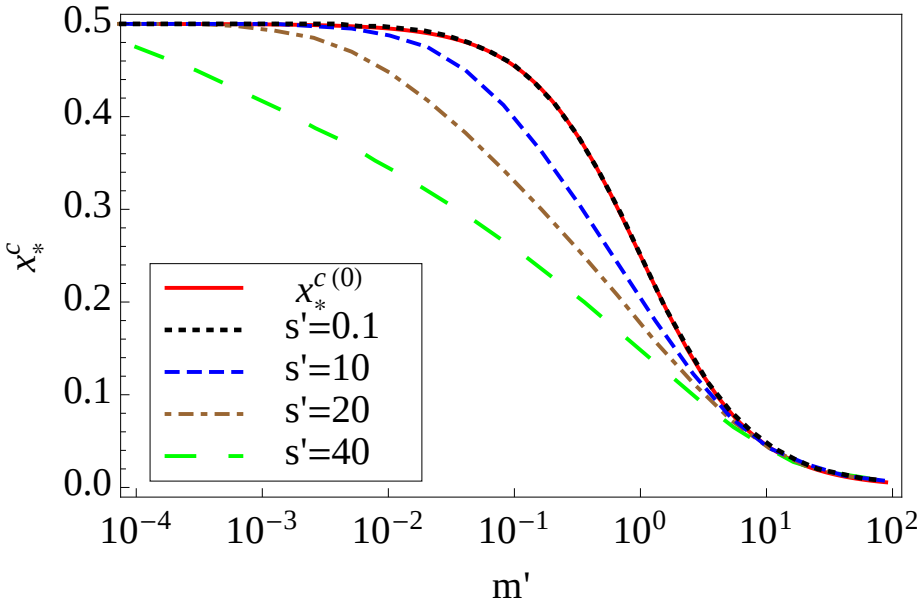

Figure 2.6: Critical value $x_*^{\rm c}$ as a function of m' for several values of s'. For $x_* < x_*^{\rm c}$ or $x_* > 1 - x_*^{\rm c}$ the system is driven deterministically to fixation for $N \to \infty$. The sold line is the estimate in Eq. (2.34), valid for small s, while the dashed lines correspond to the numerical solution of Eq. (2.32) for larger values of s'.

The global heterozygosity $H = 2\bar{x}(1-\bar{x})$ provides an index of the biodiversity of the population, as it vanishes in the absorbing states X_0 and X_1, while it does not in the active phase. In this respect it can be considered as an order parameter for the "phase transition" occurring at $x_* = x_*^{\rm c}$ and $x_* = 1 - x_*^{\rm c}$. Figure 2.7 reports H as a function of x_*, as obtained from the numerical solution of Eq. (2.32) for $s' = 1$ and for two values of m'.

The picture presented above approximately carries over to the case in which the number of demes N is not infinite but anyhow large. In this case one can heuristically assume that, in the absorbing phase $x_* < x_*^c$ or $x_* > 1 - x_*^c$, fixation to a boundary ($\bar{x} = 0$ or 1) is effectively reached when the distance of $\bar{x}$ to that boundary is smaller than $1/(\Omega N)$ (corresponding to having in the metapopulation only one individual different from the others) and therefore we expect the MFT to scale as $T_{\rm fix} \propto \log(\Omega N)$ because of the exponential law with which $\bar{x}(t)$ approaches the boundary as a function of time. Figure 2.8 reports the MFT as a function of N for various values of the optimal frequency x_*. It can be noticed that, as expected from the arguments presented above, $T_{\rm fix}/N$ increases upon increasing N in the active phase

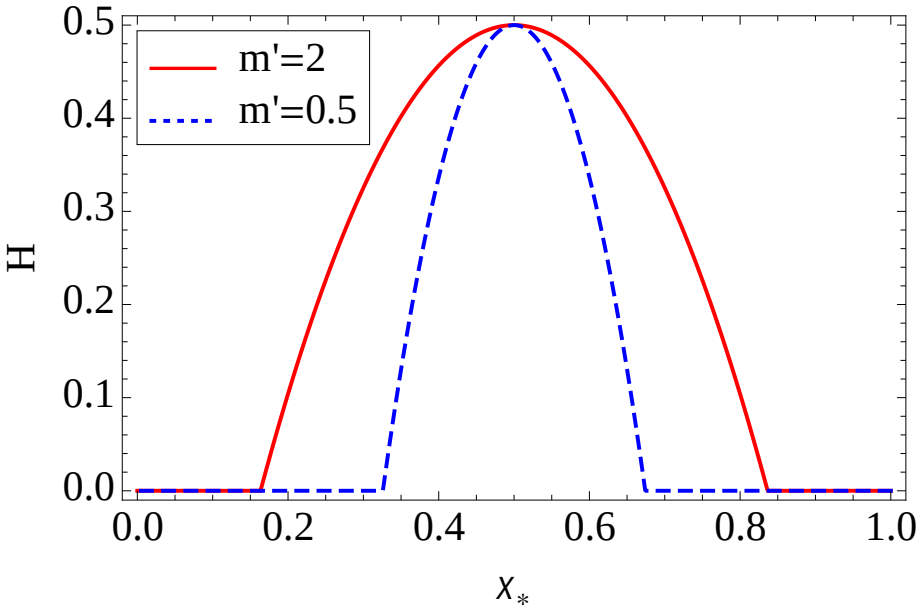

Figure 2.7: Global heterozygosity H in the stationary state $\bar{x} = x_\infty$ for $N \to \infty$, as a function of the optimal frequency x_* for $s' = 1$ and two values of m'. H reported here has been obtained by the numerical solution of Eq. (2.32).

(red squares), while it decreases in the absorbing phase (blue circles), and this supports the fact that a bona-fide phase transition should be present in the limit $N \to \infty$. A numerical interpolation reveals indeed an exponential dependence of $T_{\rm fix}/N$ (red solid line) as a function of N in the active phase while a logarithmic one (blue dashed line) of $T_{\rm fix}$ in the absorbing phase, in agreement with what anticipated above.

For finite but large N, when the corresponding system with $N = \infty$ is in the active phase, x_∞ effectively becomes a *metastable* state (with a lifetime of the order of $T_{\rm fix}$), in which the mean frequency $\bar{x}$ fluctuates around the value x_∞ before a random fluctuation eventually drives the system to fixation. As it can be seen in Fig. 2.9, in the metastable state the single-deme frequencies x_i (solid lines) can be quite different from the metastable frequency x_∞, but the fluctuations of their mean $\bar{x}$ around the value x_∞ are vanishingly small upon increasing N from panel (a) to panel (c).

2.4 Fixation for finite N

As anticipated in Sec. 2.2.1, every finite population will eventually reach fixation. In this section we estimate the MFT for the island model with balancing selection, described in Sec. 2.2.3, on the basis of the approximate description which relies on the time scale separation between the local and the global dynamics and which we presented in the same section.

The MFT $T_{\rm fix}(\overline{x})$ for the whole population with an initial mean frequency $\bar{x}$ is determined

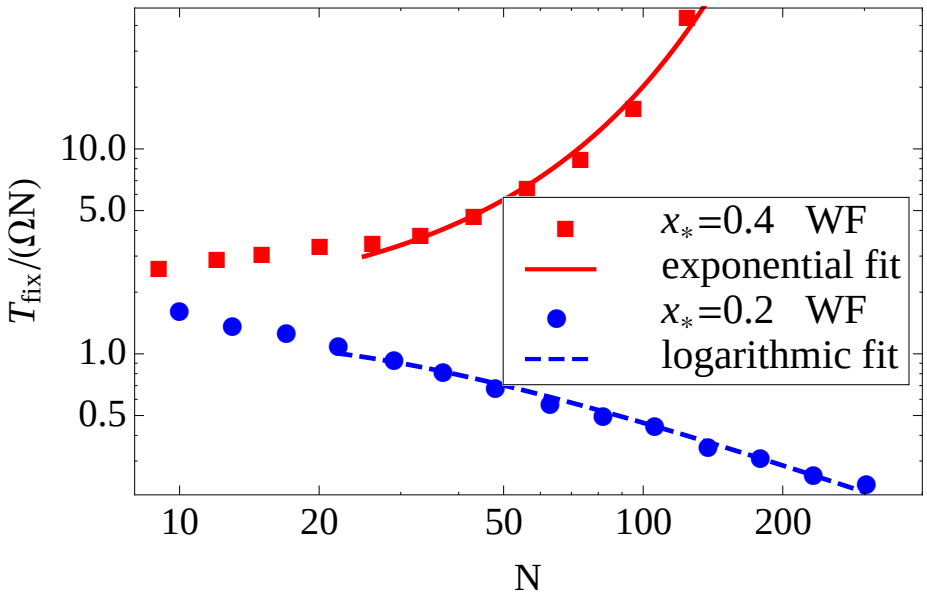

Figure 2.8: Dependence of the MFT $T_{\rm fix}$ on the size N of the metapopulation, for $\Omega = 100$, $s' = 1$ and $m' = 1$. The MFT has been determined via numerical simulations of the Wright-Fisher (WF) model. For $x_* = 0.4$ (red squares) $T_{\rm fix}/N$ shows an approximate exponential increase upon increasing N (red solid line, $T_{\rm fix}/(\Omega N) = \exp\left[0.46 + 0.025N\right]$) while for $x_* = 0.2$ (blue circles) $T_{\rm fix}$ displays an approximate logarithmic dependence on N (blue dashed line, $T_{\rm fix}/(\Omega N) = \left[-27 + 16\log N\right]/N$).

within the diffusion approximation by Eq. (1.18), which, on the basis of $M(\bar{x})$ and $V(\bar{x})$ calculated as described in Eqs. (2.18a) and (2.18b), reads (see Ref. [84])

$$V(\bar{x})T''_{\rm fix}(\bar{x})/2 + M(\bar{x})T'_{\rm fix}(\bar{x}) = -1. \tag{2.35}$$

2.4.1 Lowest order prediction in the small-α expansion

For $x_* = 1/2$, by using the lowest-order approximations [denoted by the superscript (0)] for M and V in Eqs. (2.20a) and (2.20b) and choosing the state $\bar{x} = 1/2$ (corresponding to the metastable state) as initial condition, we get

$$T^{(0)}_{\rm fix} = N_{\rm e}\int_0^1 {\rm d}y \int_0^1 {\rm d}z \frac{{\rm e}^{s_{\rm e}N_{\rm e}y(1-z^2)/4}}{1-yz^2}, \tag{2.36}$$

which reaches a constant value for $m' \gg 1$, while $T^{(0)}_{\rm fix}/(N\Omega) \simeq \log 2/m'$ for $m' \ll 1$. Figure 2.10 shows $T^{(0)}_{\rm fix}$ (solid line) as a function of m' for the population specified in the caption, together with the prediction (dashed line) which accounts for the first-order correction in $s_{\rm e}/m$ to the mean drift $M(\bar{x})$ and variance $V(\bar{x})$ (see next subsection). $T^{(0)}_{\rm fix}$ shows a marked

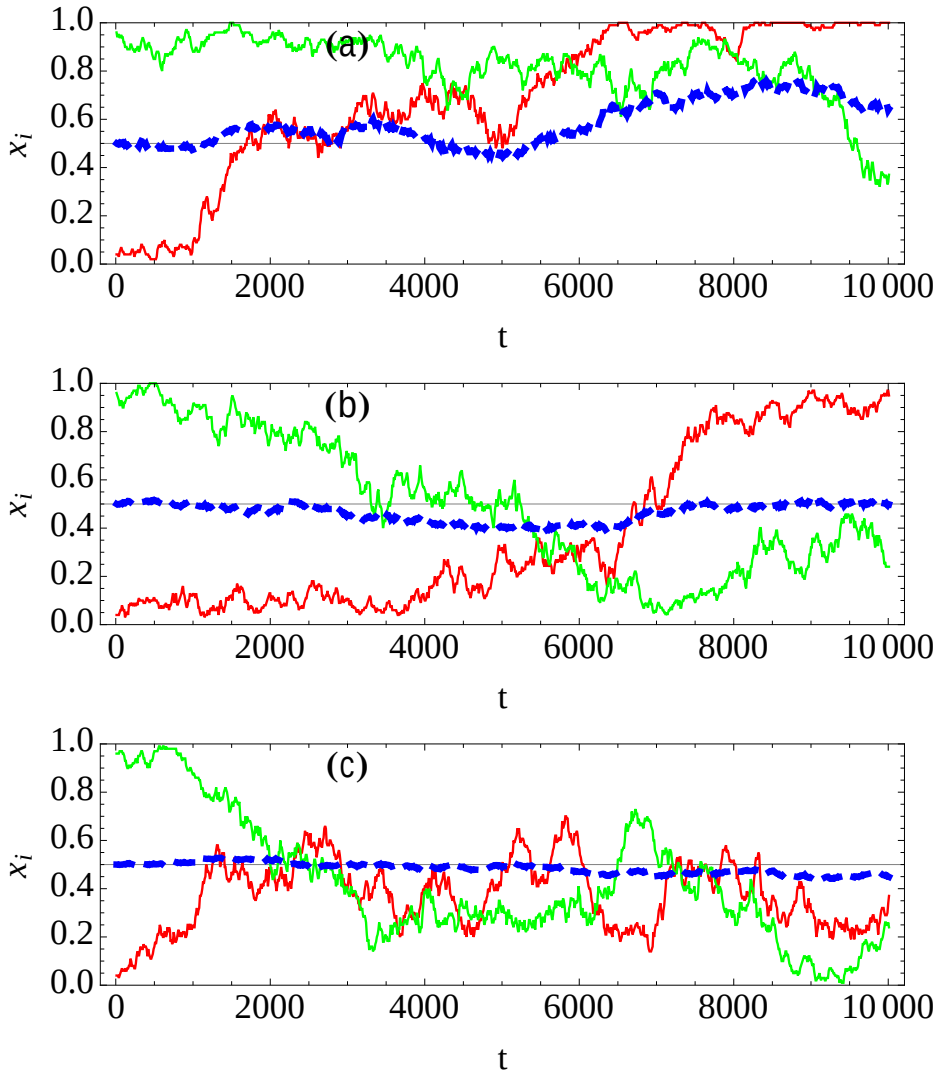

Figure 2.9: Evolution of the frequencies (thin solid lines) of two representative demes and of the mean frequency $\bar{x}$ (dashed, thick line), of a metapopulation characterized by $\Omega = 100$, $m' = 1$, $s' = 5$, $x_* = 0.5$, and by an increasing number of demes: (a) $N = 8$, (b) $N = 30$, and (c) $N = 100$. It can be noticed that the amplitude of the fluctuations of the mean frequency $\bar{x}$ around the value $x_\infty = 1/2$ decreases significantly upon increasing the number of demes. In addition, the time scale separation between the dynamics of $\bar{x}$ and of the single-deme frequencies clearly enlarges for this choice of parameters.

nonmonotonic dependence on the migration rate m', while complying with the bounds of Ref. [60] for large and small m' (dash-dotted lines). In fact, $T_{\rm fix}^{(0)}(m' \gg 1)$ approaches the value it would have in a well-mixed population of ΩN individuals, whereas for $m' \ll 1$ fixation — and thus $T_{\rm fix}$ — is controlled by the growing time scale $T_{\rm migr} \propto 1/m'$ associated with migration (c.f., Sec. 2.5 for a detailed analysis of the case of slow migration). In this respect, the limit $m' \to 0$ differs essentially from the case $m' = 0$, in which $T_{\rm fix}$ is governed by the

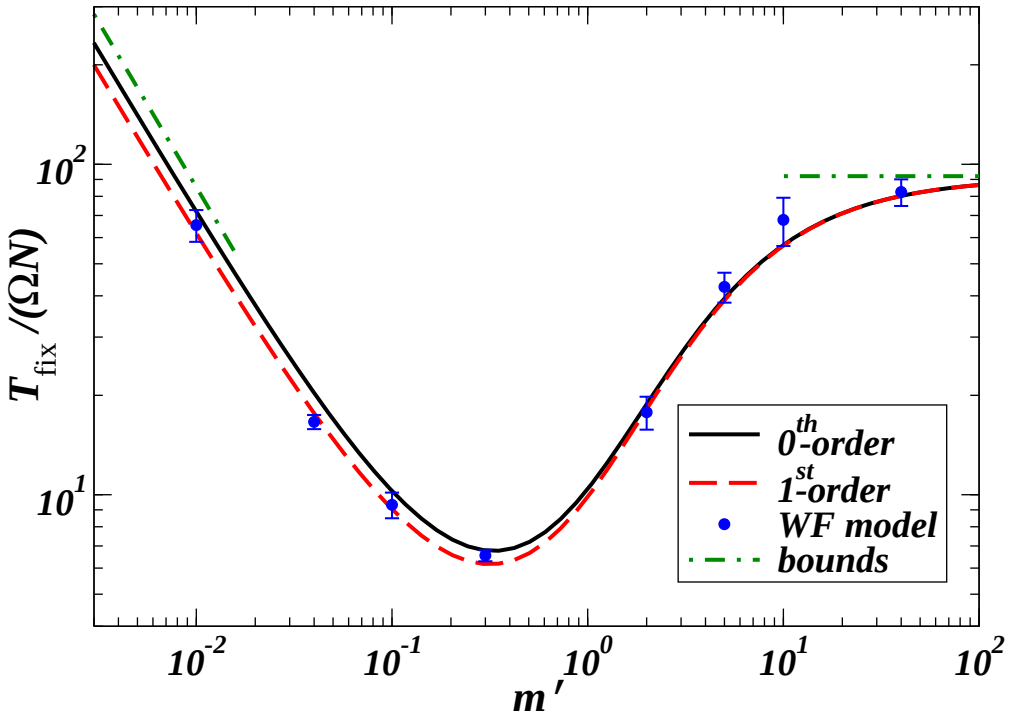

Figure 2.10: Mean fixation time $T_{\rm fix}$ as a function of the migration rate m' with $N = 30$, $\Omega = 100$, $s' = 1$, and $x_* = 0.5$. The solid line corresponds to Eq. (2.36), while the dashed line accounts for the first-order correction in α; symbols with errorbars are the results of numerical simulations of the Wright-Fisher (WF) model. The dash-dotted lines to the left and to the right of the plot indicate the upper bounds for small and large migration, predicted in Ref. [60].

single-deme fixation times, is finite, and it scales $\propto \log N$ for large N (see App. B.6 for further details). In order to demonstrate the accuracy of our analytical predictions, Fig. 2.10 reports the results (symbols with errorbars) of numerical simulations of the Wright-Fisher (WF) microscopic model with balancing selection. Their agreement with the analytical prediction of Eq. (2.36) is very good and further improves upon including the first-order corrections in α (dashed line).

This nonmonotonic dependence of $T_{\rm fix}$ on m' comes actually as a surprise and indeed, as discussed below, it emerges only within a certain range of parameters. Interestingly enough, the bounds discussed in Ref. [60] for large and small migration rates were somehow interpreted in the literature as being lower bounds. Clearly this is not the case. Figure 2.11(a) shows that the nonmonotonicity displayed in Fig. 2.10 is enhanced upon increasing $\sigma \equiv s'N$, while it disappears for $\sigma < \sigma_c$, where σ_c is a critical threshold below which the MFT behaves qualitatively as in a neutral population with $s = 0$. The value $m'_{\rm min}$ of m' at which $T_{\rm fix}$ is minimum diverges for $\sigma \to \sigma_c \simeq 5.2$ (see App. B.7 for details on the numerical estimate of σ_c) and decreases upon increasing $\sigma > \sigma_c$, as shown in Fig. 2.11(b). The value σ_c slightly depends on α if the corrections to Eqs. (2.20a) and (2.20b) are included. Figure

2.11(c) shows that the nonmonotonicity of $T_{\rm fix}^{(0)}$ persists also for $x_* \neq 1/2$, but only within an interval of values of x_* which depends on σ — as indicated by the shaded area in Fig. 2.11(d) — and which covers the entire range for $\sigma \gtrsim 10$.

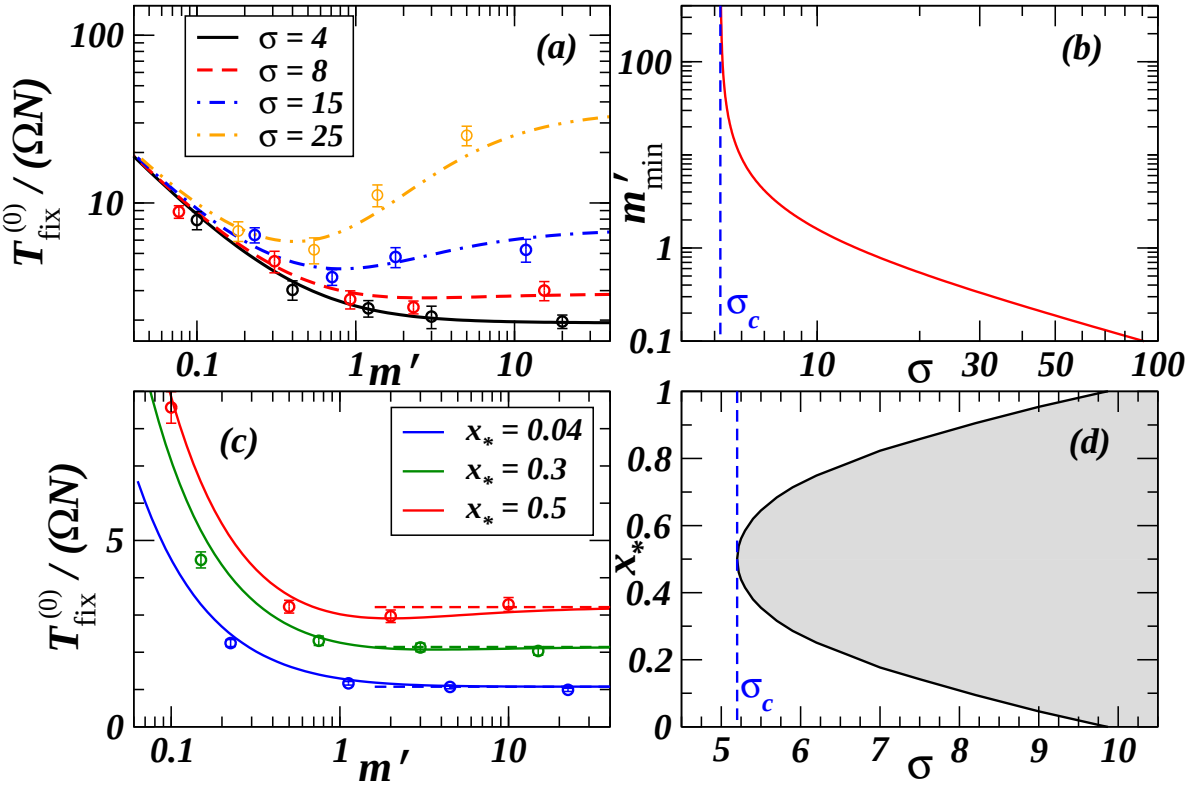

Figure 2.11: Features of the mean fixation time $T_{\rm fix}^{(0)}$ in Eq. (2.36) for a population of $N = 30$ demes with $\Omega = 100$ individuals each: (a) dependence of $T_{\rm fix}^{(0)}$ on m' for $x_* = 0.5$ and various values of σ; (b) $m'_{\rm min}$ as a function of σ; (c) $T_{\rm fix}^{(0)}$ as a function of m' for $\sigma = 9$ and various x_*; (d) region (gray) of the parameter space (σ, x_*) where $T_{\rm fix}^{(0)}$ is a nonmonotonic function of m'. Symbols with errorbars are the results of numerical simulations of the WF model.

2.4.2 Higher-order corrections in α

As a consequence of the corrections $O(\alpha)$ to the Langevin equation for $\overline{x}$, the corresponding mean fixation time (MFT) is modified compared to the value $T_{\rm fix}^{(0)}$ it has in the absence of these corrections (see Eq. (2.36)). In order to write the MFT in a compact form, it is convenient to perform first the change of variable

$$z = 4x(1-x) \tag{2.37}$$

in Eqs. (2.25) and (2.26): using the Itō-Lemma (see App. A.1 for details) and neglecting terms $O(\alpha^2)$, we obtain

$$\dot{z} = \widetilde{A}\, z(1-z)(1+\widetilde{C}z) - \widetilde{B}z(1+\widetilde{D}z) + \sqrt{4\widetilde{B}\, z(1-z)(1+\widetilde{D}z)}\,\eta, \tag{2.38}$$

where

$$\widetilde{A} = s_e(1+\alpha A)/2, \quad \widetilde{B} = (1+\alpha C)/N_e, \quad \widetilde{C} = \alpha B/[4(1+\alpha A)], \quad \widetilde{D} = \alpha D/[4(1+\alpha C)]. \tag{2.39}$$

The MFT associated with Eq. (2.38) can now be calculated via the method described in App. A.2 and its specific value depends on the initial condition of the system. When the metastable state exists (i.e., for (i) $\bar{x} \simeq 1/2$ or $m' \gg 1$, necessary to have $x_\infty \notin \{0,1\}$, and (ii) $Ns' \gg 1 + 1/m'$, necessary to have x_∞ metastable), it is reached within a typical time $T_{\rm rel}$ which is largely independent of the size N of the population and is much smaller than the MFT, which increases upon increasing the size N. Accordingly, for N large enough, the specific choice $\bar{x} = x_0$ of the initial condition does not influence significantly the total elapsed time between the initial time of the dynamics and the fixation, provided that x_0 is far enough from the boundaries. Assuming that the system starts from $\bar{x} = 1/2$ [corresponding to $z = 1$, see Eq. (2.37)], one finds

$$T_{\rm fix}^{(1)} = \frac{1}{2\widetilde{B}} \int_0^1 {\rm d}z \, \frac{{\rm e}^{-\beta z}}{\sqrt{1-z}\,(1+\widetilde{D}z)^\gamma} \int_z^1 {\rm d}\xi \frac{{\rm e}^{\beta\xi}}{\xi\sqrt{1-\xi}\,(1+\widetilde{D}\xi)^{1-\gamma}}, \tag{2.40}$$

where

$$\gamma = \widetilde{A}(\widetilde{D}-\widetilde{C})/(2\widetilde{B}\widetilde{D}^2) \quad \text{and} \quad \beta = \widetilde{A}\widetilde{C}/(2\widetilde{B}\widetilde{D}). \tag{2.41}$$

The asymptotic behavior of $T_{\rm fix}^{(1)}$ for $s' \to 0$ can be easily calculated from the previous expression

$$\frac{T_{\rm fix}^{(1)}}{\Omega N} \simeq \frac{\log 2}{m'} \left(1 - \frac{s'}{3} + O(s'^2)\right), \tag{2.42}$$

which, for $s' = 0$, renders the one found at the lowest nonvanishing order in α, reported in Eq. (2.36). As it can be noticed in Fig. 2.10, for $s' \neq 0$, the negative correction on the r.h.s. of Eq. (2.42) (red dashed line) improves the agreement with the results of the simulations of the Wright-Fisher microscopic model (symbols with errorbars) compared to the theoretical prediction with $s' = 0$ (black solid line). The asymptotic expression of $T_{\rm fix}^{(1)}$ for large migration rate $m \to \infty$, instead, is the same as the one reported below Eq. (2.36) at the lowest nonvanishing order in s: the population behaves like a well-mixed one with size ΩN and selection coefficient s.

2.4.3 Nonmonotonicity and the biodiversity

Global heterozygosity H

In order to understand how migration affects biodiversity before the eventual fixation which corresponds to $H = h = 0$ [see the discussion at the end of Sec. 2.2.2 and in particular Eqs. (2.12) and (2.13)], we assume that the population at time $t = 0$ is in the metastable state $\bar{x} = x_\infty$ such that $H(0) = 2x_\infty(1-x_\infty)$ and that it persists in this state until fixation occurs. Under this heuristic assumption, one can approximate $H(t) \simeq [1 - p_{\rm fix}(x_\infty, t)]H(0)$,

where $p_{\rm fix}(x_0, t)$ is the probability that a population prepared with $\bar{x} = x_0$ at time $t = 0$ has already fixed at time t. $p_{\rm fix}$ satisfies the backward Fokker-Planck equation (see Sec. 1.3.3)

$$\partial_t p_{\rm fix} = M(x_0)\partial_{x_0} p_{\rm fix} + \frac{1}{2} V(x_0)\partial^2_{x_0} p_{\rm fix}, \tag{2.43}$$

which can be integrated numerically. By using the expressions of M and V in Eqs. (2.20a) and (2.20b), the results of this approximation for H are presented in Fig. 2.12 as functions of m' for some values of t and they are compared with those of numerical simulations of the WF model (symbols with errorbars). Note that the estimate of $H(t)$ is expected to become less accurate as $m'\sigma$ is smaller than 1 because, correspondingly, the state $\bar{x} \simeq x_\infty$ is no longer metastable[5] For slow and fast migration $H(t) \simeq H(0)$ for a rather long time whereas $H(t)$ rapidly decreases in time for intermediate values of the migration rate. For a fixed time and as a function of m', instead, H has a minimum at $m' \simeq m'_{\rm min}$, indicating that the global biodiversity can be enhanced upon increasing migration [86, 87, 88, 89]. Our predictions agree rather well with the results of simulations, apart, as expected, from the region $m' \lesssim 1/\sigma \simeq 0.03$.

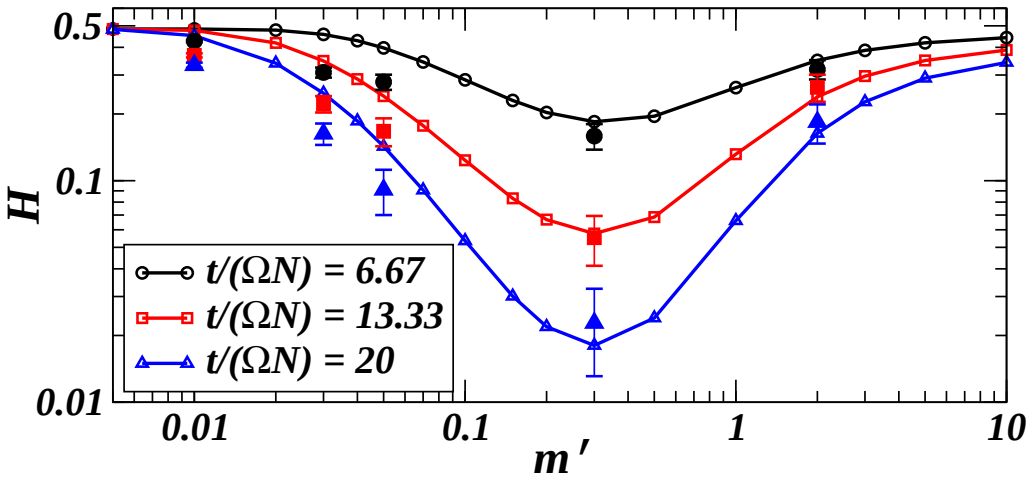

Figure 2.12: Dependence of the global heterozygosity H on the migration rate m' at various times, for a subdivided population with $\Omega = 100$, $N = 30$, $s' = 1$, and $x_* = 1/2$: the prediction of the approximation described in the text (solid lines) is compared with the results of simulations of the WF model (symbols with error-bars).

Intra-deme heterozygosity h

With a procedure analogous to the one described above for the global heterozygosity H, one can obtain an estimate for the time evolution of the intra-deme heterozygosity h. The only difference compared to the case of H is that the value of h in the metastable state —

[5] For $m'\sigma \lesssim 1$ indeed, the timescale $T_{\rm rel}$ which controls the relaxation to the metastable state becomes smaller than the timescale $T_{\rm fluct}$ associated with the lifetime of that state (see App. B.5).

which is taken to be the initial condition in our heuristic estimate — is $h(0) = \hat{h}$, determined as follows. We assume that at time $t = 0$ each deme is distributed according to the quasi-stationary distribution $P_{\rm qs}(x_i|x_\infty)$, where x_∞ is the value of $\overline{x}$ in the metastable state discussed in Sec. 2.3. In the presence of balancing selection with $x_* = 1/2$, one has $x_\infty = 1/2$ (independently of the values of m' and s') and the value $\hat{h}$ of the intra-deme heterozygosity h in the metastable state is reported in Fig. 2.13 as a function of the migration rate m' for large N (the actual behavior does not change much for smaller values of N). On the basis of

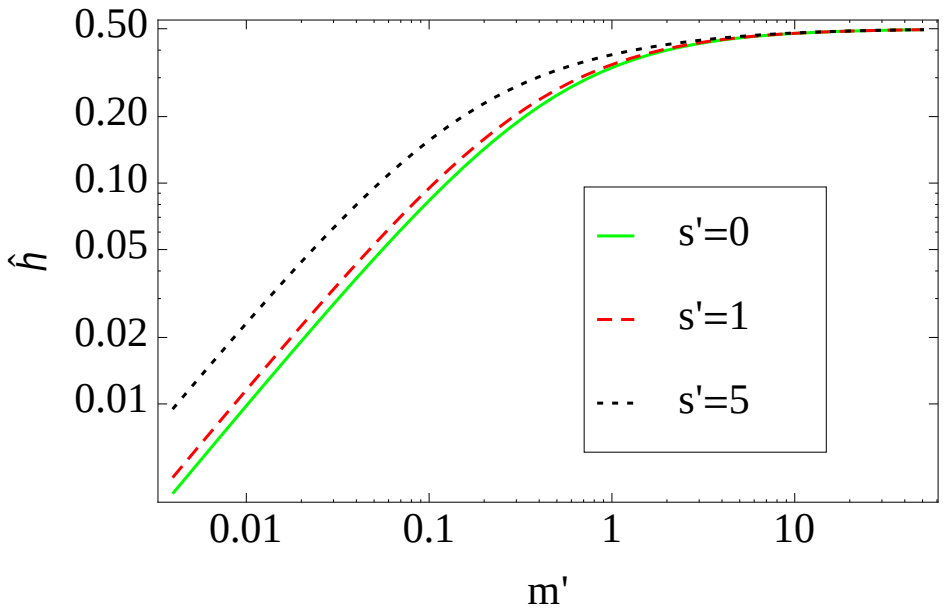

Figure 2.13: Intra-deme heterozygosity $\hat{h}$ within the metastable state $x_i \simeq \bar{x} \simeq x_\infty$ as a function of the (rescaled) migration rate m' and for various values of the (rescaled) selection rate s', in a population with $N = \infty$.

this initial value $\hat{h}$ of h, an estimate of $h(t)$ can be obtained under the same assumption as the one which was made in order to discuss $H(t)$. The corresponding evolution is reported in Fig. 2.14. For slow and fast migration, $h(t)$ remains close to $h(0)$ for a long time, whereas it rapidly decreases in time for intermediate values of the migration rate. For a sufficiently large time, instead, the profile of $h(t)$ as a function of m' develops a minimum at $m' \simeq m'_{\rm min}$. Our predictions agree rather well with the results of simulations, while they become less accurate for $m' \lesssim 1/\sigma \simeq 0.03$ which, in fact, is outside the range of validity of our approximation[6].

[6]See footnote 5.

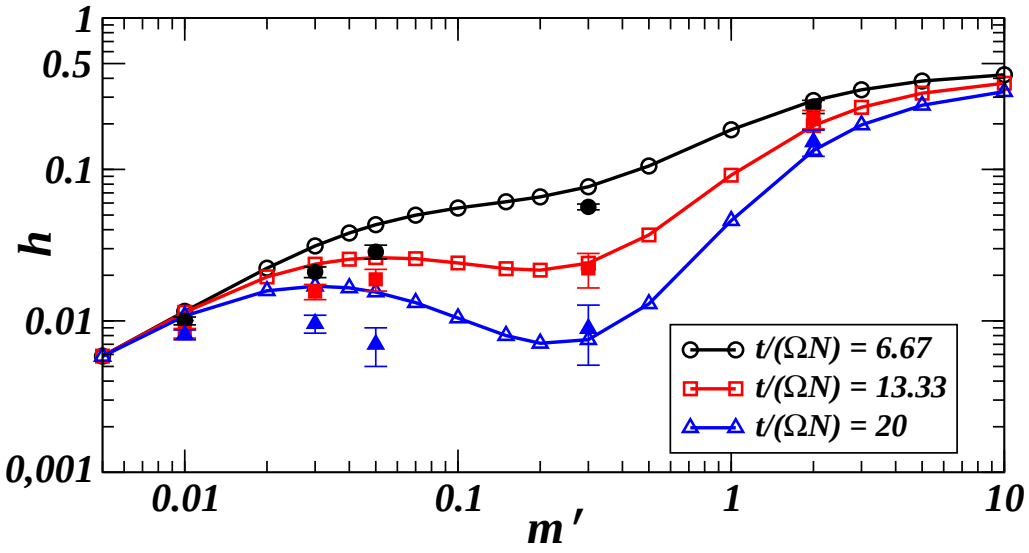

Figure 2.14: Intra-deme heterozygosity h as a function of the migration rate m' and at various times during the evolution of the subdivided population with $N = 30$, $s' = 1$, and $x_* = 0.5$. The evolution calculated on the basis of the approximation described in the main text (continuous lines) is compared with the results of the numerical simulations of the Wright-Fisher model (symbols with error-bars). The approximation is expected to become increasingly accurate as $T_{\rm rel} \ll T_{\rm fluct}$, i.e., as $m' \gg 1/\sigma \simeq 0.033$.

2.5 The case of slow migration

The effective description of the island model with migration introduced in Section 2.2.3 relies on a perturbative expansion in the parameter α. The correspondent predictions concerning the collective behavior of the metapopulation and, in particular, the mean fixation time have been derived within the region of the parameter space corresponding to small α. If the migration rate m is large, this region stretches and includes large values of the selection strength $s \simeq m$. Interestingly enough, this case can also be described by using a fast-mode elimination method recently proposed in Refs. [90, 91]. On the contrary, for small migration rate m, the approximation discussed in Sec. 2.2.3 is expected to be accurate only for a small selection coefficient s. In particular, it requires $s \ll 1/\Omega$ for the value $m \simeq 1/(\sqrt{2}\Omega)$ of the migration rate m at which the parameter α reaches its maximum as a function of m [see Eq. (2.21a) for the dependence of $s_{\rm e}$ on m]. However, numerical evidence suggests that the predictions of this approximation are actually accurate beyond the cases mentioned above; in order to rationalize this fact, in this Section we develop an alternative description of the system for small migration rate m.

2.5.1 Effective voter model

With a small but nonvanishing migration rate m — such that $0 < m' \ll T_{\rm fix1}^{-1}$ ([7]) — each deme rapidly evolves towards one of the "boundary states" $x_i = 0$ or 1, which are no longer absorbing due to $m' \neq 0$, and it spends most of the time close to it. This is illustrated in Fig. 2.15 (see also Fig. 2.3) which shows the time evolution of the allele frequencies $x_i(t)$ in the various demes of a population with $x_i(t = 0)$ either equal to 0.05 or 0.95, for two values of migration rate (a) $m' = 0.1$ and (b) $m' = 0.01$ and some values of selection strength s'. According to Eq. (2.7) one has $m'/T_{\rm fix1}^{-1} \simeq 10^{-1}$ and $\simeq 10^{-2}$ for panel (a) and (b), respectively; as anticipated, the demes in panel (b) spend most of their time into the boundary states. However, sometimes it happens that a different allele is received by a deme

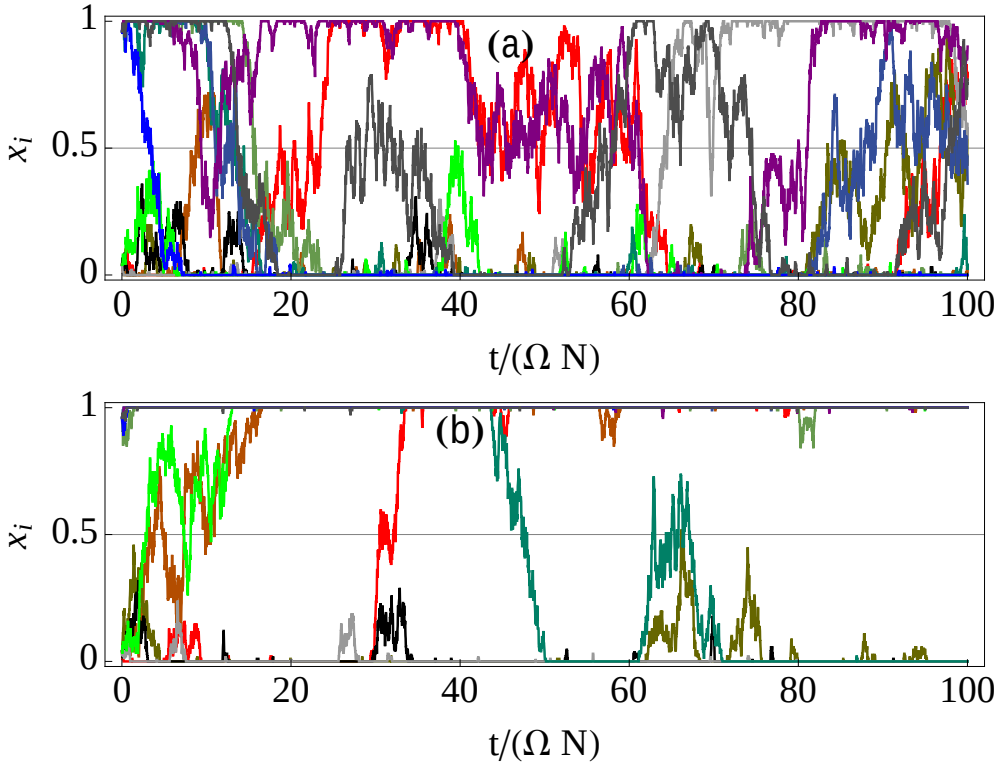

Figure 2.15: Time evolution of the frequency x_i of allele A in the various demes (represented by different colors) of a fully-connected metapopulation consisting of $N = 12$ demes with $\Omega = 100$ individuals each with migratio rate (a) $m' = 0.1$ or (b) $m' = 0.01$. These curves are obtained from the numerical simulation of the Wright-Fisher model with balancing selection characterized by $x_* = 0.5$ and (a) $s' = 5$, (b) $s' = 1$. At time $t = 0$, half of the demes have $x_i = 0.05$, while the remaining ones $x_i = 0.95$, which results in the ratio $m'/T_{\rm fix1}^{-1} \simeq 10^{-1}$ and $\simeq 10^{-2}$ for panel (a) and (b), respectively.

[7] The condition $m' \ll 1/T_{\rm fix1}$ emerges by comparing the time scale $T_{\rm fix1}$ needed by a single deme to reach fixation in the absence of migration and the typical time scale $1/m'$ associated with the occurrence of migration.

because of migration and that it rapidly fixes, causing the variable x_i to "jump" to the other boundary state. Accordingly, one can describe this dynamics in terms of an effective voter model, in which each deme of the metapopulation is mapped onto a voter with one of the two possible opinions which corresponds to the states $x_i = 0$ or 1. Migration then acts as an effective interaction among the voters, which can influence and change each other's state. More precisely, with a rate[8]

$$r = m'N/2 \tag{2.44}$$

two randomly selected voters interact and, if they are in different states, their interaction can cause one voter (or both) to change its state. In particular, as a consequence of the interaction between voters i and j with $x_i = 0$ and $x_j = 1$, they change state with probability $p = p(1|1/\Omega)$ and $q = p(0|1 - 1/\Omega)$ respectively, where $p(x'|x)$ is the probability for a single *isolated* deme to reach the value x' starting from an initial value x before fixation occurs, and is reported in Eq. (2.8). Accordingly, p quantifies the probability that an isolated deme originally in the absorbing state $x_i = 0$ (all individuals carry allele B) fixes to the opposite boundary $x_i = 1$ when, because of migration, it receives an individual carrying allele A, such that the ensuing, single-deme fast dynamics of x_i starts from the initial value $1/\Omega$. An analogous interpretation holds for q. The probability that this interaction increases (respectively decreases) by one unit the number of individuals in state 1 is therefore $p(1-q)$ (respectively $q(1-p)$). Accordingly, the rates $W_{+/-}$ at which the number of voters in state 1 increases (+) or decreases (−) by one unit are, respectively,

$$\begin{aligned} W_+ &= m'Np(1-q)\bar{x}(1-\bar{x}), \\ W_- &= m'Nq(1-p)\bar{x}(1-\bar{x}), \end{aligned} \tag{2.45}$$

where the factors $2\bar{x}(1-\bar{x})$ account for the probability that the interacting voters are in different states. When the number N of demes is large, the master equation associated with the rates in Eq. (2.45) can be approximated by a Langevin equation

$$\dot{\bar{x}} = \sigma_{\rm e}^{\rm vot}\bar{x}(1-\bar{x}) + \sqrt{\frac{\bar{x}(1-\bar{x})}{N_{\rm e}^{\rm vot}}}\,\eta, \tag{2.46}$$

where $\sigma_{\rm e}^{\rm vot} = m'(p-q)$ is an effective directional selection coefficient, $N_{\rm e}^{\rm vot} = N/[m'(p+q-2pq)]$ is an effective population size, and η the normalized Gaussian white noise such as the one in Eq. (2.3). For small s', m' and large Ω, these effective coefficients reduce to

$$\begin{aligned} \sigma_{\rm e}^{\rm vot} &= 2m's(x_* - 1/2), \\ N_{\rm e}^{\rm vot} &= \frac{N\Omega}{2m'}, \end{aligned} \tag{2.47}$$

[8]This is the rate associated with the probability $P^{\geq 1}(\delta t)$ that at least one individual is exchanged between one of the possible $N(N-1)/2$ pairs of demes of the population in the small time interval δt, thus establishing an "interaction" between the corresponding voters. In this time interval, each pair of demes exchanges an average number $\varepsilon \equiv m\Omega\delta t/(N-1)$ of individuals and, according to the Poisson counting, the probability that there is no exchange is $\mathrm{e}^{-\varepsilon} \simeq 1-\varepsilon$ in that pair and therefore $\simeq (1-\varepsilon)^{N(N-1)/2} \simeq 1 - m'N\delta t/2$ in all possible pairs. This probability equals $1 - P^{\geq 1}(\delta t)$ and thus $P^{\geq 1}(\delta t) \simeq m'N\delta t/2$, which results in the rate reported in Eq. (2.44).

and they coincide with the coefficients $\sigma_{\rm e}$, $N_{\rm e}$ evaluated in Eq. (2.30) and (2.21b), respectively. Since the expressions in Eqs. (2.47) and (2.30)-(2.21b) have been obtained via two different approaches, their agreement in the overlap between the respective regions of validity demonstrates that both of them correctly capture the dynamics of the system at a coarser scale. As it was the case in Sec. 2.2.3, the system behaves effectively as a well-mixed population with rescaled effective coefficients. Note, however, that the deterministic term in Eq. (2.46) has the same functional form (typical of directional selection) as $M^{(0)}_{\rm dir}(\bar{x})$, while the analogous of $M^{(0)}_{\rm symm}(\bar{x})$ — the footprint of balancing selection — is missing completely. This is due to the fact that the specific form of the selection does not enter into the definition of the effective voter model; on the one hand, this model provides a viable approximation for the dynamics of any metapopulation with small enough migration rate but, on the other, it fails to capture some qualitative features of balancing selection.

The MFT $T^{\rm vot}_{\rm fix}$ of the voter model can be evaluated from Eq. (2.46) via the method described in App. A.2. The result is the same as in Eq. (2.7), where the single-deme parameters s, Ω have to be replaced by the migration-dependent renormalized parameters $\sigma^{\rm vot}_{\rm e}$ and $N^{\rm vot}_{\rm e}$, while the functions $S(a,b)$ and $F(a,b)$ in Eq. (2.5), associated with balancing selection, have to be replaced by the corresponding ones for the directional selection

$$\begin{aligned} S_{\rm vot}(a,b) &= \frac{\exp[-2\sigma^{\rm vot}_{\rm e}N^{\rm vot}_{\rm e}a]-\exp[-2\sigma^{\rm vot}_{\rm e}N^{\rm vot}_{\rm e}b]}{2\sigma^{\rm vot}_{\rm e}N^{\rm vot}_{\rm e}}, \\ F_{\rm vot}(a,b) &= \int_a^b {\rm d}z \int_z^1 {\rm d}y \frac{\exp[2\sigma^{\rm vot}_{\rm e}N^{\rm vot}_{\rm e}(y-z)}{y(1-y)}. \end{aligned} \tag{2.48}$$

In the symmetric case $x_* = 1/2$ one eventually finds

$$T^{\rm vot}_{\rm fix} = \frac{N\log 2}{m'p(1-p)}. \tag{2.49}$$

This MFT $T^{\rm vot}_{\rm fix}$ is reported in Fig. 2.16 (blue dashed line) as a function of m', for $\Omega = 100$, $N = 30$, and $s' = 1$. For small values of $m' \lesssim 0.03$, $T^{\rm vot}_{\rm fix}$ is in excellent agreement with the data from numerical simulations of the Wright-Fisher microscopic model (symbols,WF), with the first-order estimate $T^{(1)}_{\rm fix}$ described in Ref. [36] (green solid line), and with the MFT $T^{\rm vi}_{\rm fix}$ (brown dashed line) obtained by introducing an intermediate state in the voter model, which we discuss next.

2.5.2 Effective voter model with an intermediate state

In the previous section, the fixation process of the single demes was considered to occur instantaneously and therefore each deme was supposed to be always in one of the two boundary states $x_i = 0$ or 1. However, the transition from one boundary state to the other — triggered by the exchange of individuals between demes — takes some time and this fact can be accounted for by introducing in the model an intermediate uncertain voter with no definite opinion. This intermediate state is associated with a single-deme frequency $x_i = x_{\rm u}$, where $x_{\rm u} \simeq x_*$ is an effective parameter, which depends on the optimal frequency x_* and

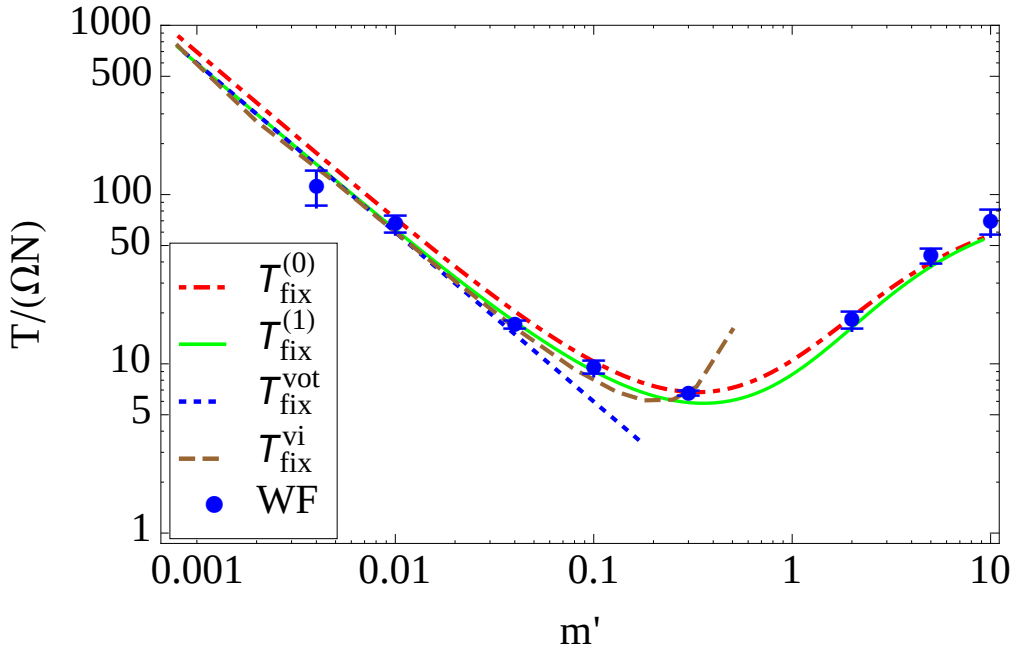

Figure 2.16: Mean fixation time as a function of the migration rate m', for a metapopulation consisting of $N = 30$ demes of $\Omega = 100$ individuals each, with $s' = 1$ and $x_* = 1/2$. Symbols correspond to the MFT of the Wright-Fisher (WF) model obtained via numerical simulations. The red dash-dotted and green solid curves correspond to the analytic prediction $T_{\rm fix}^{(0)}$ and its improvement $T_{\rm fix}^{(1)}$, respectively, described in Eq. (2.36) and in Eq. (2.40). The blue dashed line is the MFT $T_{\rm fix}^{\rm vot}$ [see Eq. (2.49)] of the effective voter model described in the main text. The brown dashed curve, instead, corresponds to the MFT $T_{\rm fix}^{\rm vi}$ of the voter model with an intermediate state (see Sec. 2.5.2), which reproduces qualitatively the nonmonotonic behavior observed in the numerical data. The "lifetime" $T_{\rm u}$ of the intermediate state introduced in Sec. 2.5.2 is estimated as described in App. B.3.

on the rates s' and m'. This state is supposed to be metastable, with a "lifetime" $T_{\rm u}$ proportional to the single-deme fixation time $T_{\rm fix1}$ reported in Eq. (2.5); this means that the intermediate state decays with a rate $1/T_{\rm u}$ into one with definite opinion $x_i = 0$ or 1. In App. B.3 we discuss a possible heuristic estimate of the effective parameter $T_{\rm u}$, which renders $T_{\rm u}/T_{\rm fix1} \simeq 0.3$. Following the line of argument outlined in the previous subsection, and the notation introduced there, the state $x_i = 1$ is reached from the intermediate state with probability $\tilde{p} = p(1|x_{\rm u})$. The presence of an intermediate state is known to change completely the nature of the ordering process of the voter model (see for instance Refs. [92, 93, 24]). Here such a state is introduced in order to mimic the effect of balancing selection and, as we discuss further below, it is sufficient to cause the emergence of an internal attractive point in the dynamics of $\bar{x}$ and nonmonotonic dependences of the MFT on the relevant parameters.

With the same rate as for the effective voter model, given in Eq. (2.44), an interaction

takes place between any pair of voters. After an interaction with a voter having a different definite opinion or an indefinite one, a voter with a definite opinion can loose its own, entering the intermediate state. In order to illustrate this in more detail, consider a voter i in the state $x_i = 0$: its interaction with a voter j in a different state ($x_j = 1$) consists in exchanging of one individual between them, which introduces in the i-th deme an individual with allele A into a background population of individuals with allele B (and viceversa in the deme j). The probability that the i-th deme, with a frequency $x_i = 1/\Omega$ after the exchange, reaches the value $x_i = x_\mathrm{u}$ is given by $P = p(x_\mathrm{u}|1/\Omega)$, which represents the probability that the i-th voter, initially in the state $x_i = 0$, reaches the intermediate state after the interaction with the j-th deme. Similarly, the probability that the voter j, initially in the state $x_j = 1$, reaches the intermediate one due to its interaction with the voter i is $Q = p(x_\mathrm{u}|1 - 1/\Omega)$. Let us consider now the case of a voter in the state $x_i = 0$ interacting with a voter j in the intermediate one: due to this interaction, i reaches the value $x_i = x_\mathrm{u}$ with probability $x_\mathrm{u}P$. Indeed, deme i receives from deme j an individual with allele A with probability x_u, in which case the frequency x_i of allele A in deme i reaches the value x_u with probability P. It is important to note that we assumed that such an interaction has no effect on the voter in the intermediate state because, for large Ω, the state $x_\mathrm{u} \pm 1/\Omega$ has almost the same fixation probability as x_u (i.e., $p(0|x_\mathrm{u} \pm 1/\Omega) \simeq p(0|x_\mathrm{u})$). For later purposes we emphasize here that generically P increases monotonically upon increasing the selection strength s', at least for $0.25 \lesssim x_* \lesssim 0.75$. This feature turns out to be crucial for understanding the nonmonotonic behavior of the MFT as a function of s' (for fixed m'), which is discussed in detail further below in this section.

In the following we denote by N_0, N_1, and N_u the numbers of voters in states 0, 1, and x_u, respectively. Since $N_0 + N_1 + N_\mathrm{u} = N$, the state of the metapopulation is fully determined by N_0 and N_1. The rates of the possible transitions previously described are, in the (N_0, N_1) space,

- $(N_0, N_1) \xrightarrow{W_A} (N_0 - 1, N_1)$,
- $(N_0, N_1) \xrightarrow{W_B} (N_0, N_1 - 1)$,
- $(N_0, N_1) \xrightarrow{W_C} (N_0 - 1, N_1 - 1)$,
- $(N_0, N_1) \xrightarrow{W_D} (N_0 + 1, N_1)$,
- $(N_0, N_1) \xrightarrow{W_E} (N_0, N_1 + 1)$,

where

$$
\begin{aligned}
W_A &= \frac{m'PN_0}{N}[N_1(1-Q)+N_{\rm u}x_{\rm u}],\\
W_B &= \frac{m'QN_1}{N}[N_0(1-P)+N_{\rm u}(1-x_{\rm u})],\\
W_C &= \frac{m'PQN_0N_1}{N},\\
W_D &= \frac{1-\tilde{p}}{T_{\rm u}}N_{\rm u},\\
W_E &= \frac{\tilde{p}}{T_{\rm u}}N_{\rm u}.
\end{aligned}
\tag{2.50}
$$

These rates define the transition matrix $W_{\vec{N}\to\vec{N}'}$ of the effective voter model with intermediate states, the stochastic evolution of which is described by the master equation [22]

$$
\partial_t P(\vec{N},t) = \sum_{\vec{N}'}\left[P(\vec{N}',t)W_{\vec{N}'\to\vec{N}} - P(\vec{N},t)W_{\vec{N}\to\vec{N}'}\right], \tag{2.51}
$$

where $P(\vec{N},t)$ is the probability to find the system in the state $\vec{N}=(N_0,N_1)$ at time t.

Numerical evaluation of the MFT

On the basis of the (forward) master equation (2.51), a backward master equation for the fixation probability $u(\vec{N},t) = P((N,0);t|\vec{N};0) + P((0,N);t|\vec{N};0)$ immediately follows [22]

$$
\partial_t u(\vec{N};t) = \sum_{\vec{N}'}\left[W_{\vec{N}\to\vec{N}'}u(\vec{N}',t) - W_{\vec{N}\to\vec{N}'}u(\vec{N},t)\right]. \tag{2.52}
$$

This equation can be solved numerically by introducing a time discretization $t_n = n\delta t$ (where δt is a time interval chosen to be small enough to ensure that $W_{\vec{N}\to\vec{N}'}\delta t \ll 1$ for every pair $(\vec{N},\vec{N}')$) and by using the finite difference approximation of the time derivative (Euler's method). The state is described by an $(N+1)\times(N+1)$ array $u_n(N_0,N_1)$ with $N_0,N_1 = 0,...,N$, whose entries are constrained to vanish for $N_0+N_1>N$. At each time step, the entries of u_n evolve according to the discrete version of Eq. (2.52).

If the system starts from a state different from the absorbing boundaries $X_1=(N_0=0,N_1=N)$ and $X_0=(N_0=N,N_1=0)$, the initial condition for the fixation probability is $u_0(N_0,N_1)=\delta_{N_0,N}\delta_{N_1,0}+\delta_{N_0,0}\delta_{N_1,N}$, where $\delta_{M,N}=1$ for $M=N$, 0 otherwise. Since we are interested in the determination of the MFT for a system which starts from the state $(N_0=N/2,N_1=N/2)$[9], we focus on the quantity $U_n \equiv u((N/2,N/2),t_n)$. The probability

[9]Since the number of uncertain voters is supposed to be small ($N_{\rm u}\ll N$), the state $\bar{x}=1/2$ of the voter model can be essentially realized only by having $(N_0=N/2,N_1=N/2)$ as the initial condition, which, for $x_*\sim 1/2$, is also a good approximation of the metastable state into which the system quickly relaxes.

density $p^{\rm fix}(t)$ for reaching one of the two absorbing states as a function of the time t is therefore given by the discrete derivative of U for sufficiently small δt , which reads

$$p_n^{\rm fix} = \frac{U_n - U_{n-1}}{t_n - t_{n-1}}. \tag{2.53}$$

In terms of this density, the MFT $T_{\rm fix}^{\rm vi}$ of the voter model with intermediate state is given, for $\delta t \to 0$, by $T_{\rm fix}^{\rm vi} = \sum_{n=1}^{\infty} t_n p_n^{\rm fix}$, which can be estimated as

$$T_{\rm fix}^{\rm vi} \simeq \sum_{n=1}^{n_{\rm max}} t_n p_n^{\rm fix} + T_{\rm tail}, \tag{2.54}$$

where the term $T_{\rm tail}$ is associated with the tail of the distribution $p^{\rm fix}(t)$ for $t > t_{\rm max} = t_{n_{\rm max}}$ and it can be conveniently estimated by fitting $u(\vec{N}, t)$ with an exponential function in the corresponding range. In fact, $U_n \simeq 1 - e^{-\mu t_n}$ for large t_n, from which we obtain

$$T_{\rm tail} \simeq \left(t_{\rm max} + \frac{1}{\mu} \right) e^{-\mu t_{\rm max}}, \tag{2.55}$$

where the value of μ is determined from the fit.

Figure 2.16 compares the various estimates of the MFT, as obtained from the simple voter model ($T_{\rm fix}^{\rm vot}$, blue dotted line), the voter model with intermediate states ($T_{\rm fix}^{\rm vi}$, brown dashed line) or from the lowest-order ($T_{\rm fix}^{(0)}$, red dash-dotted line) and first-order ($T_{\rm fix}^{(1)}$, green solid line) expansion in the small α parameter described in Section 2.2.3; symbols with errorbars, instead, correspond to the numerical results of simulations based on the Wright-Fisher model. For small m, the estimates $T_{\rm fix}^{\rm vot}$ and $T_{\rm fix}^{\rm vi}$ agree with the results of simulations and with the first-order $T_{\rm fix}^{(1)}$ in the small-s expansion. It can be noticed that the introduction of the intermediate state extends to larger values of m the range within which the approximation is accurate and, more importantly, it makes the model able to capture qualitatively the nonmonotonic behavior of the MFT as a function of m. This demonstrates that the existence of the intermediate (metastable) state plays a crucial role in determining the emergence of the nonmonotonicity in the mean fixation time.

In Fig. 2.17 we report the MFT as a function of the selection rate s' for a fixed small value of the migration rate $m' = 0.005$. It can be noticed that $T_{\rm fix}^{\rm vi}$ from Eq. (2.54) is in excellent agreement with the results of the numerical simulations of the Wright-Fisher model (symbols) also for quite large values of the selection rate s'; the introduction of the intermediate state in the voter model significantly improves the accuracy of the approximation compared to both $T_{\rm fix}^{(0)}$ and $T_{\rm fix}^{(1)}$, reported in Eqs. (2.36) and (2.40) respectively, and to $T_{\rm fix}^{\rm vot}$ of the voter model without intermediate state.

Since balancing selection tends to push all the demes towards the configuration with allele frequency x_* which is far from the boundaries (at least for $x_* \simeq 1/2$), it is heuristically expected to cause a slowing down of fixation and therefore to increase the MFT; however, Fig. 2.17 shows that this is not always the case and in fact the MFT plotted there displays a nonmonotonic behavior as a function of the selection rate. This nonmonotonicity appears for

small enough m' and it can be rationalized on the basis of the equivalent voter model with intermediate states. In fact, the MFT $T_{\rm fix}^{\rm vi}$ is expected to be proportional to the mean time $T_{\rm change}$ that a voter needs to change its opinion, which can be estimated as $T_{\rm change} \simeq T_{\rm int} + T_{\rm u}$, where $T_{\rm int}$ is the time scale associated with an interaction able to drive a voter initially in states 0 or 1 into the intermediate one $x_{\rm u}$ with "lifetime" $T_{\rm u}$. Since a voter interacts with a typical rate m' and, after this interaction, it reaches the intermediate state $x_{\rm u}$ with probability P, the rate $T_{\rm int}^{-1}$ associated with the transitions towards the intermediate state is given by $T_{\rm int}^{-1} \simeq m'P$, so that

$$T_{\rm change} \simeq \frac{1}{m'P} + T_{\rm u}. \tag{2.56}$$

For small s', the mean time $T_{\rm change}$ is predominantly determined by the term $1/(m'P)$, which in fact increases upon decreasing s', while in the opposite limit of large s' it is actually determined by $T_{\rm u}$, which increases upon increasing s'. The interplay between these two terms results in the nonmonotonic dependence of $T_{\rm change}$ — and therefore of $T_{\rm fix}^{\rm vi}$ — on s'. However, upon further increasing s', it is no longer correct to assume that each deme spends a large part of its time into a boundary state, and therefore in this regime one cannot expect $T_{\rm fix}^{\rm vot}$ and $T_{\rm fix}^{\rm vi}$ to reproduce accurately the corresponding results of numerical simulations of the Wright-Fisher model; nonetheless $T_{\rm fix}^{\rm vi}$ still captures the qualitative behavior of $T_{\rm fix}$ of such a model, as it is clearly seen in Fig. 2.17 by comparing the symbols (numerical simulations) with the dashed line.

Effective equation for the mean frequency $\bar{x}$

When the migration rate m is small (and therefore the interaction rate r among the voters is also small — see Eq. (2.44)) only a relatively small fraction of voters is in the intermediate state, i.e., $N_{\rm u} \ll N$. For large N, the evolution of $\bar{x}$ is expected to be slow compared to that of $N_{\rm u}$, because every interaction causes a change $\Delta N_{\rm u} = \pm 1$ of $N_{\rm u}$, but only a change $\Delta\bar{x} \lesssim 1/N$ of $\bar{x} \sim 1$, so that the relative variation $|\Delta N_{\rm u}|/N_{\rm u}$ of the former is significantly larger than that of the latter $|\Delta\bar{x}|/\bar{x} \ll |\Delta N_{\rm u}|/N_{\rm u}$. This time scale separation allows us to consider $N_{\rm u}$ as a fast fluctuating variable on the time scale which characterizes the dynamics of $\bar{x}$. Conversely, $\bar{x}$ can be considered as a slowly varying (or almost constant) parameter on the time scale of the dynamics of $N_{\rm u}$.

For the sake of simplicity, we focus here on the case of symmetric balancing selection ($x_* = 1/2$ and therefore $x_{\rm u} = 1/2$, $\tilde{p} = 1/2$, and $P = Q$), but the discussion below can be straightforwardly generalized to the nonsymmetric case, with similar conclusions. Considering the characteristic time scale over which the number $N_{\rm u}$ of voters in the intermediate state evolves, one finds an estimate of its average in the large-N and small-m limit by solving the stationary master equation which describes the evolution of $N_{\rm u}$ (see App. B.4.1 for details)

$$\langle N_{\rm u} \rangle \simeq \frac{2m'NPT_{\rm u}\bar{x}(1-\bar{x})}{1 - m'PT_{\rm u}/2}. \tag{2.57}$$

Note that, as expected, the average number $\langle N_{\rm u} \rangle$ of voters in the intermediate state vanishes as $m' \to 0$. On the time scales over which $\bar{x}$ varies, we can approximate $N_{\rm u}$ with its average

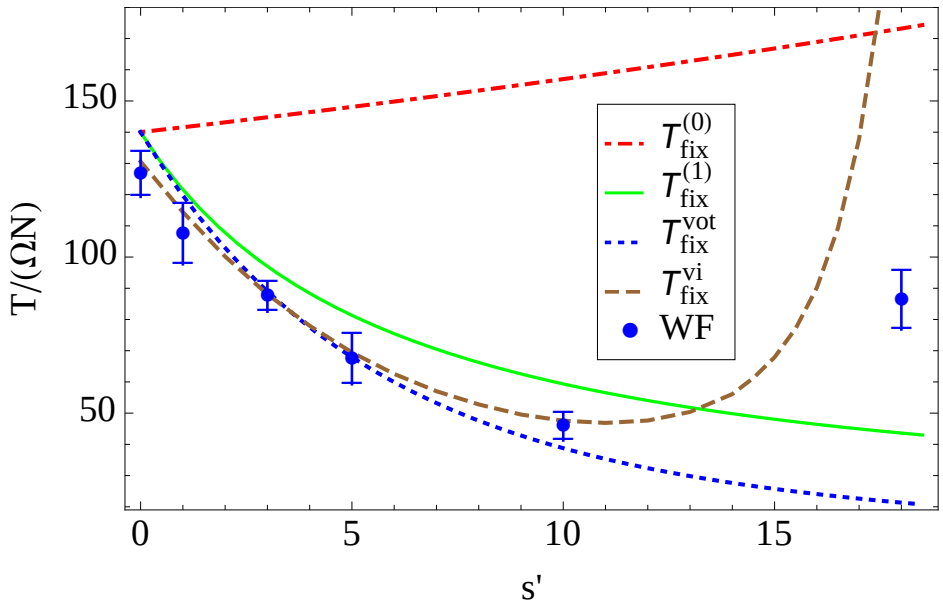

Figure 2.17: MFT for a metapopulation of $N = 30$ demes with $\Omega = 100$ individuals, $m' = 0.005$, and $x_* = 1/2$. Symbols correspond to the MFT of the Wright-Fisher (WF) model obtained via numerical simulations. The red dash-dotted and green solid lines correspond to the analytical predictions $T_{\rm fix}^{(0)}$ and $T_{\rm fix}^{(1)}$ described in Eqs. (2.36) and (2.40) respectively. The blue dashed line is the MFT $T_{\rm fix}^{\rm vot}$ [see Eq. (2.49)] of the effective voter model described in the main text. The brown dashed curve, instead, corresponds to the MFT $T_{\rm fix}^{\rm vi}$ of the voter model with an intermediate state (see Sec. 2.5.2), which reproduces qualitatively the nonmonotonic behavior observed in the numerical data. We have estimated the lifetime $T_{\rm u}$ of the intermediate state as described in App. B.3. The scenario presented here carries over to different choices of $m' \lesssim 0.05$.

$\langle N_{\rm u} \rangle$ [see Eq. (2.57)]; this allows us to write an effective Langevin equation for the evolution of the mean frequency $\bar{x}$, which reads

$$\dot{\bar{x}} = s_{\rm vi}\bar{x}(1-\bar{x})(1/2-\bar{x}) + \sqrt{\frac{\bar{x}(1-\bar{x})}{N_{\rm vi}}}\,\eta(t), \tag{2.58}$$

for large N and Ω and small m (see App. B.4.2 for a detailed derivation), where $s_{\rm vi} = m'^2P^2T_{\rm u}/(1-m'PT_{\rm u}/2)$ is an effective selection coefficient and $N_{\rm vi} = N/(m'P)$ is an effective population size. These effective parameters coincide with $s_{\rm e}$ and $N_{\rm e}$ (see Eqs. (2.21a) and (2.21b)), respectively, for large Ω and small s'. Since $s_{\rm e}$, $N_{\rm e}$ and $s_{\rm vi}$, $N_{\rm vi}$ have been obtained by following two completely different approaches, their agreement in the overlap between the respective regions of validity shows the emergence of a coherent effective dynamics at a coarser scale. Note that the deterministic term in Eq. (2.58) has an internal attractive point $\bar{x}_* = 1/2$, which is the footprint of balancing selection, and this means that the intermediate state $x_{\rm u}$ is the crucial ingredient in order to capture the main features of balancing selection;

note also that $s_{\rm vi} \propto m'^2$ for small m', where indeed the approximation in Eq. (2.46) is accurate.

2.6 Metapopulations in one spatial dimension

While the fully-connected model considered in the previous part of this chapter can be a starting point for describing subdivided populations on a network with high connectivity, the spatial arrangement of many natural populations is better captured by regular lattices. In particular, the opposite case of low connectivity realized by a quasi-one-dimensional habitat, could describe a bank of a river, a seacoast, or the front of an expanding two-dimensional population (see, e.g., Ref. [33]).

In order to investigate the effects of migration on the fixation properties of a population embedded in space, we consider here the celebrated stepping stone model [94], which involves well-mixed *demes* located on the sites of a regular lattice such as the one depicted in Fig. 2.1(b). As in the case discussed in the previous sections, each deme is subject to selection and genetic drift but now migration is possible only between pairs of neighboring demes.

2.6.1 The stepping-stone model

The one-dimensional stepping stone model [94] consists of N interacting demes of identical size Ω, labeled by an integer $i = 1, \ldots, N$ and characterized by the frequencies $\{x_1, x_2, \ldots, x_N\}$ for the occurrence of allele A, with $x_i \in [0, 1]$. The demes (green circles in Fig. **??**) are arranged on the sites of a regular one-dimensional lattice characterized by lattice spacing a. For computational convenience, we consider here periodic boundary conditions ($x_{N+1} \equiv x_1$, i.e., the demes are regularly spaced along a ring). Within each deme, the internal dynamics (assumed to be characterized by the same parameters throughout the population) proceeds as in either Moran's or Wright-Fisher's stochastic models, while neighboring demes interact by exchanging randomly picked individuals, such that the sizes Ω of the demes involved in the exchange are not affected. The rate m with which migration occurs is defined as $m = 2n_{i\leftrightarrow i+1}/\Omega$, where $n_{i\leftrightarrow j}$ is the mean number of individuals exchanged between the deme i and j in one generation. As in Sec. 2.2, we measure time in generation units, so that the time interval τ_g between two subsequent generations is set to unity ($\tau_g = 1$).

Analogously to the island model described in Sec. 2.2.2, within the Wright-Fisher model the effect of migration in the stepping stone model is typically accounted for by modifying the probability $p_r(x_i; x_{i-1}, x_{i+1})$ that a new individual in deme i carries allele A. In the absence of migrations, this probability depends only on x_i and is given by Eq. (2.1); since the migration removes on average from deme i a fraction m of its population, while it adds to it a fraction $m/2$ of the population of the demes $i-1$ and $i+1$ each, it effectively changes the frequency of deme i from x_i to $m(x_{i-1} + x_{i+1})/2 + (1-m)x_i$, so that $p_{\rm r}$ becomes

$$p_{\rm r}(x_i; x_{i-1}, x_{i+1}) = \frac{(1+\tilde{s}_i)[m(x_{i-1}+x_{i+1})/2 + (1-m)x_i]}{1+\tilde{s}_i[m(x_{i-1}+x_{i+1})/2 + (1-m)x_i]}, \tag{2.59}$$

where $\tilde{s}_i = \tilde{s}(x = m(x_{i-1} + x_{i+1})/2 + (1-m)x_i)$ is the value of the function $\tilde{s}(x)$, defined in Eq. (2.4), evaluated at the point $x = m(x_{i-1} + x_{i+1})/2 + (1-m)x_i$.

If the single-deme dynamics of the stepping stone model is based on the Moran model, the migration process affects the rate of increase/decrease of the fraction x_i of A-type individuals in the i-th deme. Similarly to the island model described in Sec. 2.2.2, for $\Omega \gg 1$ the evolution turns out to be described by the rates

$$\begin{aligned} W_{+1} &= (1+\tilde{s})x_i(1-x_i)/(1+\tilde{s}x_i) + m\left[x_{i-1}(1-x_i) + x_{i+1}(1-x_i)\right]/2, \\ W_{-1} &= x_i(1-x_i)/(1+\tilde{s}x_i) + m\left[(1-x_{i-1})x_i + (1-x_{i+1})x_i\right]/2, \end{aligned} \tag{2.60}$$

where the factors $x_{i-1}(1-x_i)$ and $x_{i+1}(1-x_i)$ on the first line of Eq. (2.60) account for the probability that, during a migration event, an individual with allele B is removed from the deme i and is replaced with an individual with allele A chosen from the deme $i-1$ and $i+1$ respectively; the terms $(1-x_{i-1})x_i$ and $(1-x_{i+1})x_i$ have an analogous origin.

For $\Omega \gg 1$ and small $m, s \ll 1$, the evolution of the allele frequency $x_i \in [0,1]$ of the i-th deme can be described (independently of the underlying Wright-Fisher or Moran dynamics) by the following Langevin equation with Itō prescription (see App. B.1)

$$\dot{x}_i = \mu(x_i) + m\left[(x_{i-1} + x_{i+1})/2 - x_i\right] + \sqrt{v(x_i)}\,\eta_i, \tag{2.61}$$

where the term $m\left[(x_{i-1} + x_{i+1})/2 - x_i\right]$ accounts for the migration of individuals between the demes, while $\mu(x_i) = \tilde{s}x_i(1-x_i)$ and $v(x_i) = x_i(1-x_i)/\Omega$ account respectively for the deterministic part and the variance of the noises of the single-deme dynamics, being η_i independent Gaussian noises with $\langle \eta_i(t)\eta_j(t')\rangle = \delta_{i,j}\delta(t-t')$.

When the number N of demes is large and the lattice size a is small (so that the size $L = Na$ of the system is finite), the stepping stone model can be described in the continuum limit, in which the space coordinate r is defined as $r_i = ia$ and Eq. (2.61) becomes

$$\partial_t x(r,t) = \mu(x(r,t)) + D_s\partial_r^2 x(r,t) + \sqrt{D_g x(r,t)[1-x(r,t)]}\,\eta(r,t), \tag{2.62}$$

where the discrete Laplacian $\left(x_{i-1} + x_{i+1} - 2x_i\right)/a^2$ in Eq. (2.61) has been replaced by its continuous version $\partial_r^2 x(r)$, meaning that migration is described in terms of a diffusion on the continuum[10] with diffusion constant $D_s = ma^2$; the strength of the noise is, instead, controlled by the constant $D_g = a/\Omega$. Note that the spatial structure of the population does not allow an effective description of the dynamics in terms of the coupling to a global (and therefore slow) variable analogous to $\bar{x}$ (see Eq. (2.14)). Accordingly, we are unable to introduce an analytic approximation analogous to the one used in Sec. 2.2.3, and we base our analysis on the numerical simulations of the microscopic models, supplemented by analytical predictions in the slow and fast migration limits.

[10]In order to avoid possible confusion, note that the diffusion term $D_s\partial_r^2 x(r,t)$ acts on the space of the positions r, i.e., on the physical space in which the population lives, and that the diffusion is due to spatial migration of the individuals. On the other hand, the diffusion approximation to which we refer in Sec. 2.2.3 concerns the Fokker-Planck equation for the probability $P(x,t)$ of the frequency x in a population, it occurs in the space of frequencies x and is due to the genetic drift (i.e., to the stochastic effect generated by death and reproduction of individuals), and is present also in a well-mixed population.

As it can be seen in Fig. 2.18, for large migration rate m' (green solid line) the frequencies of the various demes as functions of their position i along the circle are similar, and, in a first approximation, the metapopulation can be described as a well-mixed population. When the migration rate m' is small, instead, the stepping stone model allows the formation of domains (black dashed line) within which the demes fix to the same value 0 or 1; the dynamics of these domains rules the collective fixation process. These two limiting case will be analyzed in the following subsections.

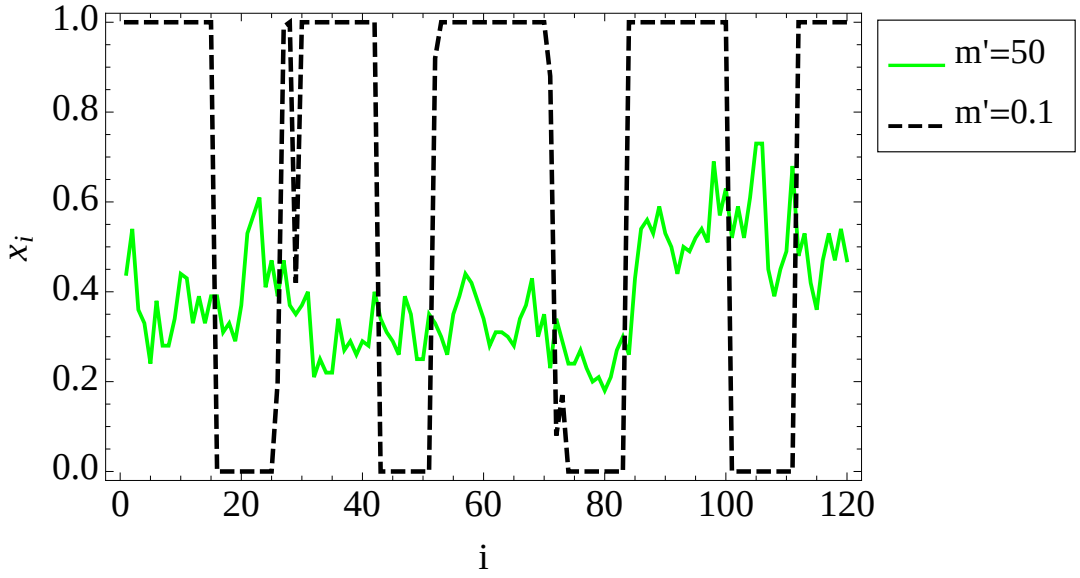

Figure 2.18: Snapshots of a one-dimensional stepping stone model with periodic boundary conditions, in which the deme frequency x_i is plotted as a function of the position i along the chain; the metapopulation is characterized by $\Omega = 100$, $N = 120$, $s' = 1$ and by two different values of m'. These snapshots have been obtained by evolving the model for ΩN generations, starting from the uniform initial condition $x_i = 1/2$.

2.6.2 The case of fast migration

The effect of migration is to wipe out possible differences among the frequencies of neighboring demes: in the absence of any other force (i.e., for $\mu(x) = 0$ and $D_g = 0$), migration makes the system homogeneous within a distance $\ell_{\rm diff}(t) = \sqrt{2D_s t}$, which increases with time. When also the genetic drift is present, it competes with migration, acting at the local level as a source of inhomogeneity. In order to make relevant changes in the local frequencies, the genetic drift requires a time $t \gtrsim T_{\rm fluct}$, where $T_{\rm fluct} = a/D_g$ is the time scale associated to local fluctuations (see App. B.5). We can therefore identify the maximal length at which the diffusion is expected to make the system homogeneous as $\ell_{\rm diff}(T_{\rm fluct}) \simeq \sqrt{2D_s T_{\rm fluct}}$; if we consider a portion of the system of length $\ll \ell_{\rm diff}(T_{\rm fluct})$, it can be considered as effectively well-mixed.

In particular, if the system size $L = Na$ is much smaller than $\ell_{\rm diff}(T_{\rm fluct})$, i.e., if

$$m \gg N^2/(2\Omega), \tag{2.63}$$

the whole system can be considered well-mixed and it can be described in terms of the mean frequency $\bar{x} = \sum_{i=1}^{N} x_i$, which evolves according to

$$\dot{\bar{x}} = \mu(\bar{x}) + \sqrt{\bar{x}(1-\bar{x})/(\Omega N)}\,\eta. \tag{2.64}$$

The mean fixation time is therefore given by Eqs. (2.5) and (2.7), in which the single deme population size Ω has to be replaced with the size ΩN of the whole system.

2.6.3 The case of slow migration

As described in Sec. 2.5.1, with a small but nonvanishing migration rate m — such that $0 < m\Omega \ll T_{\rm fix1}^{-1}$([11]) — each deme rapidly evolves towards one of the boundary states $x_i = 0$ or 1 (which are no longer absorbing due to $m \neq 0$), and it spends most of the time close to it. However, sometimes it happens that a different allele is received by a deme because of migration and it rapidly fixes, causing the variable x_i to "jump" to the other boundary state. Accordingly, one can describe this dynamics in terms of an effective voter model, in which each deme of the metapopulation is represented by a voter with one of the two possible opinions which corresponds to the states $x_i = 0$ or 1. Migration then acts as an effective interaction among the voters, which can influence and change each other's state. Indeed two neighboring demes exchange an individual with a rate $m\Omega$; if they were in different states before the interaction, then, as described in Sec. 2.5.1, the deme that was in the state $x = 0$ ($x = 1$) reaches the other boundary with probability $p = p(1|1/\Omega)$ ($q = p(0|1-1/\Omega)$), where $p(x|x')$ is defined in Eq. (2.8).

If the probabilities p, q are sufficiently small, an effective description for the interaction is the following: a voter in the state $x = 0$ ($x = 1$) with a neighbor in a different state, assumes the opinion of that neighbor with a rate $\lambda = m\Omega p$ ($\tilde{\lambda} = m\Omega q$), where the factor $m\Omega$ accounts for the rate at which the corresponding demes exchange an individual, while the factor p (q) accounts for the probability that the allele of the migrant propagates to all the other individuals of the same deme. Note that (analogously to Sec. 2.5) the specific form of selection does not enter in the definition of the effective voter dynamics, so that the latter can be generalized to any kind of selective force, as long as the single-deme fixation time is much shorter than the time scale associated with migration.

The probability $P(\{x_j\}, t)$ to find the configuration of states $\{x_j\}$ at time t satisfies the master equation (see, e.g., Refs. [22, 21])

$$\dot{P}(\{x_j\}, t) = -\sum_{\{x'_j\}} W_{\{x_j\}\to\{x'_j\}} P(\{x_j\}, t) + \sum_{\{x'_j\}} W_{\{x'_j\}\to\{x_j\}} P(\{x'_j\}, t), \tag{2.65}$$

[11] The condition $m\Omega \ll 1/T_{\rm fix1}$ emerges by comparing the time scale $T_{\rm fix1}$ needed by a single deme to reach fixation in the absence of migration and the typical time scale $1/(m\Omega)$ associated with the occurrence of migration.

where the sums run over all the possible configurations $\{x'_j\}$. For later convenience, we describe the interaction among the voters in terms of the rate $w_{\rm change}$ according to which a voter changes its state. This rate depends on the state of the voter and of its two nearest neighbours, and it reads

$$w_{\rm change}(x_i; x_{i-1}, x_{i+1}) = \tilde{\lambda} x_i \left(2 - x_{i-1} - x_{i+1}\right) + \lambda(1 - x_i)\left(x_{i-1} + x_{i+1}\right). \tag{2.66}$$

We can then rewrite Eq. (2.65) as

$$\dot{P}(\{x_j\}, t) = -\sum_{i=1}^{N} w_{\rm change}(x_i; x_{i-1}, x_{i+1}) P(\{x_j\}, t) + \sum_{i=1}^{N} w_{\rm change}(1 - x_i; x_{i-1}, x_{i+1}) P(\{x_j\}, t), \tag{2.67}$$

where we used the fact that the probability that two or more changes of opinion occur at the same time is zero and the identity $\sum_{i=1}^{N} w_{\rm change}(x_i; x_{i-1}, x_{i+1}) P(\{x_1, ...1 - x_i, ...x_N\}, t) = \sum_{i=1}^{N} w_{\rm change}(1 - x_i; x_{i-1}, x_{i+1}) P(\{x_j\}, t)$.

Estimate of the MFT

To understand how consensus is actually achieved in the voter model, we need to quantify the extent to which two distant voters agree. Such a measure is provided by the two-point correlation function (see, e.g., Ref. [95]) $G_k = \langle g_{i,i+k} \rangle$, where $g_{ij} = 2x_i x_j - x_i - x_j + 1$ equals 1 if the voters i and j have the same opinion and vanishes otherwise . Due to the translational invariance of the model, the correlator $G_k = \langle g_{i,i+k} \rangle$ depends only on the distance k. In general the evolution equation of $G_k(t)$ involves the three point function $\langle x_i x_j x_l \rangle$, but in the case of symmetric balancing selection (i.e., for $x_* = 1/2$), it actually reduces to a discrete diffusion equation (see, e.g., Ref. [95])

$$\partial_t G_k(t) = 2\lambda \left[G_{k+1} + G_{k-1} - 2G_k\right]. \tag{2.68}$$

When the number N of demes is large and the lattice size a is small, Eq. (2.68) can be rewritten in the continuum limit (analogously to what we discussed above in this section), and it becomes a diffusion equation

$$\partial_t G(r, t) = D_{\rm vot} \partial_r^2 G(r, t), \tag{2.69}$$

where $D_{\rm vot} = 2\lambda a^2$ is a diffusion constant[12]. The system is therefore expected to be homogeneous within a diffusion distance $\ell_{\rm vot}(t) = \sqrt{4 D_{\rm vot} t}$, which is an increasing function of time. An estimate of the time to reach consensus (i.e., of the MFT) can thus be obtained by equating the diffusion distance $\ell_{\rm vot}$ evaluated at the MFT $T_{\rm fix}^{\rm vot}$ to the size $L = Na$ of the system (see, e.g., Ref. [95]). This renders

$$T_{\rm fix}^{\rm vot} = \beta \frac{N^2}{4m\Omega p}. \tag{2.70}$$

[12]Note that the diffusion constant $D_{\rm vot}$ characterizing the evolution of the correlator $G(r, t)$ in the voter model approximation differs from but is of the same order as the diffusion constant $D_s = ma^2$ in the original stepping stone model (see Eq. (2.62)).

In this expression we introduced a correction factor β in order to account for the fact that, while this heuristic estimate of the MFT is expected to capture correctly the functional dependence on m, it is not generally able to predict possible proportionality constants. This factor can be fixed by comparing with numerical simulations; in the cases considered below one obtains $\beta \simeq 0.4$.

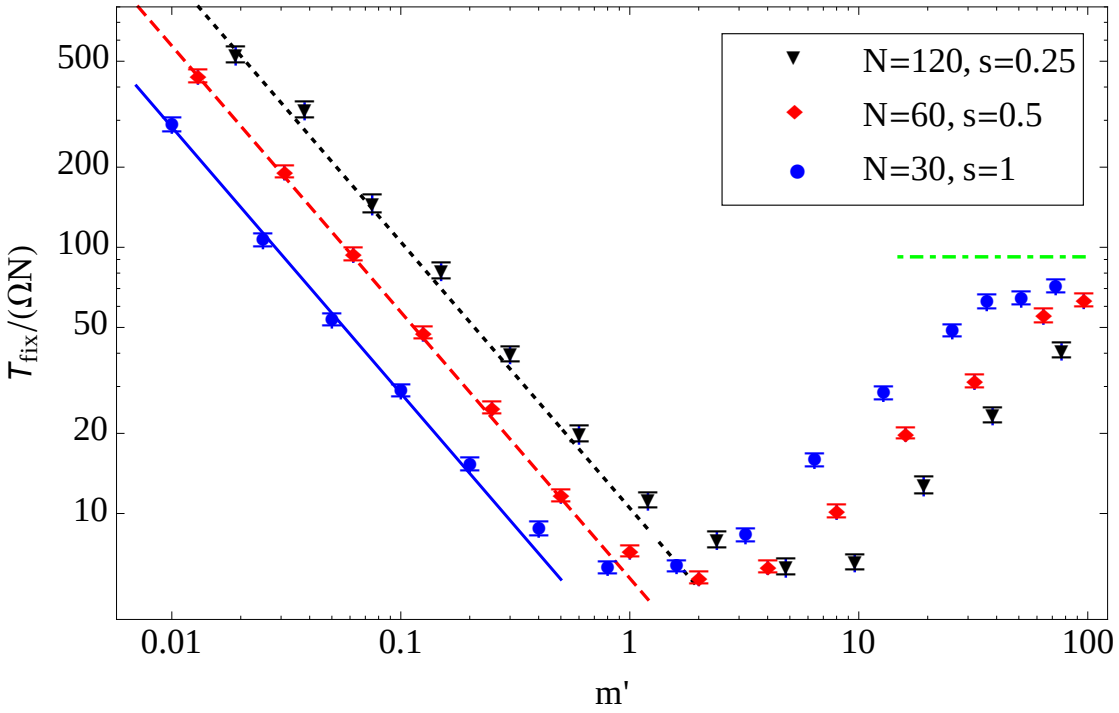

Figure 2.19: Mean fixation time as a function of the migration rate m' for the stepping stone model with balancing selection, characterized by $\Omega = 100$, $x_* = 1/2$, and by various values of N and s. Symbols with errorbars indicate the results of numerical simulations in which the single-deme dynamics is based on the Wright-Fisher model; the horizontal dot-dashed line on the right represent the estimate described in Sec. 2.6.2 for large migration rate m, while the solid, dashed, and dotted lines on the left represent the estimates for small m, based on Eq. (2.70) and obtained for $N = 30$, 60, and 120 respectively.

Figure 2.19 displays the MFT as a function of the migration rate m', obtained from numerical simulations (symbols with errorbars) of the stepping stone model in which the single-deme dynamics is based on the Wright-Fisher model with balancing selection; the population is characterized by $\Omega = 100$, $x_* = 1/2$, and by various values of N and s. The estimate of $T_{\rm fix}/(\Omega N)$ for large m discussed in Sec. 2.6.2, is represented by a dot-dashed line, while the one for small m, based on Eq. (2.70), are indicated by a solid, dashed, and dotted line, for $N = 30$, $N = 60$, and $N = 120$ respectively. A numerical interpolation renders a corrective factor $\beta \simeq 0.44$, 0.41, and 0.36 for $N = 30$, 60, and 120 respectively.

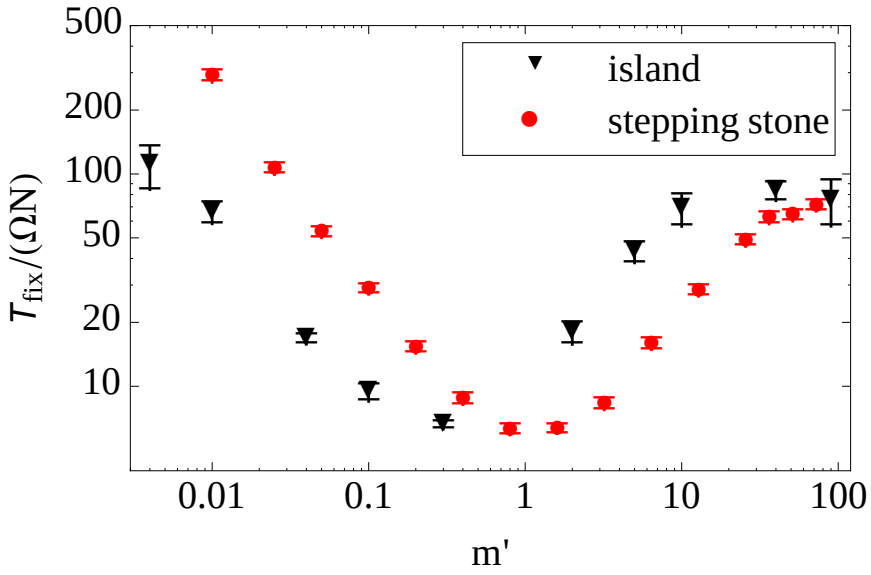

Figure 2.20: Mean fixation time as a function of the migration rate m' for the stepping stone model with balancing selection (red circles) and the island model (black triangles); in both cases the metapopulation is characterized by $\Omega = 100$, $x_* = 1/2$, $N = 30$, and $s' = 1$.

Figure 2.20 compares the dependence of the MFT on the migration rate m', as obtained from the numerical simulations of the stepping stone model (red circles) described in this section and of the island model (black triangles) described in Sec. 2.2.2; in both cases the metapopulation is characterized by $\Omega = 100$, $x_* = 1/2$, $N = 30$, and $s' = 1$. This comparison suggests that the differences between the cases of small connectivity (one-dimensional stepping stone model) and of high connectivity (island model) are quantitative but not qualitative: in both cases the MFT shows a nonmonotonic behavior, it scales as $1/m$ for small migration rate, and it approaches a horizontal plateau for large migration rate. For this reason one can heuristically expect that the same qualitative behavior carries over to metapopulations on regular structures in two and three spacial dimension, where the connectivity has intermediate values compared to the cases analyzed here.

2.7 Summary and conclusions

Balancing selection is a major mechanism responsible for promoting and maintaining biodiversity, as it favors the coexistence of different alleles in the same population. Under balancing selection, the evolution of a population might be characterized by the emergence of a long-lived metastable state (at least for sufficiently strong selection), which is eventually destabilized by stochasticity (genetic drift). When the population is subdivided in a large number of subpopulations of equal size and features, migration interacts with balancing selection and with genetic drift and determines the eventual fate of the population. In Sec. 2.2.3,

focusing on the island model [78], we have shown that, in the presence of balancing selection, the mean fixation time of a subdivided population can become a nonmonotonic function of the migration rate m. The emergence of a minimum depends on both the selection strength $\sigma \equiv s\Omega N$ exceeding a threshold and on the frequency x_* of coexistence which is promoted by the selection. While the MFT increases upon decreasing m because of the slowing down in the migration dynamics, its possible increase for sufficiently large m has a less intuitive explanation. *A posteriori* this is due to the formation of a metastable state, the "life time" of which might increase upon increasing the migration rate. Since the validity of the effective models presented in Sec. 2.2.3 relies only on the "slowness" of migration compared to the other forces driving the dynamics, these approximations could be adapted to various networks and spatial lattices (see Sec. 2.6), or even to different form of the inter-deme dynamics, as long as the migration between the demes is sufficiently slow.

In Sec. 2.3, we have shown that, as already observed above, but contrary to the heuristic expectation, balancing selection actually speeds up fixation with respect to a neutral model (i.e., a model without selection) if the allele frequency x_* promoted by balancing selection in the coexistence state is close to extinction of one of the alleles. This phenomenon, already observed in Ref. [64] for well-mixed populations, carries over to a subdivided population, where, in addition, it is responsible for the emergence of a phase transition in the limit of an infinite number N of subpopulations, each of finite size Ω. We heuristically explain this behavior in Sec. 2.3 by decomposing the effect of asymmetric balancing selection on the evolution of the mean allele frequency $\bar{x}$ as a sum of a symmetric balancing selection term $M_{\rm symm}(\bar{x})$ and a directional term $M_{\rm dir}(\bar{x})$, which favor coexistence and fixation, respectively. In fact, it turns out that $M_{\rm dir}(\bar{x})$ becomes stronger than $M_{\rm symm}(\bar{x})$ as x_* approaches one of the two boundaries $x_* = 0$ or 1, corresponding to the extinction of one of the alleles. It is then possible to characterize in detail the mean fixation time of finite populations as a function of the migration rate m and of the other relevant parameters, i.e., the selection strength s' and the optimal frequency x_*.

While the perturbative results provided in Sec. 2.2.3 are limited either to fast migration or to moderate balancing selection, we have shown in Sec. 2.5 how to extend them to slow migration and larger values of selection strength. In fact, a metapopulation with a small migration rate m can be effectively described at a coarser level by a voter model with an interaction rate proportional to the migration rate m. In Sec. 2.5.1 we demonstrate that the MFT of this effective voter model correctly reproduces the one of the original metapopulation for slow migration. However, the standard voter model fails to reproduce some qualitative features of the MFT of the subdivided population, which are recovered once we introduce into the model an additional intermediate state, corresponding to a voter with no definite opinion. This intermediate state turns out to be crucial for reproducing the nonmonotonic behavior of the MFT as a function of the migration rate; in addition, this model provides prediction for the MFT in good quantitative agreement with simulations up to larger values of the migration rate. We have also shown that an analogous nonmonotonic behavior of the MFT emerges as a function of the selection strength for a sufficiently small and fixed migration rate, in qualitative and partially quantitative agreement with numerical simulation of the microscopic model, as it can be seen in Fig. 2.17. In summary, the three-state effective

model proposed in Sec. 2.5.2 provides a coarser description of the collective behavior of the metapopulation that is useful in order to understand the mechanisms underlying the emerging phenomena observed in the population. Such a description is expected to carry over to other population models in which it is possible to identify a separation of time scales between local and global dynamics. In this respect, the metapopulation considered here has a very simple internal structure (it is a fully-connected graph), therefore it would be important to investigate whether the features discussed above are present on more general networked (or even spatially-embedded) systems and to understand their potential interplay with other dynamical phenomena, such as diffusion and coarsening.

In Sec. 2.6 we have considered a subdivided population with the same dynamics as the fully-connected model analyzed in the previous part of the chapter, but now spatially arranged on a finite ring, with migration allowed only between nearest-neighboring demes. The analysis reveals a nonmonotonicity in the MFT very similar to the one observed in the fully-connected case, strengthening thus the conclusion that this nonmonotonicity should be a quite general feature for subdivided populations with balancing selection. While in the fully connected case we traced back the origin of this nonmonotonicity to the existence of a metastable state resulting from the simultaneous interaction of a large number of demes, this behavior in the stepping stone model might be due to the formation of diffusing domains which the slow time scale is associated with. However this aspect deserves further investigation

Chapter 3

Statistical properties of tRNA binding time

This chapter is based on the results originally presented in Ref. [38].

3.1 Introduction

Recent advances in experimental physical biology are offering an unprecedented detail in the observation of the reactions occurring in living systems. In fact, single molecule sensibility techniques (see Refs. [96, 97, 98, 99, 100, 101]) are beginning to probe and unveil the intrinsic stochastic nature of life at the microscopic level. Most notably, recent *in vitro* experiments (see Refs. [102, 103]) focused on the fundamental aspects of protein translation.

Protein translation is a crucial step in gene expression, which is the process by which information from a gene in the DNA is used in order to synthetize a functional gene product, typically a protein; gene expression represents the way in which the genotype of an individual affects its phenotype (i.e., the set of all its observable characteristics). In addition, protein translation is one of the most common biochemical reactions occurring in the cell: the individual triplets of nucleotides (the codons) composing a messenger RNA (mRNA) are translated into amino acids by the ribosomes (see, for instance, Ref. [104]). This process is biologically and chemically rather well understood, but the implications of its intrinsic stochastic nature and of the presence of quantities which strongly fluctuate during the life of the cell have been not yet fully elucidated.

An intriguing question concerns the ribosome dwell time distribution (DTD), i.e., the distribution of the time intervals between two subsequent codon translation events. The form of this distribution and its dependence on the codons heavily influence the ribosome traffic along the mRNA sequences [105, 106, 107, 108], and affect the efficiency, accuracy and regulation of translation [109, 110], as well as the process of the so-called cotranslational folding (i.e., of the folding that occurs *during* the translation) of the nascent protein [111]. The translation of a codon involves several subsequent biochemical steps (see, e.g., Refs. [103, 112, 113, 114]), and the stochastic duration of each of these sub-steps is typically modeled by an exponential distribution characterized by the time scale (i.e., by the rate) of that reaction

(see Refs. [112, 114]). However, one among them (i.e., the *binding step*) requires that the ribosome binds to an additional molecular species, the transcript RNA (tRNA), which has an internal stochastic dynamics.

The tRNA molecules carry the corresponding amino acid to the ribosome, and physically recognise the codons effectively decoding the genetic code. After translation has occurred and the tRNA molecule has left the ribosome, it must be recharged with the correct amino acid[1] before it can be used again. The concurrency between these two mechanisms, consumption and recharge, determines the global fraction X of charged tRNA in the cell. The value of X is not constant during the life of the cell, and experimental evidence showed that it can significantly vary depending on the conditions and on time in a range from less than 1% up to almost 100% (see Ref. [115]). It was also shown numerically that this fact can have significant consequences on translation [116, 117]. Furthermore, the tRNA molecules have low concentrations in the cell (see, for instance, Ref. [118]): in this regime the number of tRNAs in the neighborhood of the ribosome is small, and the fluctuations in their number are relevant. The stochastic duration of the binding step (*binding time*) is directly influenced by these fluctuations, as it depends on the concentration of charged tRNA in the neighborhood of the ribosome (see Refs. [102, 119]).

In order to understand how and under which conditions the charging dynamics of tRNA can affect the binding time distribution (BTD) (i.e., the distribution of the waiting times of the ribosome for the charged tRNA), and consequently the DTD, we describe here a stochastic model which explicitly incorporates (*i*) the tRNA charging and discharging dynamics, and (*ii*) the spatial inhomogeneity and stochastic fluctuations in the number of charged tRNAs around the ribosome. This minimal model, originally presented in Ref. [38], captures these two fundamental aspects of the translation process[2]and is analytically tractable. Its solution, validated by using Monte Carlo numerical simulations, shows that the interplay between diffusion, recharging, and translation dynamics induces a coupling between the fluctuations in the number of charged and uncharged tRNAs. Due to this phenomenon, the BTD, which we obtain analytically from the model, deviates from a pure exponential, consistently with the findings in Ref. [119]. Moreover, this model asymptotically reaches a non equilibrium steady state (NESS). NESSs have attracted a lot of attention since a variety of systems in physics, chemistry, biology and engineering exhibit them, and their characterization is typically significantly more difficult than the equilibrium states (see, e.g., Refs. [120, 121, 122, 123]).

The structure of the chapter is as follows: after defining the model in Sec. 3.2, we characterize the stationary state in Sec. 3.3. The BDT is obtained in Sec. 3.4, where its main features are analyzed. In the last subsection we show how an additional biochemical step can be included, in order to get an estimate for the DTD. In Sec. 3.5, we discuss the interpretation of the parameters of the model in terms of measurable quantities and we provide, when possible, an estimate of their orders of magnitude. We conclude by summarizing and commenting our results in Sec. 3.6.

[1]The charged tRNA is a ternary complex, composed by the aminoacylated tRNA, a species-specific elongation factor, and an energy-carrying molecule (guanosine triphosphate - GTP).

[2]We did not consider secondary aspects, such as the enzymatic nature of the recharging of the tRNAs, the continuous spatial dependence of the tRNA density, or the tRNA proofreading.

3.2 The model

We model a ribosome translating an mRNA (a string of codons) into a protein (a string of amino acids), with the scope of analyzing the effects of tRNA charging dynamics and its finite availability on translation dynamics.

The fraction of charged tRNAs in the cell varies within a wide range (up to 2 orders of magnitude, depending on the tRNA species and growth conditions [115]) and exclusively affects the binding step. For this reason we focus here on this specific step, neglecting all the other biochemical reactions, which will be accounted for in Sec. 3.4.3. For simplicity, each translation event is assumed to be instantaneous: as the charged tRNA binds to the ribosome, (i) it is uncharged and released in the system, (ii) the codon is translated and the ribosome translocates to the next codon. Moreover, we treat the special case of a single tRNA species translating a single type of codons.

The ribosome consumes charged tRNAs during translation. On average, the concentration of charged tRNAs is lower close to the ribosome and rises upon moving away from it, as shown in Ref. [119]. In order to model this spatial inhomogeneity, we suppose that the ribosome can instantaneously recruit the tRNAs within a distance r from it, i.e., within a volume $V_r = 4\pi r^3/3$ around it. The tRNAs farther than r from the ribosome are considered as part of an infinite reservoir, and can diffuse closer to the ribosome. The concentrations of charged tRNAs within the volume V_r is different from that in the reservoir, and it is determined by the stochastic translation dynamics.

Let us consider a system which comprises a ribosome (translating an mRNA composed by several repeats of the same codon), n charged and m uncharged tRNAs within a distance r from it, as depicted in Fig. 3.1. Each uncharged tRNA can be recharged with rate λ_R, while each charged tRNA can bind to the ribosome with rate λ_B, becoming uncharged. We also suppose that there is a stochastic flux between the system and the infinite reservoir, i.e., that each tRNA can exit the system with rate ρ, while with rate μ ($\tilde{\mu}$) a charged (uncharged) tRNA diffuses from the reservoir into the system. We refer to ρ as the *diffusion rate*, since the exit rate from the volume V_r is determined by how fast the Brownian diffusion is (as we discuss in Sec. 3.5). This subdivision in system and reservoir encodes, in the simplest way, the spatial inhomogeneity of the charged tRNA fraction close to the ribosome.

Considering an infinitesimal time interval δt, the possible transitions (with the corresponding probabilities) are:

- $(n, m) \xrightarrow{m\lambda_R\,\delta t} (n+1, m-1)$; recharge: one uncharged tRNA gets charged.
- $(n, m) \xrightarrow{n\lambda_B\,\delta t} (n-1, m+1)$; binding: one charged tRNA gets discharged and one codon is translated.
- $(n, m) \xrightarrow{\mu\,\delta t} (n+1, m)$ and $(n, m) \xrightarrow{\tilde{\mu}\,\delta t} (n, m+1)$: a tRNA (respectively charged uncharged) enters the system from the reservoir.
- $(n, m) \xrightarrow{n\rho\,\delta t} (n-1, m)$ and $(n, m) \xrightarrow{m\rho\,\delta t} (n, m-1)$: a tRNA (respectively charged uncharged) leaves the system.

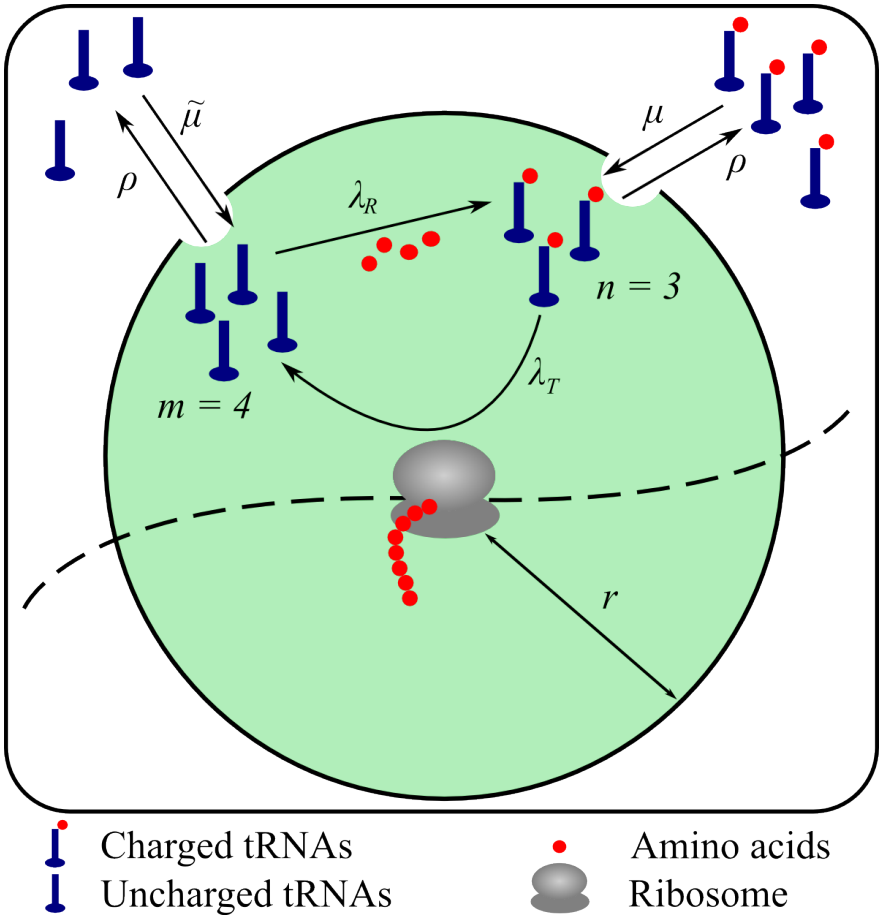

Figure 3.1: Cartoon of the model representing the possible reaction pathways. Uncharged tRNAs (blue, on the left) can either be exchanged with the reservoir or be recharged (with rate λ_R), illustrated by the addition of an amino acid (red dots). Similarly, the charged tRNAs can enter in or leave the system (green area), or bind (with rate λ_B) to the ribosome (gray), which translates an mRNA (dashed line). In the state represented here, $n = 3$ and $m = 4$.

These rates define, in general, a non-equilibrium system: the stationary state is a function of all the rates, as we show in the next section.

3.3 Stationary distribution of the number of charged tRNAs

The set of rates given in the previous section produces the following master equation for the probability $p_{n,m}(t)$ of the system being in the state characterized by the presence of n

charged and m uncharged tRNAs:

$$\begin{aligned}\dot{p}_{n,m} = {} & \lambda_R(m+1)p_{n-1,m+1}] + \lambda_B(n+1)p_{n+1,m-1}] + \mu\, p_{n-1,m} + \tilde{\mu}\, p_{n,m-1} \\ & + \rho[(n+1)p_{n+1,m} + (m+1)p_{n,m+1}] - [\lambda_R m + \lambda_B n + \mu + \tilde{\mu} + \rho(n+m)]p_{n,m}.\end{aligned} \tag{3.1}$$

We focus on the stationary state of the system by setting $\dot{p}_{n,m} = 0$. Since the system is ergodic[3], the stationary state is unique and it is reached after a relaxation time that will be discussed further below in this section.

In order to determine the stationary solution of Eq. (3.1), we introduce the generating function $G(z,w) = \sum_{n,m=0}^{\infty} p_{n,m} z^n w^m$ and we obtain

$$\lambda_R(z-w)\partial_w G + \lambda_B(w-z)\partial_z G + \rho[(1-z)\partial_z G + (1-w)\partial_w G] + \mu(z-1)G + \tilde{\mu}(w-1)G = 0, \tag{3.2}$$

the solution of which can be determined by using the method of characteristics. After imposing the condition $G(1,1) = 1$ (normalization), we have

$$G(z,w) = \exp\left[\frac{(z-1)[\lambda_R(\mu+\tilde{\mu}) + \mu\rho] + (w-1)[\lambda_B(\mu+\tilde{\mu}) + \tilde{\mu}\rho]}{\rho(\lambda_R + \lambda_B + \rho)}\right], \tag{3.3}$$

and by successive differentiation, we obtain the stationary probability

$$p_{n,m} = \left[\frac{(\partial_z)^n(\partial_w)^m}{n!\, m!} G(z,w)\right]_{\substack{z=0 \\ w=0}} = \frac{e^{-\bar{N}}\, \bar{n}^n\, \bar{m}^m}{n!\, m!}, \tag{3.4}$$

where $\bar{n}$, $\bar{m}$ and $\bar{N}$ are the mean values of the quantities n, m and $N = n + m$, respectively (with $\bar{n} + \bar{m} = \bar{N}$):

$$\begin{aligned}\bar{n} &= \langle n \rangle = \frac{\lambda_R \bar{N} + \mu}{\lambda_B + \lambda_R + \rho}, \\ \bar{m} &= \langle m \rangle = \frac{\lambda_B \bar{N} + \tilde{\mu}}{\lambda_B + \lambda_R + \rho}, \\ \bar{N} &= \langle n + m \rangle = \frac{\mu + \tilde{\mu}}{\rho}.\end{aligned} \tag{3.5}$$

The stationary distribution[4] Eq. (3.4) is a factorized Poissonian distribution in n and m: the two variables are uncorrelated *at the same time* (we anticipate here that this is not true at *different times*, as we show in Sec. 3.4).

Using the last of Eqs. (3.5), the parameters μ and $\tilde{\mu}$ can be conveniently expressed in terms of the diffusion parameter ρ and of the mean tRNA number $\bar{N}$:

$$\begin{aligned}\mu &= X\bar{N}\rho, \\ \tilde{\mu} &= (1-X)\bar{N}\rho,\end{aligned}$$

[3] According to Eq. (3.1), any state (n,m) can be reached by any other.

[4] Note that, since detailed balance does not hold in general, the system is out of equilibrium and it is not obvious how to predict a priori the stationary distribution (see, e.g., Refs. [121, 122]).

where we introduced the parameter $0 \leq X \leq 1$ which measures the fraction of charged tRNA in the reservoir. Note that X was measured *in vivo* in Ref. [115], and that, depending on the richness of the growth media, it spans the interval $X \simeq 10^{-3} \div 10^{0}$.

In order to simplify the notation, let us rescale the time such that $\lambda_B = 1$, and set $\lambda_R = \lambda$. Let us also introduce the mean fraction x of charged tRNAs into the system:

$$x \equiv \frac{\lambda + X\rho}{1 + \lambda + \rho}. \tag{3.6}$$

In these terms, the mean values for n and m can be expressed as $\bar{n} = \bar{N}x$ and $\bar{m} = \bar{N}(1-x)$.

These quantities and the stationary distribution in Eq. (3.4) behave as expected in the limit $\rho \to \infty$: the system is at equilibrium with the cell and the mean fraction x of charged tRNA therein coincides with the fraction X in the cell: $x = X$. On the other hand, if $\rho \to 0$, the diffusion is much slower than binding, and the mean number of charged tRNAs is completely determined by the internal dynamics: $x = \lambda(1+\lambda)^{-1}$. In this case the effect of diffusion amounts at a slow but not negligible fluctuation of the tRNA number $N = n + m$.

The exponential relaxation to the stationary distribution is ruled by the two time scales $t_1 = \rho^{-1}$ and $t_2 = (\lambda + \rho + 1)^{-1}$ (with $t_1 > t_2$), which are deduced from the time-dependent solution of Eq. (3.1) (see App. C.1 for details). The stationary state is reached when the observation time T_{obs} is larger than the largest of these time scale: $T_{\text{obs}} \gg \rho^{-1}$.

Finally, we observe that the detailed balance condition is satisfied only for $\rho = 0$ (i.e., in the absence of diffusion), or for $\lambda = X/(1-X)$ (see App. C.2 for the proof). In the latter case the stationary mean values for the charged fraction of tRNA of both the internal and the diffusive dynamics coincide, and $x = X$. Apart from these two special points, the stationary state is a non-equilibrium one.

3.4 Statistics of binding times

Since every charged tRNA gives a unitary contribution (remember that we set $\lambda_B = 1$) to the total binding rate, the mean binding time per codon predicted by this model is simply $1/\bar{n}$. In general, however, when the distribution is not exponential, the mean does not fully characterize the behavior of the random variable. In this section we therefore calculate analytically the probability density function for the time intervals between two subsequent binding events.

The derivation is carried out by writing down a master equation which accounts for an auxiliary variable s which counts the number of time steps elapsed since the last binding event (see below). This procedure allows the calculation of the cumulative distribution of the binding times and finally of the binding time distribution.

Let us consider a discrete-time dynamics where δt is the unit time interval. The state of the system is described by $(n, m; s)$, where the counter s, at each time interval, is either set to zero if a binding event occurs, or increased by one otherwise. Without loss of generality, we set $\lambda_B = 1$ from the outset. The possible transitions are:

- $(n, m; s) \xrightarrow{m\lambda\,\delta t} (n+1, m-1; s+1)$: one uncharged tRNA gets recharged

- $(n,m;s) \xrightarrow{n\,\delta t} (n-1,m+1;0)$: one codon is translated and one charged tRNA gets discharged
- $(n,m;s) \xrightarrow{\mu\,\delta t} (n+1,m;s+1)$ and $(n,m;s) \xrightarrow{\tilde{\mu}\,\delta t} (n,m+1;s+1)$: a tRNA (respectively charged uncharged) enters the system from the reservoir
- $(n,m;s) \xrightarrow{n\rho\,\delta t} (n-1,m;s+1)$ and $(n,m;s) \xrightarrow{m\rho\,\delta t} (n,m-1;s+1)$: a tRNA (respectively charged uncharged) leaves the system to the reservoir
- $(n,m;s) \xrightarrow{1-\delta t[n+\lambda m+\mu+\tilde{\mu}+\rho n+\rho m]} (n,m;s+1)$: nothing happens and the counter s is increased.

This set of rates leads to the discrete-time master equation for the probability $q_{n,m;s}(t)$ of being in the state $(n,m;s)$ at time t

$$\begin{aligned}\frac{q_{n,m;s}(t+\delta t)}{\delta t} &= \lambda(m+1)\,q_{n-1,m+1;s-1}(t) + \mu\,q_{n-1,m;s-1}(t) + \tilde{\mu}\,q_{n,m-1;s-1} + \\ &+ \rho(n+1)q_{n+1,m;s-1}(t) + \rho(m+1)q_{n,m+1;s-1} + \frac{q_{n,m;s-1}(t)}{\delta t} + \\ &- \big[n+\lambda m+\mu+\tilde{\mu}+\rho n+\rho m\big]q_{n,m;s-1}(t) + \delta_{s,0}\sum_{s'=0}^{\infty}(n+1)q_{n+1,m-1;s'}(t). \quad (3.7)\end{aligned}$$

In order to obtain a well-defined limit for $\delta t \to 0$, we set $\tau = s\delta t$, such that $q_{n,m;s}(t+\delta t) \to q_{n,m}(\tau,t) + \delta t\partial_\tau q_{n,m}(\tau,t)$, $q_{n,m;s-1}(t) \to q_{n,m}(\tau,t) - \delta t\partial_\tau q_{n,m}(\tau,t)$ and Eq. (3.7) results in the following partial differential equation:

$$\begin{aligned}\partial_t q_{n,m}(\tau,t) &= -\partial_\tau q_{n,m}(\tau,t) + \lambda(m+1)q_{n-1,m+1}(\tau,t) - (n+\lambda m)q_{n,m}(\tau,t) + \\ &+ \rho\big[(n+1)q_{n+1,m}(\tau,t) + (m+1)q_{n,m+1}(\tau,t) - (n+m)q_{n,m}(\tau,t)\big] + \mu\,q_{n-1,m}(\tau,t) + \\ &+ \tilde{\mu}\,q_{n,m-1}(\tau,t) - (\mu+\tilde{\mu})q_{n,m}(\tau,t) + (n+1)\delta(\tau)p_{n+1,m-1}(t), \quad (3.8)\end{aligned}$$

where $p_{n,m}(t) = \int_0^\infty d\tau\, q_{n,m}(\tau,t)$ is the solution of Eq. (3.1). The differential equation for the stationary probability is obtained by setting $\partial_t q_{n,m}(\tau,t) = 0$, and it reads

$$\begin{aligned}\partial_\tau q_{n,m}(\tau) &= \lambda(m+1)q_{n-1,m+1}(\tau) - (n+\lambda m)\,q_{n,m}(\tau) + \rho\Big[(n+1)q_{n+1,m}(\tau) + \\ &+ (m+1)q_{n,m+1}(\tau) + X\bar{N}\,q_{n-1,m}(\tau) + (1-X)\bar{N}\,q_{n,m-1}(\tau) + \\ &- (n+m+\bar{N})q_{n,m}(\tau)\Big] + \delta(\tau)\,\alpha_{n+1,m-1}, \quad (3.9)\end{aligned}$$

where $\alpha_{n,m} = n\,p_{n,m}$ and $p_{n,m}$ is provided by Eq. (3.4).

Similarly to the previous case, we introduce the generating function

$$G(z,w;\tau) = \sum_{n=0}^{\infty}\sum_{m=0}^{\infty} q_{n,m}(\tau)z^n w^m, \quad (3.10)$$

and Eq. (3.9) becomes

$$\partial_\tau G = \lambda(z-y)\partial_y G - z\partial_z G + \rho\Big[(1-z)\partial_z + (1-w)\partial_w + \bar{N}X(z-1) + \bar{N}(1-X)(w-1)\Big]G + \delta(\tau)f(z,w), \quad (3.11)$$

where

$$f(z,w) = \sum_{n=0}^{\infty}\sum_{m=1}^{\infty} \alpha_{n+1,m-1} z^n w^m = \bar{n}\, w\, \exp[\bar{n}(z-1) + \bar{m}(w-1)]. \quad (3.12)$$

Although Eq. (3.11) could be solved in full generality, here we are interested in the particular value $G(1,1,\tau_*)$, because it coincides with the probability density

$$Q(\tau_*) = \sum_{n,m=0}^{\infty} p_{n,m}(\tau_*) \quad (3.13)$$

to find a value τ_* for the auxiliary variable τ. This distribution is particularly interesting, since it is proportional to the probability $P(\tau_*)$ for the time interval between two subsequent binding events to be larger than τ_*. In fact, the probability $Q(\tau_*)$ to find a value τ_* for the auxiliary variable τ is proportional to the mean number of times the function $\tau(t)$ exceeds the value τ_* within the observation time, i.e., to the mean number of binding times with a duration larger than τ_*, as depicted in Fig. 3.2. The fraction $Q(\tau_*)/Q(0)$ represents therefore the mean fraction of binding events with duration larger than τ_*, i.e., $P(\tau_*) = Q(\tau_*)/Q(0)$.

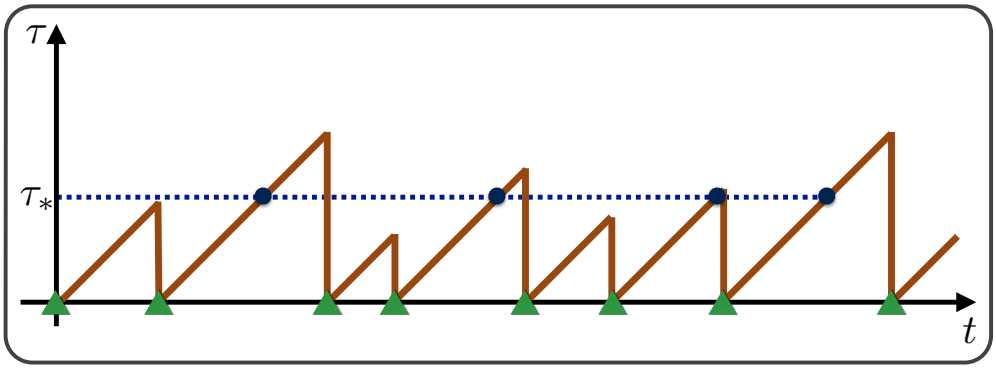

Figure 3.2: Schematic representation of the value of the auxiliary variable τ as a function of the time t. After each binding event (green triangle on the t-axis), $\tau(t)$ increases linearly in time, until another binding occurs. The probability density $Q(\tau_*)$ to find the auxiliary variable with a value τ_* is proportional to the mean number of binding times with a duration larger than τ_*.

By solving Eq. (3.11) with $w = z$, we obtain the generating function $G(z,z;\tau)$ and the

probability $P(\tau)$

$$P(\tau) = \left[R + \frac{\lambda}{\lambda - 1}\left(\frac{e^{-\tau(\rho+1)}}{\rho+1} - \frac{e^{-\tau(\rho+\lambda)}}{\rho+\lambda}\right)\right] e^{-\tau R\bar{N}x} \times \exp\left[\frac{\lambda\bar{N}x}{\lambda-1}\left(\frac{e^{-\tau(\rho+1)}-1}{(\rho+1)^2} - \frac{e^{-\tau(\rho+\lambda)}-1}{(\rho+\lambda)^2}\right)\right], \quad (3.14)$$

where

$$R = \frac{\rho(\rho+\lambda+1)}{(\rho+1)(\rho+\lambda)} \quad (3.15)$$

is always smaller than 1, and x is the fraction of charged tRNAs in the system, given by Eq. (3.6).

For further reference, note that the function $P(\tau)$ can be written as $P(\tau) = \partial_\tau A(\tau)$, with

$$A(\tau) = -\frac{1}{\bar{N}x}\exp\left[-\tau R\bar{N}x + \frac{\lambda\bar{N}x}{\lambda-1}\left(\frac{e^{-\tau(\rho+1)}-1}{(\rho+1)^2} - \frac{e^{-\tau(\rho+\lambda)}-1}{(\rho+\lambda)^2}\right)\right]. \quad (3.16)$$

Let us now observe that $P(\tau)$ is the complement of the cumulative distribution for the BTD $p(t)$, which is therefore given by

$$p(t) = -\partial_\tau P(\tau)|_{\tau=t}. \quad (3.17)$$

Some realizations of $p(t)$ are shown in Fig. (3.3), where we also compare the analytical prediction of the stationary distribution in Eq. (3.17) with the numerical Monte Carlo simulations of the dynamics described by Eq. (3.7). We did not observe any significant deviation between the theoretical results and the simulations. Interestingly enough, for small times and small values of $\bar{N}$, the BTD deviates significantly from an exponential (as highlighted in the log-plot insets of Fig. 3.3). On the other hand, these deviations are milder for small values of λ and large values of ρ. The relevant features of $p(t)$ are analyzed in the next section.

3.4.1 Characterization of the binding time distribution

In order to characterize the binding time distribution $p(t)$, we calculate its first two moments. We compare the second moment of the BTD with that of an exponential distribution having the same mean, observing that the BTD is overdispersed with respect to the latter distribution.

The first moment — i.e., the mean of the BTD — is given by

$$\langle t\rangle = \int_0^\infty \mathrm{d}t\, tp(t) = \int_0^\infty \mathrm{d}\tau\, P(\tau) = \frac{1}{\bar{N}x}, \quad (3.18)$$

and coincides with the inverse of the mean number $\bar{n}$ of charged tRNAs in the system, as expected. The second moment is given by

$$\langle t^2\rangle = \int_0^\infty \mathrm{d}t\, t^2 p(t) = 2\int_0^\infty \mathrm{d}t\, tP(t) = -2\int_0^\infty \mathrm{d}t\, A(t), \quad (3.19)$$

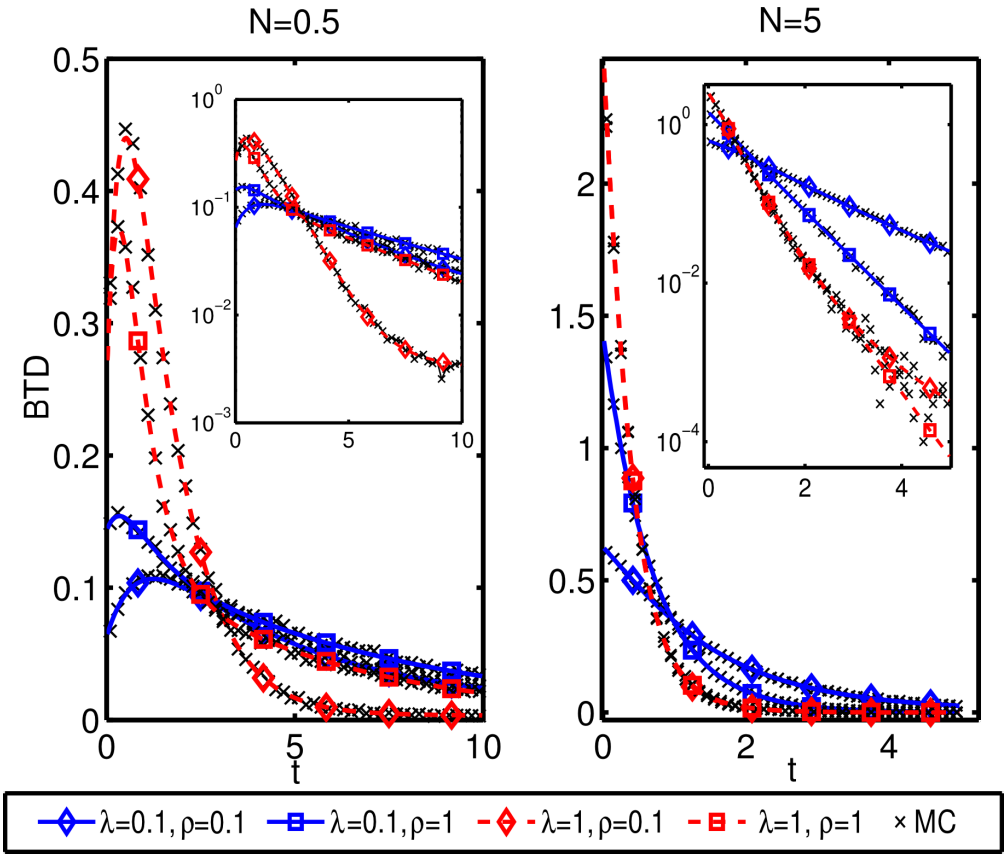

Figure 3.3: Probability density function $p(t)$ of the binding time (BTD) for various choices of the parameters λ (blue and solid lines for $\lambda = 0.1$, red and dashed lines for $\lambda = 1$), ρ (diamonds for $\rho = 0.1$, squares for $\rho = 1$) and $\bar{N}$ ($\bar{N} = 0.5$ in the left panel, $\bar{N} = 5$ in the right one). The parameter X is kept fixed to 0.5. The black crosses are the results of Monte Carlo simulations, and do not show any significant deviation from the theoretical predictions. As the two log-plot insets show, deviations from a pure exponential (which would correspond to a straight line) are marked for small $\bar{N}$, where the fluctuations play a relevant role.

where $A(t)$ is given by Eq. (3.16), and can be written as

$$\langle t^2 \rangle = \frac{2}{\bar{N}x} \exp\left[\frac{\lambda \bar{N}x}{\lambda - 1}\left(\frac{1}{(\rho+\lambda)^2} - \frac{1}{(\rho+1)^2}\right)\right] \times \int_0^1 dy\, y^{R\bar{N}x-1} \exp\left[\frac{\lambda \bar{N}x}{\lambda - 1}\left(\frac{y^{\rho+1}}{(\rho+1)^2} - \frac{y^{\rho+\lambda}}{(\rho+\lambda)^2}\right)\right]. \quad (3.20)$$

Equation (3.20) can be numerically evaluated in order to determine the variance $\sigma_t^2 = \langle t^2 \rangle - \langle t \rangle^2$. In Fig. 3.4 we plot the ratio $\sigma_t^2/\sigma_{\rm exp}^2$ for various values of the parameters, where $\sigma_{\rm exp}$ is the variance of the exponential distribution

$$p_{\rm exp}(t) = x\bar{N}e^{-x\bar{N}t}, \quad (3.21)$$

fixed to having the same mean as the BTD. By inspection, we did not find any point in the parameter space such that $\sigma_t < \sigma_{\rm exp}$: the BTD is overdispersed with respect to the exponential distribution in Eq. (3.21). This observation can be further characterized by comparing the small and large t expansions of the two distributions: first, by analyzing the Taylor expansion around $t = 0$ of the two probability distributions, we observe that $p(t) - p_{\rm exp}(t) \sim \lambda t + O(t^2)$. Short binding times are under represented in the exponential distribution. Also note that for $\lambda = 0$ the two distributions coincide and the ratio $\sigma_t/\sigma_{\rm exp} = 1$, as shown in Fig. 3.4.

The tails of the two distributions also differ at large times. For $t \to \infty$, in fact, Eq. (3.17) behaves as

$$p(t) \propto e^{-Rx\bar{N}t}. \tag{3.22}$$

Comparing this expression with Eq. (3.21) and noting that $R < 1$ (by definition), we see that large binding times are under represented in the exponential distribution.

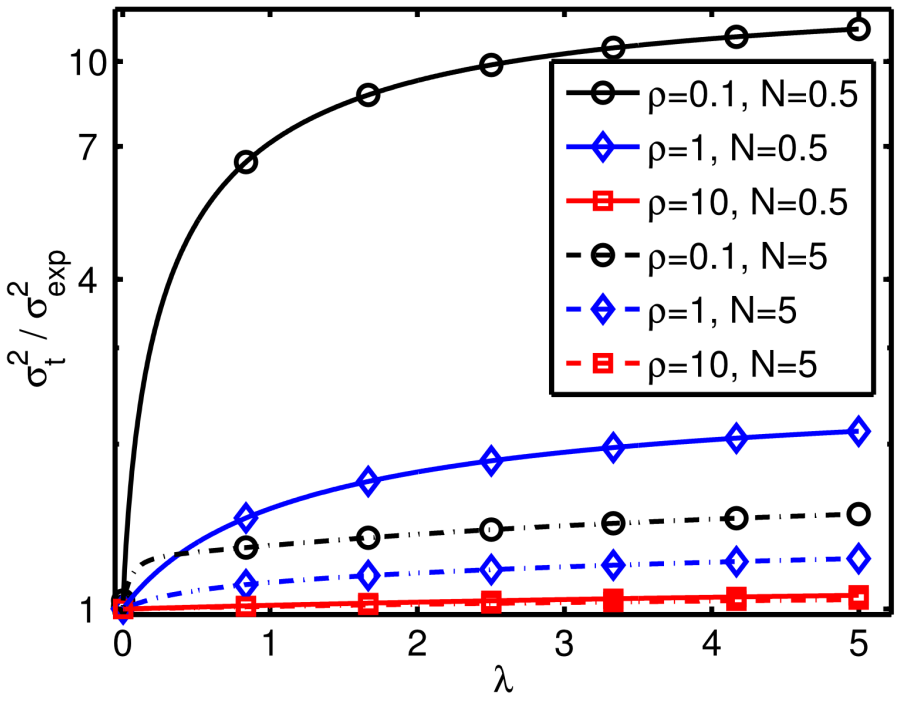

Figure 3.4: Ratio between the variances σ_t^2 of the BTD, and $\sigma_{\rm exp}^2$ of the exponential with the same mean Eq. (3.21), as a function of λ, for various values of $\bar{N}$ and ρ (the specific value of the parameter X does not change qualitatively the results and is set to $X = 1/2$). For $\lambda \to 1$ the BTD converges to an exponential distribution, as shown by Eq. (3.23), and the ratio $\sigma_t^2/\sigma_{\rm exp}^2 \to 1$. In general, however, the BTD is over dispersed with respect to the exponential distribution.

Finally, the BTD in Eq. (3.17) reduces to an exponential for small recharge rate $\lambda \to 0$,

where

$$p(t) \to x\bar{N}e^{-x\bar{N}t}, \tag{3.23}$$

and in the fast diffusion limit $\rho \to \infty$:

$$p(t) \to X\bar{N}e^{-X\bar{N}t}. \tag{3.24}$$

In the latter case, the charged fraction x of tRNA in the system coincides with the fraction X in the reservoir, consistently with the expectation that in the fast diffusion limit the fluctuations of charged tRNAs are determined by the exchange with the bath and are uncorrelated in time. As we show in the next section, these two limits have an interesting physical interpretation.

3.4.2 Time-correlations of n and m

Here we show that the deviation of the BTD from an exponential arises due to a nontrivial coupling between the fluctuations of n and m.

First, let us introduce the mean value $\langle n(t)\rangle_{\rm nb}$ of n at time t after a binding event (the binding happened at time 0), conditioned to the fact that no other binding events were recorded up to time t. The BTD is related to $\langle n(t)\rangle_{\rm nb}$ by

$$p(t) = \langle n(t)\rangle_{\rm nb} \exp\left(-\int_0^t \mathrm{d}t' \, \langle n(t')\rangle_{\rm nb}\right), \tag{3.25}$$

as proven in App. C.3. Quite interestingly, Eq. (3.25) shows that the deviations from an exponential of the BTD appear as soon as $\langle n(t)\rangle_{\rm nb}$ departs from a constant and acquires a time dependence.

In the stationary regime, a binding event occurs with probability proportional to np_n, where $p_n = \sum_{m=0}^{\infty} p_{mn}$ is the marginal stationary probability for n, obtained from Eq. (3.4). More precisely, the distribution for n at the instant before a binding event is:

$$p_n^{\rm b^-} = \frac{\bar{n}^{n-1}}{(n-1)!}e^{-\bar{n}}, \tag{3.26}$$

with mean $\bar{n}_{\rm b^-} = \bar{n} + 1$: a binding event typically occurs when a fluctuation increases the number of charged tRNAs close to the ribosome (i.e., within the volume V_r). Note that the number m of uncharged tRNAs is not influenced. Because of the translation event $n \to n-1$ and $m \to m+1$, and therefore, immediately after translation, $\bar{n}_{\rm b^+} = \bar{n}$ and $\bar{m}_{\rm b^+} = \bar{m} + 1$: the fluctuation on n has propagated to m. Now, if $\lambda > 0$ and $\rho < \infty$, this fluctuation can again propagate to n with a characteristic time scale, producing a loop which induces a time dependence in $\langle n(t)\rangle_{\rm nb}$. This mechanism is suppressed if $\lambda = 0$ and it is negligible if $\rho \to \infty$. In the former case, in fact, the dynamics of n is not affected by the dynamics of m (as it can easily be seen from the rates described at the beginning of Sec. 3.2). This intuition is confirmed by the numerical simulations in Fig 3.5, where it is shown that the mean $\langle n(t)\rangle_{\rm nb}$ reduces to a constant for $\lambda \to 0$. For $\rho \to \infty$ the fluctuations on m are immediately dissipated in the thermal bath before they can propagate back to n.

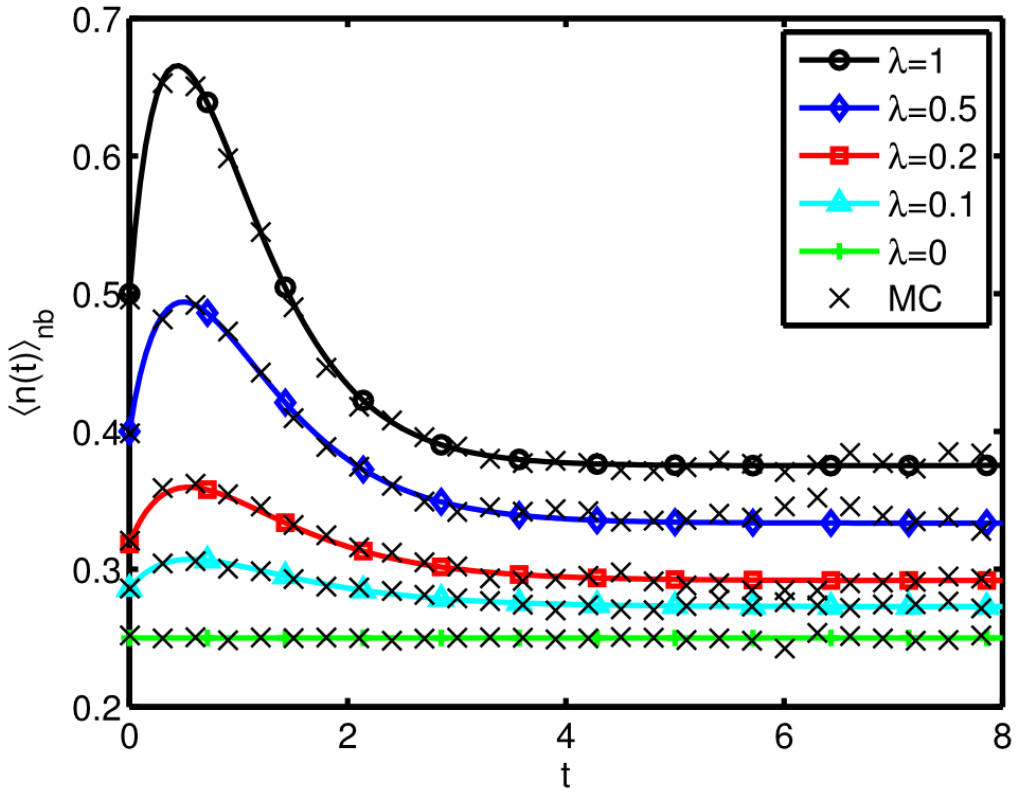

Figure 3.5: Mean number of charged tRNAs in the system $\langle n(t)\rangle_{\rm nb}$ conditioned to the fact that no binding event occurred up to time t after the one at $t = 0$, plotted for various values of λ, estimated analytically (see Eq. (C.19), solid lines), and numerically by Monte Carlo simulations (black crosses). The other parameters were set to $\bar{N} = 1$, $\rho = 1$ and $X = 1/2$. As λ approaches 0, the function $\langle n(t)\rangle_{\rm nb}$ becomes independent of time.

As a further check, we can quantify the influence of m at a given time on the future dynamics of n — and vice versa — by studying the two-time correlators

$$C_{mn}(t) \equiv \langle m(0)n(t)\rangle - \bar{n}\bar{m} = \bar{m}\lambda\frac{e^{-\rho t} - e^{-t(\lambda+\rho+1)}}{\lambda+1}, \tag{3.27}$$

$$C_{nm}(t) \equiv \langle n(0)m(t)\rangle - \bar{n}\bar{m} = \bar{n}\frac{e^{-\rho t} - e^{-t(\lambda+\rho+1)}}{\lambda+1}, \tag{3.28}$$

which are derived in App. C.1.

The correlation between $m(\tau)$ and $n(\tau + t)$ in Eq. (3.27) vanishes identically for $\lambda = 0$ or $\rho \to \infty$. The dynamics of n decouples from that of m because the fluctuations of m cannot propagate to n. Note, however, that the reverse is not true: the two variables are not independent when $\lambda = 0$, as shown by the fact that the correlator $C_{nm}(t)$ in Eq. (3.28) does not vanish. On the other hand, for $\lambda > 0$ and $\rho < \infty$, the correlator Eq. (3.27) is a linear combination of two exponentials with different decay times. It is not monotonic in

t, as it vanishes at $t = 0$ (as expected from the factorisation of the stationary probability) and has a maximum for $t = (1 + \lambda)^{-1} \log[\rho^{-1}(\lambda + \rho + 1)]$. The fact that $C_{nm}(t) \neq C_{mn}(t)$ implies that time reversal symmetry is broken; this highlights the nonequilibrium nature of this stationary process, which is further analyzed in App. C.2.

Let us finally observe that the finding of an exponential BTD in the limits $\lambda = 0$ and $\rho \to \infty$ is coherent with the absence of memory in the time series of n in the same limits. The BTD, indeed, is directly dependent only on the time series of n, and not on m. In the process in which only the n variable is observed (i.e., the projection of the original process on the n variable) the information on m is lost. In general, the future evolution of n is not completely determined by its present state, i.e., the projection on the n variable of the process is not Markovian. In the two limits $\lambda = 0$ and $\rho \to \infty$, however, n is effectively decoupled from the evolution of m: the time-series of n is Markovian and memoryless, and the BTD is exponential, as the exponential is the only memoryless continuous distribution [124]. The complete model, however, is always Markovian, as its time evolution exclusively depends on the current state (n, m) and not on the past history.

3.4.3 Additional biochemical steps

The derivation of the BDT $p(t_B)$ reported in Eq. (3.17) was carried out in the limit where the binding step is rate limiting, i.e., by neglecting the additional biochemical steps which are required to translate a codon [112, 114]. Here we show how these additional steps can be accounted for by using a simple approximation, under the assumption that a time distribution describing their duration is known.

Let us split the dwell time t_D of the ribosome into the binding time t_B, and the time t_A taken by the additional biochemical reactions, such that $t_D = t_B + t_A$, as schematically depicted in Fig. 3.6. As a first approximation, let us assume that t_A is described by a Poisson process with rate λ_A, modeling one additional biochemical step. Accordingly, the times t_A are drawn from the exponential distribution

$$p_A(t_A) = \lambda_A e^{-\lambda_A t_A}. \tag{3.29}$$

During t_A the binding is suppressed, while recharge and exchange with the reservoir continue normally. Since the value of t_A influences the tRNA charging level in the binding step, the two time intervals t_A and t_B are not independent random variables, and we expect that the distribution $p(t_B)$ is no longer accurately described by Eq. (3.17).

The influence of t_A on Eq. (3.17) can be effectively treated by rescaling the rates to the effective values

$$\lambda^{\mathrm{e}} = \gamma\lambda, \quad \rho^{\mathrm{e}} = \gamma\rho, \tag{3.30}$$

with

$$\gamma = \frac{\bar{t}_A + \bar{t}_B}{\bar{t}_B}, \tag{3.31}$$

where $\bar{t}_A$ and $\bar{t}_B$ are the mean values of t_A and t_B, respectively. This amounts at assuming that recharge and diffusion occur during the binding step only, with effective rates given by

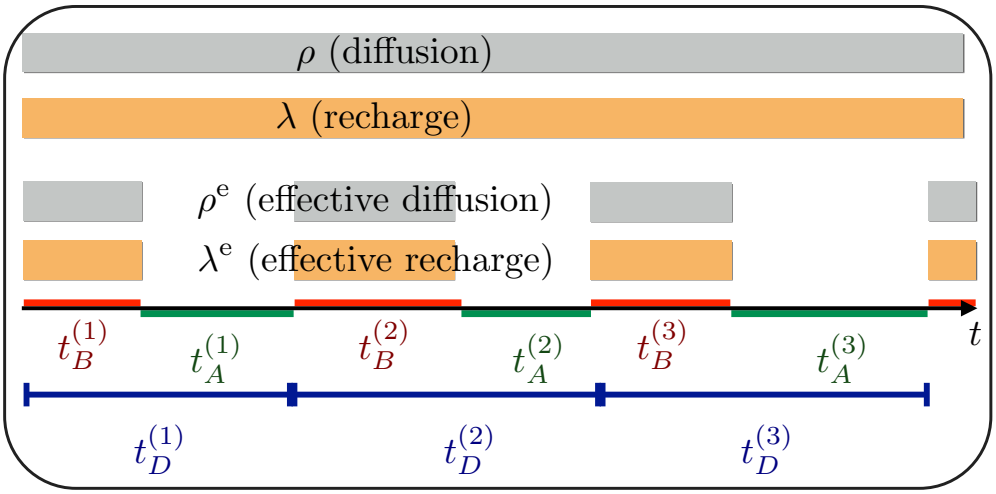

Figure 3.6: Schematic representation of the alternation between binding steps (of duration $t_B^{(i)}$) and "additional steps" ($t_A^{(i)}$); recharge and diffusion occur with a rate λ and ρ, respectively, independently of the ribosome being involved in a binding or in an "additional" process. However, the process can be described in terms of effective recharge and effective migration, occurring only during the binding process with rates λ^{e} and ρ^{e}, respectively, given in Eq. (3.30).

Eq. (3.30), as schematically depicted in Fig. 3.6. This simplified approach is most accurate if $\bar{t}_B \gg \bar{t}_A$ (i.e., when the binding step is rate limiting [125]) or if $\bar{t}_B \gg 1/\rho$ (i.e., when diffusion is very fast and therefore, after each translation, $n(t)$ quickly reaches its stationary value).

The mean binding time $\bar{t}_B$ in Eq. (3.31) can be calculated by plugging the effective parameters λ^{e} and ρ^{e} in Eq. (3.18), and by substituting this value into Eq. (3.31). Then, solving the equation for $\gamma(\lambda^{\mathrm{e}}, \rho^{\mathrm{e}})$, and substituting this value in Eqs. (3.30), we obtain the bare parameters (ρ, λ) as functions of the rescaled ones (ρ^{e}, λ^{e}). By inverting these relations, we calculate the rescaling factor γ as a function of the rate λ_A and of the bare parameters:

$$\gamma = \frac{k + \sqrt{k^2 + 4(\lambda + \rho)}}{2(\lambda + \rho)}, \tag{3.32}$$

where $k = \lambda + \rho - 1 + \bar{N}(\lambda + \rho X)/\lambda_A$.

In general, the distribution of the *dwell time* $t_D = t_A + t_B$ can be obtained by convolving the probability distributions for t_A and t_B. Here we use the exponential distribution Eqs. (3.29) and (3.17), respectively, which produce

$$\begin{aligned} p_{\mathrm{D}}(t_D) &= \int_0^{t_D} dt_B\, p(t_B) p_A(t_D - t_B) \\ &= \lambda_A \left[e^{-\lambda_A t_D} \left(1 + \lambda_A \int_0^{t_D} dt_B\, e^{\lambda_A t_B} P(t_B) \right) - P(t_D) \right] \end{aligned} \tag{3.33}$$

Table 3.1: Data for E.Coli.

Typical radius of a ribosome [1]	$L_R \simeq 1 \times 10^{-8}\,\mathrm{m}$
Molar concentration of the tRNA [2]	$c_\mathrm{t} \simeq (0.3 \div 30) \times 10^{-6}\,\mathrm{M}$
Number concentration of the tRNA [2]	$C_\mathrm{t} \simeq (1.8 \div 180) \times 10^{20}\,\mathrm{m}^{-3}$
Diffusion constant of the tRNA [3]	$D \simeq (0.2 \div 2) \times 10^{-12}\,\mathrm{m^2 s^{-1}}$
Mean translation rate [4]	$\Theta \simeq (10 \div 20)\,\mathrm{codons\,s^{-1}}$
Codon length	$\ell_\mathrm{cod} \simeq 1\,\mathrm{nm}$
Total binding rate [5]	$\lambda_B^\mathrm{tot} \simeq x c_\mathrm{t} \times 110\,(\mu\mathrm{M\,s})^{-1}$

[1] From Ref. [126].
[2] Considering a single species of tRNA, from Ref. [118].
[3] From Ref. [127].
[4] From Ref. [128].
[5] From Ref. [112]; note that xc_t is the molar concentration of a charged tRNAs of a specific species.

where $P(t)$ is the cumulative distribution of binding times provided by Eq. (3.14).

Note that the mean dwell time $\bar{t}_D$ is simply the sum of the mean binding time $\bar{t}_B$ and the mean time $\bar{t}_A$ for the additional biochemical steps, i.e.,

$$\bar{t}_D = \frac{\rho^\mathrm{e} + \lambda^\mathrm{e} + 1}{\bar{N}(\lambda^\mathrm{e} + \rho^\mathrm{e} X)} + \frac{1}{\lambda_A}. \tag{3.34}$$

This is in agreement with the heuristic intuition based on the fact that $t_D = t_A + t_B$, as schematically depicted in Fig. 3.6.

3.5 Discussion and interpretation of the parameters

In order to understand the physical implications of the findings reported in the previous sections, it is necessary to obtain an estimate of the parameters ρ, $\bar{N}$, X, λ_R and λ_B in terms of physical and biological measurable quantities.

Let us first consider the effective volume V_r around the ribosome, introduced in Sec. 3.2. This volume is delimited by a radius r which corresponds to the maximal distance from the ribosome such that a tRNA has a non-negligible probability of diffusing towards (and being captured by) the ribosome. As shown in Ref. [129], the probability of being absorbed by a target of radius L_R centered at the origin, for a point-like random walker starting from radius r', is L_R/r'. Therefore, we expect that r is of the same order of magnitude as the ribosome radius L_R, i.e., $r = \omega L_R$, with $1 < \omega < 10$.

The mean number of a certain species of tRNAs is found by fixing the concentration in the volume V_r to be the same as in the cell (C_t). We obtain $\bar{N} = V_r C_\mathrm{t} \simeq \omega^3(10^{-3} \div 10^{-1})$. The wide range of variation is due to two facts: first, different species of tRNA have very different concentrations. Second, the concentration of a given species of tRNA changes accordingly to the variation in the environmental conditions experienced by the cell.

The parameter X measures the fraction of charged tRNAs in the cell. Its range, measured *in vivo* for E. Coli in Ref. [115], spans the interval $X \simeq 10^{-3} \div 10^{0}$, depending on the richness of the growth media. A dynamic range was also observed in numerical simulations [116].

The tRNA exchanges between system and reservoir are ruled by ρ, which can be obtained in terms of the diffusion constant D of the tRNA molecules, the ribosome velocity $v_{\rm rib}$ and the system size r. Assuming that each tRNA performs a Brownian motion, its mean square displacement in the time T is $\ell^2 = \langle \sum_i \Delta x_i^2 \rangle = 6DT$, and the typical exit time from the sphere of radius r is

$$T_{\rm exit} = \frac{r^2}{6D}. \tag{3.35}$$

Neglecting the ribosome motion, we equate $T_{\rm exit}$ to the mean exit time $1/\rho$ in the stochastic model, obtaining

$$\rho = \frac{6D}{r^2} \simeq \omega^{-2}(1 \div 70) \times 10^3\,{\rm s}^{-1}. \tag{3.36}$$

The motion of the ribosome produces an additional flux[5] $\rho_T \simeq v_{\rm rib}/r$. Using the data in Tab. 3.1, the ribosome speed reads $v_{\rm rib} = \Theta \ell_{\rm cod} \simeq (10 \div 20)\,{\rm nm/s}$. This produces $\rho_T \simeq \omega^{-1}(1 \div 2)\,{\rm s}^{-1}$, which is negligible compared to the estimate in Eq. (3.36).

The binding rate λ_B can be obtained by equating the total binding rates in our model ($\bar{n}\lambda_B$) with the experimental one, adapted from Ref. [112] ($\lambda_B^{\rm tot}$, in Tab. 3.1). Solving for λ_B produces the estimate $\lambda_B = \lambda_B^{\rm tot}/(xC_{\rm t}V_r) \simeq 4 \times 10^4 \omega^{-3}\,{\rm s}^{-1}$.

The rate λ_A can be readily estimated from the rates of the biochemical steps in Ref. [112] to be $\lambda_A \simeq 1.26\,{\rm s}^{-1}$. However, this value is not compatible with the mean translation rate Θ measured *in vivo* for E.Coli. In fact, as reported in Tab. 3.1, $\Theta \simeq (10 \div 20)\,{\rm cod/s}$, while from Eq. (3.34), we expect that $1/\Theta = \bar{t} \geq 1/\lambda_A$. This lack of consistency between different measures (which also affects negatively the estimate of the rescaling factor, which, from Eq. (3.31), is $\gamma = \lambda_A/(\lambda_A - \Theta)$) could be due to the fact that the rates in Ref. [112] were obtained *in vitro*.

The last unknown parameter is the recharge rate λ_R, which can be in principle estimated by restoring in Eq. (3.34) the λ_B-dependence and by equating to the inverse of the mean experimental translation rate Θ:

$$\frac{1}{\Theta} = \frac{\rho^{\rm e} + \lambda_R^{\rm e} + \lambda_B}{\bar{N}\lambda_B(\lambda_R^{\rm e} + \rho^{\rm e} X)} + \frac{1}{\lambda_A}. \tag{3.37}$$

The estimate obtained with the values in Tab. 3.1, however, is affected by the aforementioned inconsistency.

By measuring all the involved quantities under the same experimental conditions, it would instead be possible to consistently estimate all the parameters, and therefore to quantify the predicted deviation of the BTD from an exponential distribution.

[5] In the reference frame of the ribosome there is a drift $v_{\rm rib}$ in the tRNAs motion, which determines, in the small time δt, the exit from the system of an mean number $N_{\rm exit} \simeq r^2 v_{\rm rib} \delta t C_{\rm t} \simeq v_{\rm rib} \delta t N/r$ of tRNAs (while, of course, the same mean number of tRNAs is entering in the system). The same mean number $N_{\rm exit}$ would be caused by a stochastic flux with individual exit rate $\rho_T \simeq v_{\rm rib}/r$

The deviation of the BTD from the exponential distribution could be also directly measured experimentally with the techniques employed in Refs. [102, 103]: it would be necessary to introduce the tRNA recharging in the experimental setup (by adding the relative enzymes), and to carefully analyze how and how much the binding time affects the total translation time. The binding time seems to be rate-limiting in the experimental conditions employed in Ref. [102], as the mean translation time changes linearly with the inverse of the tRNA concentration. In this case the BTD should be adequately approximated by Eq. (3.17). The same does not hold for the experiments in Ref. [103], where several timescales are evidently present. In this latter case, in order to disentangle the effects due to the binding time from those due to the additional biochemical steps, it would be particularly useful to run a series of experiments at different concentrations of tRNA ($C_{\rm t}$), because a change in C_t affects only the binding step, and leaves all the other biochemical steps unchanged. The interpretation of these results would be potentially possible by refining the framework introduced in Sec. 3.4.3.

3.6 Conclusions

In this chapter we presented a microscopic model which describes the binding of the tRNA (charged with the proper amino acid) to the ribosome during the translation of an mRNA sequence into a protein. This fundamental step strongly depends on the conditions in the cell, and, in particular, on the concentration of charged tRNAs around the ribosome [102, 119, 117]. We consider the recharge dynamics and the diffusion of the tRNA molecules by assuming that each tRNA can be either charged with the relative amino acid, or uncharged. The charging occurs with rate λ_R, and the charged tRNAs can bind to the ribosome with rate λ_B. Spatial inhomogeneity and stochastic fluctuations of the number of charged tRNAs around the ribosome are accounted for, and diffusion-driven exchanges with the reservoir (representing the rest of the cell) are allowed. This model neglects the additional biochemical steps which are required to translate a codon, meaning that it is per se valid if the binding step is rate limiting (i.e., if the mean duration of the binding step is much larger than that of the other steps). A mean-field approach is introduced in Sec. 3.4.3 in order to estimate the effect of these additional reactions.

We describe this non-equilibrium system via its master equation, which in fact is not symmetric under time-reversal and violates detailed balance. We mainly focus on the stationary solution, but we also manage to solve the time dependent master equation from which we extract the relaxation time scales to the stationary solution, and the two-time correlators for the variables n and m (respectively, the number of charged and uncharged tRNAs in the system). We are able to obtain the analytical expression of the binding time distribution (BTD), i.e., the distribution of the time intervals spent by the ribosome waiting for a charged tRNA. This distribution substantially deviates from the exponential distribution typically used to model the BDD: specifically, the short and long binding times are under represented in the exponential estimate. Besides, we numerically checked within a wide range of parameters that the BTD is overdispersed with respect to the exponential distribution with the same mean. This fact could be measured experimentally with the techniques employed in Refs. [102, 103], by utilizing experimental conditions such that (i) the recharge of the tRNAs

is allowed and (*ii*) the binding step is rate limiting (as in Ref. [102]). When the condition (*ii*) is not met, it would still be possible to estimate the effects of the binding time on the total translation time by refining the framework sketched in Sec. 3.4.3; in this case, in order to study the BTD, it would be particularly useful to repeat the experiment with different concentrations of tRNA.

We also showed that, from the mathematical point of view, the appearance of a non exponential BTD is related to the coupling of the fluctuations of m and n. More specifically, we showed that the qualitative mechanism is as follows: (*i*) a binding event typically happens when the number of charged tRNAs is increased due to a fluctuation, on average $\bar{n}_{\mathrm{b}^-} = \bar{n}+1$, (*ii*) during the binding event, a charged tRNA gets discharged and the fluctuation on n propagates to m, $\bar{m}_{\mathrm{b}^+} = \bar{m} + 1$, (*iii*) if $\lambda > 0$, this fluctuation on m can propagate again on n with a characteristic timescale, producing a "bump" in the time-series of n as in Fig. 3.5. The size of this effect is larger the smaller the mean number of tRNAs $\bar{N}$ is, i.e., the larger the relative size of the fluctuations is.

An interesting direction of investigation could be the generalization of the model presented in this chapter to the more realistic case in which various different species of tRNA and codons are present. Concluding, we think that this kind of models, by analytically dissecting a small set of phenomena, can be very helpful in understanding the quantitative small scale dynamics of the translation process, and in discriminating the main effects from the corrections.

Appendix A

A.1 Langevin equations with multiplicative noise

The Langevin equations with multiplicative noise are a particular instance of *stochastic differential equations* which is widely used in many areas of physics and beyond to model a variety of stochastic processes (see, e.g., Refs. [22, 21]). The Langevin equations considered in this work are of the form

$$\dot{x}(t) = \mu(x(t)) + \sigma(x(t))\eta(t), \tag{A.1}$$

where $\mu(x)$ and $\sigma(x)$ are smooth functions, while $\eta(t)$ is a stochastic noise with zero mean and characterized by $\langle \eta(t)\eta(t') \rangle = \delta(t-t')$. Equation (A.1) is properly defined only after one specifies its *interpretation*, i.e., the rules according to which it has to be discretized or, alternatively, according to which one has to interpret its integral form. Typically Langevin equations are interpreted either with the Itō or with the Stratonovich conventions, although different interpretations are in principle possible. Here we summarize how Itō and Stratonovich Langevin equations are defined.

A.1.1 Itō interpretation

First of all we rewrite Eq. (A.1) in its integral form:

$$x(t) - x(0) = \int_0^t \mathrm{d}t'\, \mu(x(t')) + \int_0^t \mathrm{d}W(t')\, \sigma(x(t')), \tag{A.2}$$

where $\mathrm{d}W(t)$ is the differential Wiener process. The stochastic integral on the r.h.s. of Eq. (A.2) can now be interpreted (i.e., discretized) in various forms. If this is done *à la Itō*, it is understood as the mean-square-limit of the sum performed over the discrete time intervals (see, e.g., Refs. [22, 21])

$$\int_0^t \mathrm{d}W(t')\, \sigma(x(t')) = \operatorname*{ms\,lim}_{n\to\infty} \sum_{k=1}^{n} [W(t_k) - W(t_{k-1})]\, \sigma(x(t_{k-1})), \tag{A.3}$$

where $W(t)$ is the integral Wiener process. The distinctive feature of the Itō definition of the stochastic integral is the fact that the function $\sigma(x(t))$ is evaluated at the earlier time of every time interval; this specific choice would be inconsequential in the case of a constant function $\sigma(x)$ or for an ordinary integral, but it is relevant for a stochastic integral.

A.1.2 Stratonovich interpretation

In the Stratonovich interpretation, the stochastic integral in Eq. (A.2) is defined as the mean-square-limit of the sum

$$\int_0^t \mathrm{d}W(t')\,\sigma(x(t')) = \underset{n\to\infty}{\mathrm{ms}\lim} \sum_{k=1}^{n} [W(t_k) - W(t_{k-1})]\,\sigma\!\left(\frac{x(t_k)+x(t_{k-1})}{2}\right). \tag{A.4}$$

In this case the function $\sigma(x)$ is evaluated at the arithmetic mean between the values $x(t_{k-1})$ and $x(t_k)$ that the function x has at the two extremes of each time interval.

Every Itō-interpreted Langevin equation can be translated in the Stratonovich convention, and vice versa. For instance, if Eq. (A.1) is interpreted in the Itō convention, it is equivalent to the following Stratonovich-interpreted Langevin equation [22, 21]

$$\dot{x}(t) = \mu(x(t)) - \frac{1}{2}\sigma(x(t))\sigma'((x(t)) + \sigma(x(t))\,\eta(t). \tag{A.5}$$

A.1.3 Change of variable

A change of variable $z = z(x)$ can be implemented in Eq. (A.1) Itō interpreted by using the so-called Itō lemma (see, e.g., Refs. [22, 21]); the first step consists of writing Eq. (A.1) in its differential form

$$\mathrm{d}x = \mu(x)\mathrm{d}t + \sigma(x)\mathrm{d}W. \tag{A.6}$$

Heuristically, one has then to consider the second order expansion of $\mathrm{d}z = \frac{\partial z}{\partial x}\mathrm{d}x + \frac{1}{2}\frac{\partial^2 z}{\partial x^2}(\mathrm{d}x)^2$ as a function of $\mathrm{d}x$. In fact, according to the Itō lemma, the only relevant contribution from the second-order term comes from the square of the differential Wiener process, which gives $(\mathrm{d}W)^2 = \mathrm{d}t$, so that the relationship between the differentials finally reads (see, e.g., Refs. [22, 21])

$$\mathrm{d}z = \left[\frac{\partial z}{\partial x}\mu(x) + \frac{1}{2}\frac{\partial^2 z}{\partial x^2}\sigma^2(x)\right]_{x=x(z)} \mathrm{d}t \;+\; \left[\frac{\partial z}{\partial x}\sigma(x)\right]_{x=x(z)} \mathrm{d}W\,, \tag{A.7}$$

where $x(z)$ is the inverse of the function $z(x)$.

A.2 Derivation of the mean fixation time

If the functions $\mu(x)$ and $\sigma(x)$ in Eq. (A.1) (Itō-interpreted) are such that the states $x = 0$ and $x = 1$ are absorbing and that the variable x is confined within the interval $x \in [0, 1]$, one can define the mean fixation time $T_{\mathrm{fix}}(x)$ to reach either of the two absorbing states starting from the initial condition x. $T_{\mathrm{fix}}(x)$ satisfies the backward Fokker-Planck equation (see Sec. 1.3.3)

$$\frac{1}{2}\sigma^2(x)\partial_x^2 T_{\mathrm{fix}}(x) + \mu(x)\partial_x T_{\mathrm{fix}}(x) + 1 = 0, \tag{A.8}$$

which, in terms of the function $f(x) = \partial_x T_{\rm fix}(x)$, takes the simpler form

$$f'(x) = -\frac{2\mu(x)}{\sigma^2(x)}\, f(x) - \frac{2}{\sigma^2(x)}. \tag{A.9}$$

Equation (A.9) can be straightforwardly integrated

$$\begin{aligned} f(x) &= f(x_0) \exp\left[-\int_{x_0}^{x} \mathrm{d}\xi\, \frac{2\mu(\xi)}{\sigma^2(\xi)}\right] + \int_{x_0}^{x} \mathrm{d}y\, \left(-\frac{2}{\sigma^2(y)}\right) \exp\left[-\int_{y}^{x} \mathrm{d}\xi\, \frac{2\mu(\xi)}{\sigma^2(\xi)}\right] \\ &= f(x_0)\frac{s(x)}{s(x_0)} + 2s(x)\int_{x}^{x_0} \mathrm{d}y\, m(y), \end{aligned} \tag{A.10}$$

where $s(x) = \exp\big[-\int^x \mathrm{d}y \frac{2\mu(y)}{\sigma^2(y)}\big]$, $m(x) = \frac{1}{s(x)\sigma^2(x)}$, and x_0 is an arbitrary point within the interval $[0,1]$. By setting, e.g., $x_0 = 1$ and by integrating, one obtains (see, e.g., Refs. [84, 51])

$$T_{\rm fix}(x) = \frac{f(1)}{s(1)} \int_0^x \mathrm{d}z\, s(z) + 2\int_0^x \mathrm{d}z\, s(z) \int_z^1 \mathrm{d}\xi\, m(\xi), \tag{A.11}$$

where we used the boundary condition $T_{\rm fix}(0) = 0$. The value of $f(1)$ can be obtained by imposing the remaining boundary condition, i.e., $T_{\rm fix}(1) = 0$, which gives

$$f(1) = \frac{-2s(1)}{\int_0^1 \mathrm{d}z\, s(z)} \int_0^1 \mathrm{d}z s(z) \int_z^1 \mathrm{d}\xi\, m(\xi). \tag{A.12}$$

By substituting this expression into Eq. (A.11) and after some algebraic manipulations, one obtains the expression for the MFT

$$T_{\rm fix}(x) = \frac{2}{S(0,1)} \left[S(x,1)\int_0^x \mathrm{d}\xi\, m(\xi) S(0,\xi) + S(0,x)\int_x^1 \mathrm{d}\xi\, m(\xi) S(\xi,1)\right], \tag{A.13}$$

where $S(x_1,x_2) = \int_{x_1}^{x_2} \mathrm{d}x\, s(x)$ is nothing but Eq. (1.17a) in the main text.

A.3 Solution of Eq. (1.24)

For $y < 1$, equation (1.24) in the main text can be conveniently rewritten by reabsorbing the factor $\sigma^2/2$ via the change of variable

$$u = \left(\frac{2}{\sigma^2}\right)^{\frac{1}{2(1-y)}} x, \tag{A.14}$$

and by defining the function $\psi(u,t) = |u|^{2y} P(u,t|u',0)$. In terms of these quantities, Eq. (1.24) reads

$$\partial_t \psi(u,t) = |u|^{2y} \partial_u^2 \psi(u,t). \tag{A.15}$$

By introducing the Laplace transform in time of $\psi(u,t)$, i.e., $\tilde{\psi}(u,s) = \int_0^\infty \mathrm{d}t\, \psi(u,t)\mathrm{e}^{-st}$, this equation can be rewritten as

$$|u|^{2y}\partial_u^2\tilde{\psi}(u,s) - s\tilde{\psi}(u,s) = -|u|^{2y}\delta(u-u'), \tag{A.16}$$

where $u' = (2/\sigma^2)^{\frac{1}{2(1-y)}}\, x'$ and we used the initial condition $\psi(u,0) = |u|^{2y}\delta(u-u')$, which corresponds to $P(x,0|x',0) = \delta(x-x')$. In terms of the variable $z = \frac{1}{1-y}|u|^{1-y}$, Eq. (A.16) reads

$$\left[-(1-2\nu)\frac{1}{z}\partial_z + \partial_z^2 - s\right]\tilde{\psi}(z,s) = -\left(\frac{1}{2\nu}\right)^{2\nu-1} z^{2\nu-1}\delta(z-z'), \tag{A.17}$$

where $\nu = 1/[2(1-y)]$ and $z' = \frac{1}{1-y}u'^{1-y}$. The homogeneous part of Eq. (A.17) can be recognized to be a variant of Bessel's equation; the general solution of this homogeneous part can therefore be written as a linear combination of the functions

$$\begin{aligned}\tilde{\psi}_1^{(\mathrm{o})}(z,s) &= z^\nu K_\nu(\sqrt{s}z),\\ \tilde{\psi}_2^{(\mathrm{o})}(z,s) &= z^\nu I_\nu(\sqrt{s}z),\end{aligned} \tag{A.18}$$

where $I_\nu(w)$ and $K_\nu(w)$ are the modified Bessel functions of first and second kind, respectively (see, e.g., Ref. [130]). In order to obtain a smooth probability distribution $P(x,t|x',0)$ for $t>0$, we require the continuity of $\tilde{\psi}(u,s)$ at the points $u=0$ and $u=u'$; $\partial_u\tilde{\psi}(u,s)$ has to be continuous at the point $u=0$, while it should have a proper discontinuity at the point $u=u'$, in order to generate the inhomogeneous term in Eq. (A.17) (see, e.g., Ref. [130]). The solution of Eq. (A.16) reads then

$$\tilde{\psi}(u,s) = (2\nu)^\nu A(s)|u|^{1/2}K_\nu(2\nu\sqrt{s}|u|^{\frac{1}{2\nu}}) + 2\nu\theta(u)(uu')^{1/2}I_\nu(2\nu\sqrt{s}u_<^{\frac{1}{2\nu}})K_\nu(2\nu\sqrt{s}u_>^{\frac{1}{2\nu}}), \tag{A.19}$$

where $u_< = \min\{u,u'\}$ and $u_> = \max\{u,u'\}$. By calculating the inverse Laplace transform and by implementing the inverse of the change of variables in Eq. (A.14), one obtains Eqs. (1.25) and (1.27).

Appendix B

B.1 Diffusion approximation for the microscopic models

Given a microscopic model (e.g., Wright-Fisher) with certain transition rates, one can write the evolution equation for the probability $P(x,t)$ of finding the model in a certain configuration x in the form of a master equation. The diffusion approximation then consists in approximating this equation with a Fokker-Planck (or equivalently, a Langevin) equation, i.e., with a diffusion equation with suitable x-dependent drift and diffusion coefficients. In particular, only the mean value $\langle \Delta x \rangle$ and the variance $\langle (\Delta x)^2 \rangle$ of the change Δx per unit time of the variable x resulting from the implementation of these microscopic dynamical transitions are accounted for in the evolution equation. Although this approach is known to fail in some cases, for example for the susceptiple-infected-susceptible (SIS) model of epidemiology (see e.g., Ref. [83]), it turns out to be quite accurate for the Wright-Fisher and Moran models discussed in the present work [36, 80, 81, 82].

B.1.1 Wright-Fisher model

For sufficiently large values of the subpopulation size Ω, one can rely on the diffusion approximation of the Wright-Fisher model defined by the rates discussed in Sec. 2.2. For a well-mixed population characterized by the binomial sampling with the probability $p_{\rm r}(x)$ given in Eq. (2.1), one readily finds

$$\begin{aligned} \mu(x) &= \langle \Delta x \rangle = \tilde{s} x(1-x) + O(\tilde{s}^2), \\ v(x) &= \langle (\Delta x)^2 \rangle = \frac{x(1-x) + O(\tilde{s})}{\Omega} + O(\tilde{s}^2). \end{aligned} \tag{B.1}$$

For a subdivided population characterized by binomial sampling with the probability $p(x_i, \bar{x})$ given in Eq. (2.10), instead, one finds

$$\begin{aligned} \mu(x_i) &= \langle \Delta x_i \rangle = \tilde{s} x_i(1-x_i) + m(\bar{x} - x_i) + O(\tilde{s}^2, \tilde{s}m), \\ v(x_i) &= \langle (\Delta x_i)^2 \rangle = \frac{x_i(1-x_i) + O(m, \tilde{s})}{\Omega} + O(\tilde{s}^2, m^2, m\tilde{s}). \end{aligned} \tag{B.2}$$

Accordingly, as anticipated in Sec. 2.2, the dynamics of the Wright-Fisher model within this diffusion approximation, and for sufficiently small rates $\tilde{s}$ and m, is described by the

single-deme Langevin equations (2.3) and (2.14) which have to be interpreted with the Itō prescription.

B.1.2 Moran model

The time evolution of the probability distribution $P(\{x_i\},t)$ of the deme frequencies $\{x_i\}_i$ can be determined from the corresponding master equation with the rates given by Eq. (2.11). For large Ω and in the limit of continuous time $\delta t \to 0$ (where δt denotes the duration of a step in the dynamics of the Moran model), standard expansions, such as the Kramers-Moyal expansion [22], lead to the Fokker-Planck equation

$$\begin{aligned}\partial_t P(\{x_i\},t) = &-\sum_{j=1}^{N} \partial_{x_j}[\mu(x_j)P(\{x_i\},t)] \\ &+\frac{1}{2}\sum_{j=1}^{N} \partial^2_{x_j}[v(x_j)P(\{x_i\},t)],\end{aligned} \tag{B.3}$$

in which the drift μ and the variance v are given by

$$\begin{aligned}\mu(x_i) &= \frac{W_1 - W_{-1}}{\Omega\,\delta t} = \frac{\tilde{s}}{2}x_i(1-x_i) + \frac{m}{2}(\bar{x}-x_i) + O(\tilde{s}^2), \\ v(x_i) &= \frac{W_1 + W_{-1}}{\Omega^2\,\delta t} = \frac{x_i(1-x_i) + O(\tilde{s},m)}{\Omega},\end{aligned} \tag{B.4}$$

where we have chosen the temporal step to be $\delta t = 2/\Omega$. With this choice of time scales, the resulting genetic drift $v(x_i)$ for small $\tilde{s}$ and m is the same as the one of the Wright-Fisher model for a population of the same size, see Eq. (B.2). Note that, in order to recover the same expression also for the drift $\mu(x_i)$, it is necessary to rescale the migration and the selection coefficients as $m \to 2m$ and $\tilde{s} \to 2\tilde{s}$, respectively. Equation (B.3) is nothing but the Fokker-Planck equation associated with the set of N single-deme Langevin equations (2.14), which, as we argued above, also describe the dynamics of the Wright-Fisher model in the presence of migration.

B.2 Migration in the microscopic models

While the Wright-Fisher [77, 78] and Moran [79] models are typically employed in order to describe the single-population dynamics, below we discuss how one can modify their microscopic rules in order to account for the possibility of having migration from one population to another in the form of exchanges of individuals within different demes of an island model.

B.2.1 Wright-Fisher model

A standard way to introduce migration in the Wright-Fisher model is to modify the probability with which a new generation is sampled. In the migration process, which occurs

between two subsequent generations, a mean number $m\Omega$ of randomly chosen individuals leaves each deme and it is then randomly redistributed in the other demes. One can effectively think of all the individuals leaving the N demes as merging in a sort of "reservoir", with a mean of $m\Omega N$ individuals, and a mean fraction of type-A individuals determined by the inter-deme mean frequency (IDMF) $\bar{x} = \sum_{i=1}^{N} x_i$. Individuals are then randomly chosen from this reservoir in order to replace those that migrated from each deme. Accordingly, the mean fraction of type A-individuals arriving in the i-th deme because of this redistribution is $m\Omega\bar{x}$, while the mean fraction of A-type individuals leaving deme i is $m\Omega x_i$. Accordingly, the original fraction x_i has changed into $m\bar{x} + (1-m)x_i$ because of migration, with this process affecting all the demes. This simplified description of the migration process neglects fluctuations in the number and in the composition of migrants during each generation and in fact, it accounts for migration only by modifying the probability p_r that a new individual carries allele A [36, 62, 58].

B.2.2 Moran model

Let us consider an island model in which the single deme dynamics is based on the Moran model. In the absence of migration, because of death and reproduction, each deme evolves according to the rates in Eq. (2.2) in the main text. Because of migration, during each step of the evolution, there can be an additional variation of the allele frequency x_i. More precisely, the probability that in the i-th deme the number Ω_A of individuals carrying allele A increases (decreases) by one unit is given by $W_1^{\rm m}\delta t$ ($W_{-1}^{\rm m}\delta t$), where $\delta t = O(\tau_g/\Omega)$ is the duration of the evolutionary step and the rates are given by

$$\begin{aligned} W_1^{\rm m} &= m\bar{x}(1-x_i), \\ W_{-1}^{\rm m} &= m(1-\bar{x})x_i, \end{aligned} \tag{B.5}$$

where we neglect the $O((m\delta t)^2)$ probability that more than one individual per deme migrates within one evolutionary step.

Because of the simultaneous action of death, reproduction, and migration, the probability Q_k to have a change $k = \pm 1, \pm 2$ in the number of alleles A in the i-th deme between two subsequent generations is given by

$$\begin{aligned} Q_2 &= W_1\delta t\, W_1^{\rm m}\delta t, \\ Q_1 &= W_1\delta t\left[1-(W_1^{\rm m}+W_{-1}^{\rm m})\delta t\right] \\ &\quad + \left[1-(W_1+W_{-1})\delta t\right] W_1^{\rm m}\delta t, \\ Q_{-1} &= W_{-1}\delta t\left[1-(W_1^{\rm m}+W_{-1}^{\rm m})\delta t\right] \\ &\quad + \left[1-(W_1+W_{-1})\delta t\right] W_{-1}^{\rm m}\delta t, \\ Q_{-2} &= W_{-1}\delta t\, W_{-1}^{\rm m}\delta t. \end{aligned} \tag{B.6}$$

If one neglects the contribution of order $O(\delta t^2)$, these probabilities generate the rates anticipated in Eq. (2.11) in the main text.

B.3 Estimate of the "lifetime" T_u of the intermediate state

If the migration rate m' is sufficiently small, such that $0 < m' < T_{\rm fix}^{-1}$ [1] , each deme spends most of its time into one of the two boundary states, till it receives, due to migration, one individual different from the majority. In turn, this individual triggers an attempt to leave the boundary state which leads to the intermediate one x_u (and possibly to the opposite boundary) with an overall rate $m'P$, as discussed in Sec. 2.5.2. Under our assumption of small migration rate, this transition takes place before any other individual is exchanged by the deme with the rest of the population, and therefore it occurs as in an isolated deme, i.e., it takes a mean time $T_{\rm fix1}$. During this transition, the deme will spend a mean time T_u close to the intermediate state x_u before reaching the final boundary. Figure B.1 provides a schematic representation of the time evolution of the allele frequencies of the various demes (indicated by solid and dashed lines of different colors) in the regime described above. In particular, the deme represented by the solid line has received an individual with allele A from another deme and has fixed it after a time $T_{\rm fix1}$, of which T_u spent close to the intermediate state promoted by balancing selection. Other demes of the metapopulation (indicated by dashed lines) evolve similarly, i.e., they move from one boundary state to the other, with possible unsuccessful attempts.

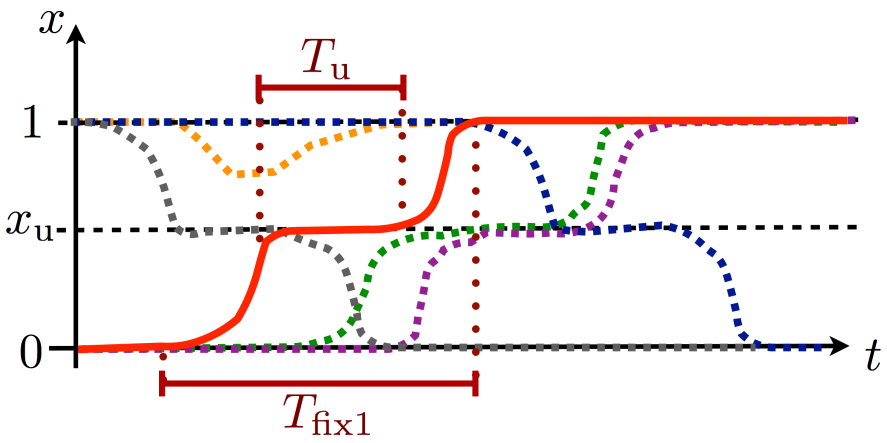

Figure B.1: Schematic representation of the evolution of the frequencies x_i of various demes (represented by different colors) in a metapopulation with small migration rate $m' \ll T_{\rm fix1}^{-1}$. Under this assumption, the possible transition between the two boundary states is triggered with a typical time scale $\sim 1/m'$ which is much longer than the one $T_{\rm fix1}$ taken by the transition itself, where $T_{\rm fix1}$ is the single-deme MFT. Part of this time, corresponding to the "lifetime" T_u, is spent by the various demes in the vicinity of the intermediate state.

In order to estimate T_u, we focus on the ratio $\rho = T_u/T_{\rm fix1}$, i.e., on the fraction of the time spent outside the boundaries in which the deme is actually close to x_u; in the quasi-stationary state associated with a certain value of the mean frequency $\bar{x}$ (and described by

[1] The condition $m' \ll 1/T_{\rm fix1}$ emerges by comparing the time scale $T_{\rm fix1}$ needed by a single deme to reach fixation in the absence of migration and the typical time scale $1/m'$ associated with the occurrence of migration.

the density $P_{\rm qs}(x|\bar{x})$), ρ can be estimated as the ratio of the corresponding probabilities, i.e., of the probability to find a deme close to the intermediate state (that is $x \simeq x_{\rm u}$) to the one of finding it outside the boundaries. In order to specify properly the condition of x_i being "close to" $x_{\rm u}$, hereafter we focus for simplicity on the symmetric case with $x_* = x_{\rm u} = 1/2$. In the effective voter model with the intermediate state, the continuous interval of states $x \in [0,1]$ is represented by the three coarse states $\{0, 1/2, 1\}$. It is then natural to associate to every value of x in the interval $[0,1]$ its closest representative state. With this definition, the probability $P_{\rm u}$ to find the deme close to the intermediate state is

$$P_{\rm u}(\bar{x}) = \int_{1/4}^{3/4} {\rm d}x\, P_{\rm qs}(x|\bar{x}). \tag{B.7}$$

On the other hand, the probability to find the deme outside the boundary states can be estimated as

$$P_{\rm non-fix}(\bar{x}) = \int_{1/\Omega}^{1-1/\Omega} {\rm d}x\, P_{\rm qs}(x|\bar{x}), \tag{B.8}$$

where a minimal distance $1/\Omega$ of the deme frequency from a boundary corresponds to having one individual different from the background. The ratio ρ can therefore be approximated as

$$\rho(\bar{x}, s', m') = \frac{P_{\rm u}(\bar{x})}{P_{\rm non-fix}(\bar{x})}. \tag{B.9}$$

A numerical study of the estimate of ρ according to Eq. (B.9) is reported in Fig. B.2 as

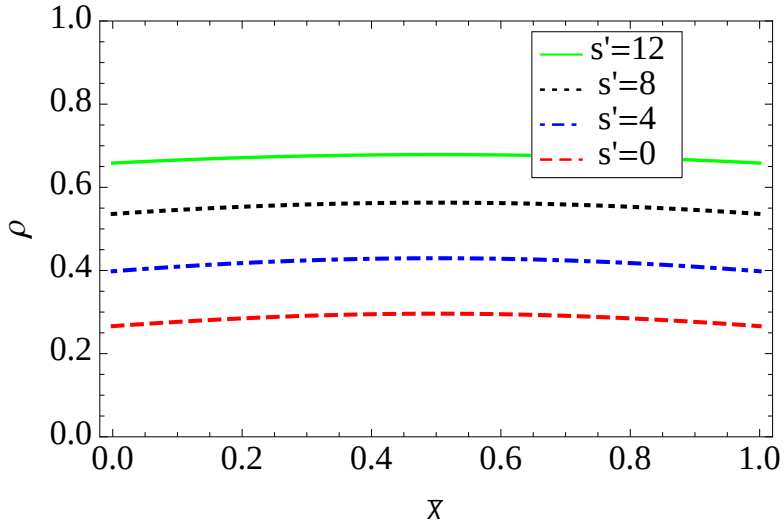

Figure B.2: Estimate of the ratio $\rho = T_{\rm u}/T_{\rm fix1}$ as a function of $\bar{x}$ for $m' = 0.2$, $x_{\rm u} = x_* = 1/2$, $\Omega = 100$ and $s' = 0$, 4, 8, and 12 from bottom to top, calculated as explained in the main text on the basis of the quasi-stationary distribution.

a function of $\bar{x}$ for $m' = 0.2$, $x_{\rm u} = x_* = 1/2$, $\Omega = 100$, and for various values of s'. It

particular ρ turns out to increase uniformly as s' increases, which indicates that $T_{\rm u}$ grows faster than $T_{\rm fix1}$ as a function of this parameter. It can be noticed that, while generically ρ depends on $\bar{x}$, this dependence becomes increasingly less important as m' decreases. The typical $\bar{x}$-independent estimate of ρ (and therefore of $T_{\rm u}$) can be obtained by considering the mean value

$$\rho(s', m') = \int_0^1 {\rm d}\bar{x}\, A(\bar{x})\rho(\bar{x}, s', m'), \tag{B.10}$$

which depends on the *a-priori* distribution $A(\bar{x})$ of the frequency $\bar{x}$. However, as we pointed out above, $\rho(\bar{x}, s', m')$ is approximately independent of $\bar{x}$ at least for sufficiently small m' and therefore the specific form of $A(\bar{x})$ is inconsequential, so that we can set $A \equiv 1$ in Eq. (B.10). Figure B.3 shows the dependence of ρ on the migration rate m', as obtained from the numerical integration of Eq. (B.10) for various values of the selection coefficient s'. We note again that ρ is an increasing function of the selection coefficient s', and this can be heuristically understood from the fact that balancing selection favors the location of the deme frequency x_i around the optimal frequency x_*. Using Eq. (B.10), it is straightforward to obtain a numerical estimate for the lifetime of the intermediate state as $T_{\rm u} \simeq \rho T_{\rm fix1}$.

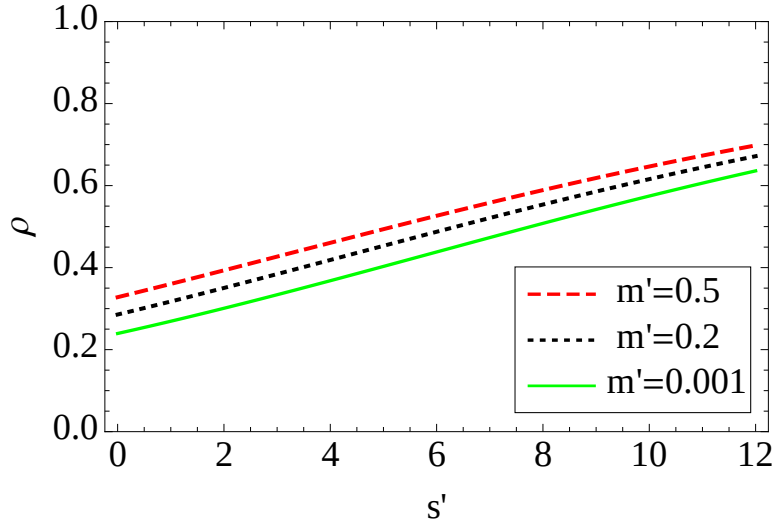

Figure B.3: Mean fraction ρ of time that a deme spends close to the intermediate state $x_{\rm u}$ as a function of the migration rate m', for $x_{\rm u} = x_* = 1/2$, $\Omega = 100$, and $m' = 0.001$, 0.2, and 0.5 from bottom to top; these values of ρ have been estimated on the basis of Eq. (B.10) with an uniform *a-priori* distribution $A(\bar{x}) \equiv 1$.

B.4 Effective equation for $\bar{x}$ in the voter model with intermediate state

In Sec. 2.5.2 we introduced a simplified description of the metapopulation consisting of N demes in terms of a voter model with N individuals which can have a definite (0,1) or no

definite opinion. Each deme of the original island model is represented by a voter, with opinion 0 or 1 depending on whether the deme has almost fixed at the values $x = 0$ or 1 of the frequency x of allele A, while individuals with no definite opinion correspond to demes with $x = x_{\rm u} \simeq x_*$ fluctuating in an intermediate long-lived state. The dynamics of the island model can therefore be described at this coarser level by following the evolution of the numbers $N_{\rm u}$, N_0, and $N_1 = N - N_{\rm u} - N_0$ of individuals with intermediate opinion, or opinions 0 and 1, respectively.

B.4.1 Evolution of $N_{\rm u}$

Under the assumption that $\bar{x} = (N_1 + x_{\rm u} N_{\rm u})/N$ is constant (or slowly varying), the behavior of $N_{\rm u}$ is described by a conditional quasi-stationary distribution $P_{\rm qs}(N_{\rm u}|\bar{x})$; this distribution is the stationary solution of the master equation

$$0 = \sum_{n=-1,1,2} [W_{N_{\rm u}-n\to N_{\rm u}} P_{N_{\rm u}-n} - W_{N_{\rm u}\to N_{\rm u}+n} P_{N_{\rm u}}] \tag{B.11}$$

where, for small $N_{\rm u}/N$ and considering the symmetric case $x_{\rm u} = x_* = 1/2$ for simplicity, the rates in Sec. 2.5.2 can be written as

$$\begin{aligned} W_{N_{\rm u}\to N_{\rm u}+1} &= m' P[2N(1-P)\bar{x}(1-\bar{x}) + N_{\rm u}/2], \\ W_{N_{\rm u}\to N_{\rm u}+2} &= m' N P^2 \bar{x}(1-\bar{x}), \\ W_{N_{\rm u}\to N_{\rm u}-1} &= N_{\rm u}/T_{\rm u}, \end{aligned} \tag{B.12}$$

where $P = p(x_{\rm u}|1/\Omega)$ is the probability that a deme with initial frequency $x = 1/\Omega$ reaches the intermediate state $x = x_{\rm u}$ before fixation. Since the rates $W_{N_{\rm u}\to N'_{\rm u}}$ are linear functions of $N_{\rm u}$, the evolution of the mean value $\langle N_{\rm u}\rangle = \sum_{N_{\rm u}=0}^{\infty} N_{\rm u} P_{\rm qs}(N_{\rm u}|\bar{x})$ can be written in closed form:

$$\partial_t \langle N_{\rm u}\rangle = \sum_n n W_n(\langle N_{\rm u}\rangle). \tag{B.13}$$

The approximate expression reported in Eq. (2.57) in the main text can be obtained from the stationary condition $\partial_t \langle N_{\rm u}\rangle = 0$, under the assumption of large N and small m'.

B.4.2 Evolution of $\bar{x}$

We study here the evolution of $\bar{x}$ by considering the fluctuations of $N_{\rm u}$ around its mean given in Eq. (2.57) in the main text; for the sake of simplicity we focus on the symmetric case $x_* = 1/2$, but the discussion below carries over to a generic value of x_*. Because of the presence of demes in the intermediate state, the value of $\bar{x}$ receives a contribution of the form

$$\bar{x} = \frac{N_1}{N} + \frac{N_{\rm u}}{2N}, \tag{B.14}$$

and therefore

$$\begin{aligned} N_1 &= N\bar{x} - N_{\rm u}/2, \\ N_0 &= N(1-\bar{x}) - N_{\rm u}/2. \end{aligned} \tag{B.15}$$

These relations can now be used in order to express the rates $W_{A,\dots,D}$ in Eq. (2.50) in the main text as functions of $N_{\rm u}$. For large Ω these expressions can be further simplified by taking into account that P, $Q \propto 1/\Omega$ for s' not too large (we recall here that $P = p(x_{\rm u}|\Omega^{-1})$, $Q = p(x_{\rm u}|1-\Omega^{-1})$ — see Sec. 2.5.2 — with p given in Eq. (2.8)), and that $T_{\rm u} \propto T_{\rm fix1} \propto \Omega$; one eventually finds

$$\begin{aligned} W_A &= m'NP\left\{\bar{x}(1-\bar{x}) - \frac{N_{\rm u}}{N}\frac{\bar{x}}{2}\right\} + O(1/\Omega^2), \\ W_B &= m'NP\left\{\bar{x}(1-\bar{x}) - \frac{N_{\rm u}}{N}\frac{1-\bar{x}}{2}\right\} + O(1/\Omega^2), \\ W_C &= O(1/\Omega^2), \\ W_D &= W_E = N_{\rm u}/(2T_{\rm u}). \end{aligned} \tag{B.16}$$

As discussed in Sec. 2.5.2, the evolution of $\bar{x}$ can be described by an effective Langevin equation (diffusion approximation, see Appendix B.1) in the large N limit,

$$\dot{\bar{x}} = M_{\rm vi}(\bar{x}) + \sqrt{V_{\rm vi}(\bar{x})}\,\eta(t), \tag{B.17}$$

where the drift and variance are given by

$$\begin{aligned} M_{\rm vi}(\bar{x}) &= \sum_{i=A,B,C,D,E} W_i \Delta\bar{x}_i, \\ V_{\rm vi}(\bar{x}) &= \sum_{i=A,B,C,D,E} W_i (\Delta\bar{x}_i)^2, \end{aligned} \tag{B.18}$$

and the relevant increments are $\Delta\bar{x}_A = \Delta\bar{x}_E = 1/(2N)$ and $\Delta\bar{x}_B = \Delta\bar{x}_D = -1/(2N)$. Then, by replacing $N_{\rm u}$ with its mean $\langle N_{\rm u}\rangle$ reported in Eq. (2.57), we eventually obtain the result anticipated in Eq. (2.58) in the main text.

B.5 Time scales associated with Eq. (2.17)

There are two time scales emerging from Eq. (2.17) in the main text: a *relaxation time* associated with the deterministic term $M(\bar{x})$ and a *fluctuation time* associated with the stochastic term controlled by $V(\bar{x})$.

Relaxation time. — By neglecting the stochastic fluctuations in Eq. (2.17) in the main text one obtains $\dot{\bar{x}} = M(\bar{x}) = s_{\rm e}\bar{x}(1-\bar{x})(x_* - \bar{x})$, where we used the expression for $M(\bar{x})$ from Eq. (2.20a) in the main text, which is valid under the assumption that the separation of time

scales discussed above (and in Sec. 2.2.3) holds. This deterministic drift can be expanded around the metastable value $\bar{x} = \hat{x} \simeq x_*$ and the linear contribution is responsible for a relaxation towards the value $\bar{x} = x_*$ which occurs exponentially in time, with a time scale

$$T_{\rm rel} = \frac{1}{s_{\rm e} x_* (1 - x_*)}. \tag{B.19}$$

Fluctuation time. — Equation (2.17) in the main text can be rewritten as

$$\mathrm{d}\bar{x} = M(\bar{x})\mathrm{d}t + \sqrt{V(\bar{x})}\mathrm{d}w, \tag{B.20}$$

where $\mathrm{d}w$ is a Wiener process with unit variance. In order to associate a time scale $T_{\rm fluct}$ to the diffusion-like contribution of fluctuations, we note that the variance $V(\bar{x})\mathrm{d}t + O(\mathrm{d}t^2)$ of $\overline{x}$ resulting from Eq. (B.20) becomes of order unity for

$$T_{\rm fluct} \simeq 1/V(\bar{x}) \simeq \frac{N_{\rm e}}{x_*(1 - x_*)}, \tag{B.21}$$

where we used again Eq. 2.17 in the main text (which is valid if there is a separation of time scales) and we took the optimal value x_* as the typical value for the IDMF $\bar{x}$.

By using the expression for $N_{\rm e}$ and $s_{\rm e}$ reported in Eqs. (2.21b) and (2.21a) in the main text, the condition $T_{\rm fluct} \gg T_{\rm rel}$ becomes (cp. Eqs. (B.21) and (B.19))

$$s' N \gg 1 + \frac{1}{m'}, \tag{B.22}$$

which turns into $s'm'N = sm\Omega^2 N \gg 1$ for $m' \ll 1$. This condition must be satisfied for the existence of a collective metastable state in the large-N limit.

Separation of time scales. — The separation of time scales assumed in Sec. 2.2.3 in the main text, which allows one to determine the quasi-stationary distribution of each single deme and then use it in order to calculate approximate expressions for the higher-order moments $\overline{x^k}$ — amounts at requiring that the time scale $T_{\rm migr} \simeq 1/m$, associated with the response of x_i to a change in $\bar{x}$ is much shorter than the one which characterizes the dynamics of $\bar{x}$. Since the latter involves essentially two different time scales, i.e., $T_{\rm fluct}$ and $T_{\rm rel}$ discussed above, $T_{\rm migr}$ must be much shorter than both of them:

$$T_{\rm migr} \ll \min\{T_{\rm fluct}, T_{\rm rel}\}. \tag{B.23}$$

Under the assumption that this inequality holds — which can be verified a posteriori — $T_{\rm rel}$ and $T_{\rm fluct}$ are given by Eq. (B.19) and (B.21), respectively. Accordingly, the minimum on the r.h.s. of the previous equation is $T_{\rm rel}$ for $Ns' > 1 + 1/m'$ and $T_{\rm fluct}$ otherwise. In the former instance, Eq. (B.23) becomes $T_{\rm migr} \ll T_{\rm rel}$, i.e., $s_{\rm e}/m \ll 1$ (where one can neglect the factor $x_*(1 - x_*)$, which is $\simeq 1/4$ within the range of parameters considered in the main text). The remaining case $Ns' < 1 + 1/m'$ amounts at requiring $Nm'[1 + 1/(2m')] \gg 1$, which is satisfied whenever $N \gg 1$.

In summary, the separation of time scales discussed here requires $s_{\rm e}/m \ll 1$ for $Ns' > 1 + 1/m'$, while it always holds (when N is large) for $Ns' < 1 + 1/m'$.

B.6 Global fixation in the absence of migration

In the absence of migration ($m = 0$), each deme fixes independently of the others, but global fixation of the subdivided population occurs only when the last deme has fixed. The fixation probability $p(x_0, t)$ is defined as the probability to have $x(t) \in \{0, 1\}$, assuming that the evolution of the stochastic variable x started from $x(0) = x_0$ at time $t = 0$; accordingly, p is the cumulative distribution of the fixation times conditioned to the initial condition $x(0) = x_0$ [131]. Here we focus on the initial condition $\bar{x}_0 = 1/2$ (which approximately characterizes the metastable state), denoting by $P_N(t)$ the probability that all N demes have already reached fixation at time t with $x_i(0) = 1/2$ for all of them. Due to the independence of the demes (for $m = 0$), this probability can be expressed in terms of the single-deme fixation probability $P_1(t) = p_{\rm fix1}(x_i = 1/2, t)$ as $P_N(t) = P_1^N(t)$. The probability density associated with the global fixation time is then given by $\dot{P}_N(t) = -\dot{Q}_N(t)$ where $Q_N(t) = 1 - P_N(t)$ and therefore, the mean global fixation time is

$$T_{\rm fix}^{(m=0)} = \int_0^\infty {\rm d}t\, t\, \dot{P}_N(t) = \int_0^\infty {\rm d}t\, Q_N(t) = \sum_{k=1}^{N} \binom{N}{k} (-1)^{k+1} \int_0^\infty {\rm d}t\, Q_1^k(t), \tag{B.24}$$

where $Q_1(t) = 1 - P_1(t)$. Assuming that the large fluctuations which cause fixation are independent Poisson processes, the probability that the system has not fixed after time t is exponentially distributed around the mean fixation time $T_{\rm fix1}$ of a deme, namely, $Q_1(t) \simeq {\rm e}^{-t/T_{\rm fix1}}$. We checked numerically that this approximation is quite accurate in practice. Accordingly, from Eq. (B.24) we find

$$T_{\rm fix}^{(m=0)} \simeq T_{\rm fix1}[\gamma + \psi(1 + N)], \tag{B.25}$$

where γ is the Euler constant and $\psi(z)$ is the digamma function, with an asymptotic behavior

$$T_{\rm fix}^{(m=0)} \simeq T_{\rm fix1} \ln N \quad \text{for} \quad N \gg 1. \tag{B.26}$$

We point out that the MFT depends logarithmically on N, while in presence of migration such a dependence is at least linear (or even exponential, in the limit of large N).

B.7 Numerical estimate of σ_c

The lowest-order estimate $T_{\rm fix}^{(0)}$ of the MFT (Eq. (2.36) in the main text) can be written in terms of

$$\widetilde{T}_{\rm fix}^{(0)}(\sigma, m') \equiv \frac{T_{\rm fix}^{(0)}}{N\Omega} = \left(1 + \frac{1}{2m'}\right) f(X), \tag{B.27}$$

where $X = \sigma m'/[4(m' + 1)]$ and

$$f(X) = \int_0^1 {\rm d}y \int_0^1 {\rm d}z\, \frac{{\rm e}^{Xy(1-z^2)}}{1 - yz^2}. \tag{B.28}$$

The stationary condition $\partial_{m'} T^{(0)}_{\rm fix} = 0 = \partial_{m'} \widetilde{T}^{(0)}_{\rm fix}(\sigma, m')$ therefore becomes an implicit equation in terms of m'

$$m' = 2[f(X) - Xf'(X)]/[2Xf'(X) - f(X)], \tag{B.29}$$

which admits $m' = m'_{\rm min}(\sigma)$ as a solution. Figure 2.11(b) of the main text shows that, upon approaching the threshold value σ_c of σ at which $T^{(0)}_{\rm fix}(m')$ develops a non-monotonicity, $m'_{\rm min}(\sigma)$ diverges. By requiring the r.h.s. of Eq. (B.29) to diverge for $\sigma \to \sigma_c$ we find numerically that $X_c \simeq 1.3$ and therefore $\sigma_c = 4X_c \simeq 5.2$.

B.8 Fixation probability

The cumulative distribution of fixation times $p(\bar{x}, t)$, where $\bar{x}$ indicates the initial value of the IDMF, satisfies the backward Fokker-Planck (FP) equation

$$\partial_t p(\bar{x}, t) = M(\bar{x}) \partial_{\bar{x}} p(\bar{x}, t) + V(\bar{x}) \partial^2_{\bar{x}} p(\bar{x}, t)/2, \tag{B.30}$$

where we assume the drift M and variance V given by Eqs. (2.20a) and (2.20b) in the main text. We have solved a discretized version of Eq. (B.30) on a grid in the $(\bar{x}, t)$ plane with spacings $(\Delta\bar{x}, \Delta t)$ given by $\Delta\bar{x} = 1/500$ and Δt ranging from 0.02 to 0.001, depending on the specific value of m'. We checked numerically that the algorithm we employed for the solution of the differential equation converges upon decreasing suitably $\Delta\bar{x}$ and Δt.

Figure B.4 demonstrates that the probability $p(\bar{x} = 1/2, t)$ to reach fixation starting from the metastable state $\bar{x} = 1/2$ evaluated from the numerical solution of Eq. (B.30) is, as a function of time t, quite well approximated by an exponential law $\simeq 1 - \exp(-t/T_{\rm fix,fit})$, for a suitable choice of $T_{\rm fix,fit}$. As a further test of the accuracy of the diffusive approximation also for determining rare events, we compare the solution of Eq. (B.30) with the results of numerical simulations of the Wright-Fisher model described in Sec. 2.2.1. In particular, we computed the fixation time of the model by averaging over about 500 realizations of the dynamics. The resulting cumulative distribution is reported in Fig. B.4 (red solid line) and it displays a good agreement with the numerical solution of Eq. (B.30) (blue dotted line). The decay time $T_{\rm fix,fit}$ which characterizes the exponential law reported in Fig. B.4 (green dotted line) is chosen such that to fit the MFT resulting from the simulation of the Wright-Fisher model. As it can be seen from Fig. 2.10 in the main text, within the range of parameters considered there, $T_{\rm fix,fit}$ computed from the WF simulations agrees rather well with $T^{(0)}_{\rm fix}$ determined according to Eq. (2.36) of the main text. We point out that, in the absence of migration, the single-deme fixation probability (i.e., the cumulative distribution of $T_{\rm fix1}$ discussed in Sec. 2.2.1) satisfies Eq. (B.30), where the functions $M(\overline{x})$ and $V(\overline{x})$ are given by Eqs. (2.20a) and (2.20b) of the main text in which, however, the effective parameters $s_{\rm e}$ and $N_{\rm e}$ are replaced by s and Ω, respectively, which refer to the single deme. Accordingly, the resulting distribution of $T_{\rm fix1}$ has the same qualitative behavior as the fixation time discussed here, though with a different time scale.

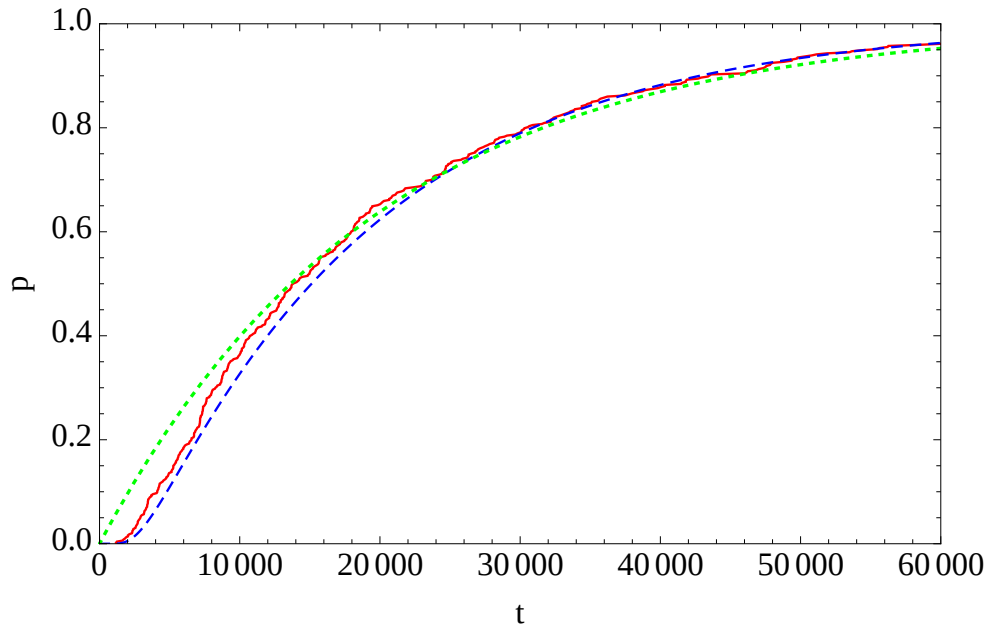

Figure B.4: Fixation probability $p(\bar{x}, t)$ as a function of time, for a population which starts from the initial value $\overline{x} = 1/2$. The numerical solution of Eq. (B.30) (blue, dashed line), is compared with the results of numerical simulations of the Wright-Fisher model (red, solid line) and with an exponential law $1 - \exp(-t/T_{\mathrm{fix,fit}})$ (green dotted). This plot refers to a population with $\Omega = 100$, $N = 30$, $s' = 1$, $m' = 0.3$, and $x_* = 1/2$.

Appendix C

C.1 Solution of Eq. (3.1) and two-points correlators

In this appendix we solve the time-dependent master equation, Eq. (3.1), in order to characterize the relaxation dynamics of the model toward the stationary state. Moreover, by using the properties of the characteristic function, we are able to compute the different-time correlators between n and m.

In order to simplify the notation, let us first introduce the quantities

$$\begin{aligned} E &= e^{-t(\lambda+\rho+1)}, \\ F &= e^{-\rho t}. \end{aligned} \tag{C.1}$$

The solution of the differential equation for the generating function $G(z,w;t)$ associated to Eq. (3.1) can be easily obtained with the method of characteristics. Using the initial condition $p_{n,m}(0) = \delta_{n,n_0}\delta_{m,m_0}$, we have

$$\begin{aligned} G(z,w;t) = \exp\Bigg[& \frac{\bar{N}\rho(w-z)[X(\lambda+1)-\lambda]}{(\lambda+1)(\lambda+\rho+1)}E + \bar{N}\frac{1-w+\lambda(1-z)}{\lambda+1}F \\ & + \bar{N}\frac{w-1+\lambda(z-1)+\rho[zX-1+w(1-X)]}{\lambda+\rho+1}\Bigg] \\ \times & \left(1+\frac{z-w}{\lambda+1}E+\frac{w-1+\lambda(z-1)}{\lambda+1}F\right)^{n_0}\left(1+\frac{\lambda(w-z)}{\lambda+1}E+\frac{w-1+\lambda(z-1)}{\lambda+1}F\right)^{m_0}. \end{aligned} \tag{C.2}$$

By differentiation we obtain the time-dependent probability distribution for (n,m):

$$\begin{aligned} p_{n,m}(t) &= \left[\frac{(\partial_z)^n}{n!}\frac{(\partial_w)^m}{m!}G(z,w;t)\right]_{z=w=0} \\ &= \frac{e^{\bar{N}(F-1)}}{n!m!(\lambda+1)^{n+m}}\sum_{r=0}^{n}\sum_{s=0}^{m}A^{n-r}B^{m-s}\sum_{j=0}^{r}\sum_{k=0}^{s}\binom{r}{j}\binom{s}{k}(1-F)^{n_0+m_0-r-s} \\ &\times \frac{n_0!m_0!\,\lambda^j(E+\lambda F)^{r-j}(\lambda E+F)^k(F-E)^{s+j-k}}{(n_0-r+j-s+k)!(m_0-j-k)!}\,\theta(n_0-r+j-s+k)\theta(m_0-j+k), \end{aligned} \tag{C.3}$$

where $\theta(x)$ is the Heaviside step function and

$$\begin{aligned} A &= (\lambda+1)\bar{n} - \frac{\bar{N}\rho[X(\lambda+1)-\lambda]}{\lambda+\rho+1}E - \bar{N}\lambda F, \\ B &= (\lambda+1)\bar{m} + \frac{\bar{N}\rho[X(\lambda+1)-\lambda]}{\lambda+\rho+1}E - \bar{N}F. \end{aligned} \tag{C.4}$$

It can be noticed that in the case $n_0 = m_0 = 0$, being the exponent linear in z and w, the time-dependent probability distribution is factorized (like the stationary one): $p_{n,m}(t) = p_n(t)p_m(t)$. In this case it reduces to:

$$\begin{aligned} p_{n,m}(t) = &\frac{1}{n!}\left[\bar{n} - \frac{\bar{N}}{\lambda+1}\left(\rho\frac{X(\lambda+1)-\lambda}{\lambda+\rho+1}E + \lambda F\right)\right]^n \\ &\times \frac{1}{m!}\left[\bar{m} + \frac{\bar{N}}{\lambda+1}\left(\rho\frac{X(\lambda+1)-\lambda}{\lambda+\rho+1}E - \lambda F\right)\right]^m e^{-\bar{N}(1-F)}. \end{aligned} \tag{C.5}$$

For generic initial conditions we can write a large-t (i.e., a small E, F) expansion, in order to see how $p_{n,m}(t)$ relaxes to the stationary value $p^{\rm st}_{n,m}$, Eq. (3.4):

$$p_{n,m}(t) = p^{\rm st}_{n,m}\left[1 + \alpha E + \beta F + O(E^2, F^2, EF)\right], \tag{C.6}$$

where

$$\begin{aligned} \alpha =& \frac{\bar{N}\rho[X(\lambda+1)-\lambda]}{(\lambda+1)(\lambda+\rho+1)}\left(\frac{m}{\bar{m}} - \frac{n}{\bar{n}}\right) + \frac{n_0\theta(n_0-1) - \lambda m_0\theta(m_0-1)}{\lambda+1}\left(\frac{1}{\bar{n}} - \frac{1}{\bar{m}}\right), \\ \beta =& \bar{N} - (n_0+m_0) - \frac{\bar{N}}{\lambda+1}\left(\frac{\lambda n}{\bar{n}} + \frac{m}{\bar{m}}\right) + \frac{n_0\theta(n_0-1) + m_0\theta(m_0-1)}{\lambda+1}\left(\frac{\lambda}{\bar{n}} + \frac{1}{\bar{m}}\right). \end{aligned} \tag{C.7}$$

The leading term for large times is therefore associated with E and F, i.e., with the relaxation-times:

$$\begin{aligned} t_1 &= \frac{1}{\rho}, \\ t_2 &= \frac{1}{\lambda+\rho+1}. \end{aligned} \tag{C.8}$$

The first time scale t_1 is associated with the diffusion process, while the second one is the inverse of the sum of all rates (if we restore the λ_B dependence we have $1/t_2 = \lambda_R + \rho + \lambda_B$).

Given the analytic expression of the generating function $G(z, w; t)$ in Eq. (C.2), it is straightforward to evaluate the correlators, for instance:

$$\begin{aligned} \langle n(0)m(t)\rangle &= \sum_{n_0,m_0}\sum_{n,m} n_0 m\, p_{n_0,m_0}\left[p_{n,m}(t)\right]_{\substack{n(0)=n_0 \\ m(0)=m_0}} \\ &= \sum_{n_0,m_0} n_0\, p_{n_0,m_0}\left[\partial_w G(z,w;t|n_0,m_0)\right]_{\substack{z=1 \\ w=1}}. \end{aligned} \tag{C.9}$$

In particular, we find:

$$\begin{aligned}
C_{nn}(t) &\equiv \langle n(0)n(t)\rangle - \bar{n}^2 = \bar{n}\frac{\lambda e^{-\rho t} + e^{-t(\lambda+\rho+1)}}{\lambda+1},\\
C_{mm}(t) &\equiv \langle m(0)m(t)\rangle - \bar{m}^2 = \bar{m}\frac{e^{-\rho t} + \lambda e^{-t(\lambda+\rho+1)}}{\lambda+1},\\
C_{nm}(t) &\equiv \langle n(0)m(t)\rangle - \bar{n}\bar{m} = \bar{n}\frac{e^{-\rho t} - e^{-t(\lambda+\rho+1)}}{\lambda+1},\\
C_{mn}(t) &\equiv \langle m(0)n(t)\rangle - \bar{n}\bar{m} = \bar{m}\lambda\frac{e^{-\rho t} - e^{-t(\lambda+\rho+1)}}{\lambda+1}.
\end{aligned} \tag{C.10}$$

The first two correlators in (C.10) are monotonically decreasing, as they are linear combinations (with positive coefficients) of the exponentials characterized by the decay times of Eq. (C.8).

The other two correlators are again linear combinations of the same exponentials, but the coefficients of such linear combination have different signs, which makes them non-monotonic. The maximum is at time

$$t_{\max} = \frac{1}{\lambda+1}\log\left[\frac{\lambda+\rho+1}{\rho}\right]. \tag{C.11}$$

C.2 Violation of detailed balance

The model can be interpreted as a random walk on the two dimensional (n, m) lattice, with site- and direction-dependent transition rates, as depicted in Fig. C.1.

We use this analogy to check for eventual violation of detailed balance (DB) in the stationary state described by Eq. (3.4). As it can be seen from Fig. C.1, there are three directions for the single step jumps:

- Along the vertical direction $(n, m) \leftrightarrow (n, m+1)$ the DB condition is

$$(1-X)\rho\bar{N}\, p_{n,m} = (m+1)\rho\, p_{n,m+1}, \tag{C.12}$$

  which is satisfied if

$$\rho = 0 \quad \text{or} \quad \rho \to \infty \quad \text{or} \quad \lambda = \frac{X}{1-X}. \tag{C.13}$$

- Along the horizontal direction $(n, m) \leftrightarrow (n+1, m)$ the DB condition is

$$X\bar{N}\rho\, p_{n,m} = (n+1)\rho\, p_{n+1,m}. \tag{C.14}$$

  Again, its solution is Eq. (C.13).

- Along the diagonal direction $(n, m) \leftrightarrow (n-1, m+1)$ the DB condition is

$$n\, p_{n,m} = \lambda(m+1)\, p_{n-1,m+1}, \tag{C.15}$$

  whose solution is

$$\rho = 0 \qquad \text{or} \qquad \lambda = \frac{X}{1-X}. \tag{C.16}$$

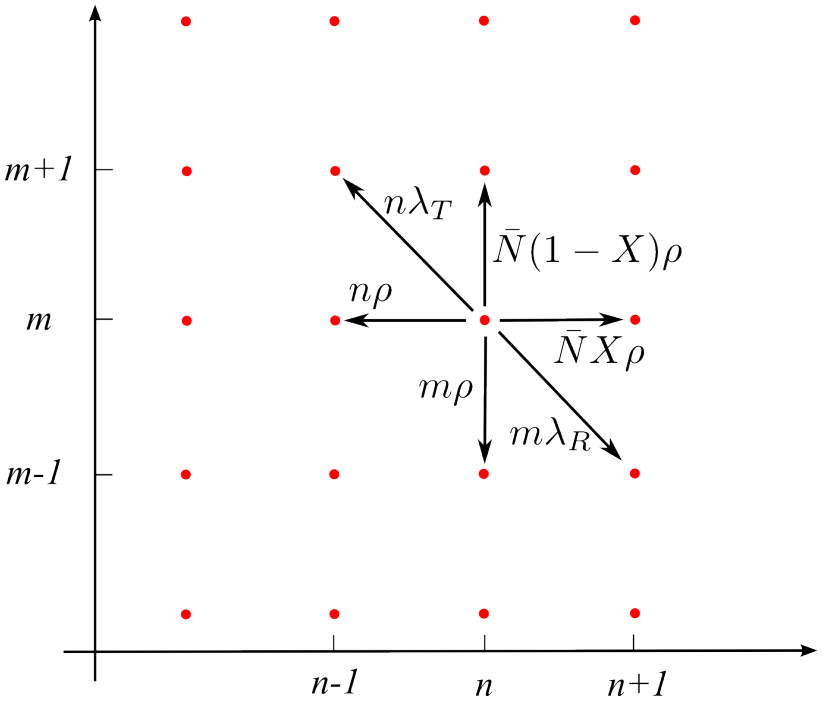

Figure C.1: (Color online) The model as a random walk on the (n, m) lattice. The transition rates depend on the direction and on the position on the lattice.

We conclude that the only values of the parameters satisfying DB are those in Eq. (C.16), while for $\rho \to \infty$ DB is "almost satisfied", being the violation vanishingly small.

The first value of Eq. (C.16) coincides with the trivial case where diffusion is suppressed, while the second one is the value where the stationary points of the internal (recharge and binding) and diffusive dynamics coincide.

In all other cases there are current probability loops and the stationary state is out of equilibrium [121].

C.3 BTD and mean number of charged tRNAs

Let us consider the time dependent mean of the number of charged tRNAs $\langle n(t)\rangle_{\rm nb} = \sum_{n=0}^{\infty} n\, p_n(t|\text{no binding})$, where at $t = 0^-$ a binding event occurred and no binding events were recorded between 0 and t.

In discrete time with temporal step δt, we can write the probability that a binding event happens at time $t > \tau_k = k\delta t$ as

$$P(\tau_k) = \prod_{i=0}^{k}(1 - \langle n(\tau_i)\rangle_{\rm nb}\delta t) \sim \exp\left(-\sum_{i=0}^{k}\langle n(\tau_i)\rangle_{\rm nb}\delta t\right). \tag{C.17}$$

In the continuous time limit we obtain

$$P(\tau) = \exp\left(-\int_0^\tau dt\, \langle n(t)\rangle_{\mathrm{nb}}\right). \tag{C.18}$$

By substituting Eq. (C.18) into 3.17, we obtain Eq. (3.25). Furthermore, by inverting Eq. (C.18), we can write

$$\langle n(t)\rangle_{\mathrm{nb}} = -\partial_\tau \log P(\tau)_{|\tau=t}. \tag{C.19}$$

This relation is utilised in Fig. 3.5 to plot the theoretical predictions.

Bibliography

[1] M. B. Green, J. H. Schwarz, and E. Witten. *Superstring theory - volume 1.* Cambridge University Press, 1987.

[2] J. F. Donoghue, E. Golowich, and B. R. Holstein. *Dynamics of the standard model.* Cambridge University Press, 1994.

[3] S. Weinberg. *The quantum theory of fields.* Cambridge University Press, 1996.

[4] B. Zwiebach. *A first course in string theory.* Cambridge University Press, 2004.

[5] E. Fermi. *Thermodynamics.* Dover Publications, 1936.

[6] M. Zemansky. *Heat and thermodynamics.* McGraw-Hill, 1957.

[7] L. E. Reichl. *Modern course in statistical physics.* Arnold Publishers, 1980.

[8] H. Callen. *Thermodynamics and an introduction to thermostatistics.* John Wiley, 1985.

[9] G. Carrington. *Basic thermodynamics.* Oxford University Press, 1994.

[10] M. Le Bellac, F. Mortessagne, and G. G. Batrouni. *Equilibrium and non-equilibrium statistical thermodynamic.* Cambridge University Press, 2004.

[11] K. Huang. *Statistical mechanics.* John Wiley, 1963.

[12] R. Kubo. *Statistical mechanics.* North Holland, 1965.

[13] W. Pauli. *Thermodynamics and the kinetic theory of gases.* Dover Publications, 1973.

[14] L. D. Landau and E. M. Lifshift. *Stastical physics.* Pergamon Press, 1980.

[15] G. Parisi. *Statistical field theory.* Addison-Wesley, 1994.

[16] G. Mussardo. *Statistical field theory.* Oxford University Press, 2010.

[17] R. J. Baxter. *Exactly solvable models in statistical mechanics.* Academic Press, 1982.

[18] D. J. Amit. *Field theory, the renormalization group, and critical phenomena.* World Scientific, 1978.

[19] J. L. Cardy. *Conformal invariance in phase transitions and critical phenomena.* Academic Press, 1987.

[20] P. Di Francesco, P. Mathieu, and D. Sénéchal. *Conformal field theory.* Springer, 1997.

[21] N. G. Van Kampen. *Stochastic processes in physics and chemistry.* Elsevier, 1981.

[22] C. W. Gardiner. *Handbook of stochastic methods for physics, chemistry and natural sciences.* Springer, 1983.

[23] J. W. Essam. Percolation theory. *Rep. Prog. Phys.*, 43:833, 1980.

[24] H. Hinrichsen. Nonequilibrium critical phenomena and phase transitions into absorbing states. *Adv. Phys.*, 49:815, 2000.

[25] M. Henkel, H. Hinrichsen, and S. Lúbeck. *Non-equilibrium phase transitions.* Springer, 2008.

[26] H. K. Janssen. On the non-equilibrium phase-transition in reaction-diffusion systems with an absorbing stationary state. *Z. Phys. B*, 42:151, 1981.

[27] O. Al Hammal, H. Chaté, I. Dornic, and M. A. Muñoz. Langevin description of critical phenomena with two symmetric absorbing states. *Phys. Rev. Lett.*, 94:230601, 2005.

[28] W. Horsthemke and R. Lefever. *Noise-induced transitions.* Springer Complexity, 2006.

[29] W. Bialek. *Biophysics: searching for principles.* Princeton University Press, 2002.

[30] R. Brown. A brief account of microscopical observations. 1827.

[31] A. Einstein. Über die von der molekularkinetischen theorie der wärme geforderte bewegung von in ruhenden flüssigkeiten suspendierten teilchen. *Annalen der Physik*, 322:549, 1905.

[32] T. Rogers, A. J. McKane, and A. G. Rossberg. Spontaneous genetic clustering in populations of competing organisms. *Phys. Biol.*, 9:066002, 2012.

[33] K. S. Korolev, M. Avlund, O Hallatschek, and D. R. Nelson. Genetic demixing and evolution in linear stepping stone models. *Rev. Mod. Phys.*, 82:1691, 2010.

[34] B. P. Lee. *Critical behavior in non-equilibrium systems.* PhD thesis, University of California, 1994.

[35] B. P. Lee and J. L. Cardy. Renormalization group study of the a+b->0 diffusion-limited reaction. *J. Stat. Phys.*, 80:971, 1995.

[36] P. Lombardo, A. Gambassi, and L. Dall'Asta. Nonmonotonic effects of migration in subdivided populations. *Phys. Rev. Lett.*, 112:148101, 2014.

[37] P. Lombardo, A. Gambassi, and L. Dall'Asta. Fixation and phase transition in subdivided populations with balancing selection. arXiv:1407.4656.

[38] L. Caniparoli and P. Lombardo. Nonequilibrium stochastic model for trna binding time statistics. *Phys. Rev. E*, 89:012712, 2014.

[39] J. C. Cox. Notes on option pricing i: constant elasticity of diffusions. Stanford University, 1975.

[40] J. C. Cox and S. A. Ross. The valuation of options for alternative stochastic processes. *J. Fin. Econ.*, 3:145, 1976.

[41] D. C. Emanuel and J. D. MacBeth. Further results of the constant elasticity of variance call option pricing model. *J. Fin. Quant. Anal.*, 4:533, 1982.

[42] A. Lindsay and D. Brecher. Results on the cev process, past and present. Working paper, 2010.

[43] M. A. Muñoz. Multiplicative noise in non-equilibrium phase transitions: a tutorial. *published in the book "Advances in condensed matter and statistical physics"*, 2004.

[44] T. Halpin-Healy and Y. C. Zhang. Kinetic roughening phenomena, stochastic growth, directed polymers and all that. aspects of multidisciplinary statistical mechanics. *Phys. Rep.*, 254:215, 1995.

[45] M. Kimura. Process leading to quasi-fixation of genes in natural populations due to random fluctuation of selection intensity. *Genetics*, 39, 1954.

[46] D. Ludwig, D. D. Jones, and C. S. Holling. Qualitative analysis of insect outbreak systems: the spruce budworm and forest. *J. Anim. Ecol.*, 47:315, 1978.

[47] H. K. Janssen. Survival and percolation probabilities in the field theory of growth models. *J. Phys. Cond. Matt.*, 17:S1973, 2005.

[48] A. Göing-Jaeschke and M Yor. A survey and some generalizations of bessel processes. *Bernoulli*, 9:313, 2003.

[49] I. Gikman and A. V. Skorokhod. *The theory of stochastic processes.* Springer-Verlag, 1974.

[50] W. Feller. Diffusion processes in one dimension. *Trans. Amer. Math. Soc.*, 77:1, 1954.

[51] S. Karlin and H. M. Taylor. *A second course in stochastic processes.* Academic Press, 1981.

[52] W. Genovese and M. A. Muñoz. Recent results on multiplicative noise. *Phys. Rev. E*, 60:69, 1999.

[53] R. A. Blythe and A. J. McKane. Stochastic models of evolution in genetics, ecology and linguistics. *J. Stat. Mech.*, (P07018), 2007.

[54] E. Lieberman, C. Hauert, and M. A. Nowak. Evolutionary dynamics on graphs. *Nature*, 433:312, 2005.

[55] I. Hanski. *Metapopulation ecology*. Oxford University Press, 1999.

[56] G. J. Baxter, R. A. Blythe, and A. J. McKane. Fixation and consensus times on a network: a unified approach. *Phys. Rev. Lett.*, 101:258701, 2008.

[57] M. W. Nachman and S. L. Crowell. Estimate of the mutation rate per nucleotide in humans. *Genetics*, 156:297, 2000.

[58] J. L. Cherry and J. Wakeley. A diffusion approximation for selection and drift in a subdivided population. *Genetics*, 163:421, 2003.

[59] T. Maruyama. On the fixation probability of mutant genes in a subdivided population. *Genet. Res.*, 15:221, 1970.

[60] M. Slatkin. Fixation probabilities and fixation times in a subdivided population. *Evolution*, 35:477, 1981.

[61] M. C. Whitlock. Fixation probability and time in subdivided populations. *Genetics*, 164:767, 2003.

[62] J. L. Cherry. Selection in a subdivided population with dominance or local frequency dependence. *Genetics*, 163:1511, 2003.

[63] M. Hamilton. *Population genetics*. Wiley-Blackwell, 2009.

[64] A. Robertson. Selection for heterozygotes in small populations. *Genetics*, 47:1291, 1962.

[65] M. Nei and A. K. Roychoudhury. Probability of fixation and mean fixation time of an overdominant mutation. *Genetics*, 74:371, 1973.

[66] A. L. Hughes and M. Nei. Pattern of nucleotide substitution at major histocompatibility complex class i loci reveals overdominant selection. *Nature*, 335:167, 1988.

[67] N. Takahata. A simple genealogical structure of strongly balanced allelic lines and trans-species evolution of polymorphism. *PNAS*, 87:2419, 1990.

[68] S. Wright. The distribution of self-sterility alleles in populations. *Genetics*, 24:538, 1939.

[69] A. D. Richman, M. K. Uyenoyama, and J. R. Kohn. Allelic diversity and gene genealogy at the self-incompatibility locus in the solanaceae. *Science*, 273:1212, 1996.

[70] M. Aidoo, D. J. Terlouw, M. S. Kolczak, P. D. McElroy, F. O. ter Kuile, B. L. Nahlen, A. A. Lal, and V. Udhayakumar. Protective effects of the sickle cell gene against malaria morbidity and mortality. *Lancet*, 359:1311, 2002.

[71] S. A. Schroeder, D. M. Gaughan, and M. Swift. Protection against bronchial asthma by cftr df508 mutation: A heterozygote advantage in cystic fibrosis. *Nat. Med.*, 1:703, 1995.

[72] D. J. Weatherall. Thalassaemia and malaria, revisited. *Ann. Trop. Med. Parasitol.*, 91:885, 1997.

[73] D. M. Abrams and S. H. Strogatz. Modelling the dynamics of language death. *Nature*, 424:900, 2003.

[74] M. A. Nowak and K. Sigmund. Evolutionary dynamics of biological games. *Science*, 303:793, 2004.

[75] A. Traulsen, J. C. Claussen, and C. Hauert. Coevolutionary dynamics: From finite to infinite populations. *Phys. Rev. Lett.*, 95:238701, 2005.

[76] J. B. Xavier. Social interaction in synthetic and natural microbial communities. *Mol. Syst. Biol.*, 7:483, 2011.

[77] R. A. Fisher. *The genetical theory of natural selection.* Clarendon Press, 1930.

[78] S. Wright. Evolution in mendelian populations. *Genetics*, 16:97, 1931.

[79] P. A. P. Moran. *The statistical processes of evolutionary theory.* Clarendon Press, 1962.

[80] M. Kimura. Solution of a process of random genetic drift with a continuous model. *PNAS*, 41:144, 1955.

[81] S. N. Ethier and M. F. Norman. Error estimate for the diffusion approximation of the wright-fisher model. *PNAS*, 74:5096, 1977.

[82] E. Aalto. The moran model and validity of the diffusion approximation in population genetics. *J. Theor. Biol.*, 140:317, 1989.

[83] C. R. Doering, K. V. Sargsyan, and L. M. Sander. Extinction times for birth-death processes: exact results, continuum asymptotics, and the failure of the fokker-planck approximation. *Multiscale Model. Simul.*, 3:283, 2008.

[84] M. Kimura and T. Ohta. The average number of generations until extinction of an individual mutant gene in a finite population. *Genetics*, 61:763, 1969.

[85] M. Kimura. On the probability of fixation of mutant genes in a population. *Genetics*, 47:713, 1962.

[86] M. H. Schierup. The number of self-incompatibility alleles in a finite, subdivided population. *Genetics*, 149:1153, 1998.

[87] M. H. Schierup, X. Vekemans, and D. Charlesworth. The effect of subdivision on variation at multi-allelic loci under balancing selection. *Genet. Res.*, 76:51, 2000.

[88] C. A. Muirhead. Consequences of population structure on genes under balancing selection. *Evolution*, 55:1532, 2001.

[89] J. Nishino and F. Tajima. Effect of population structure on the amount of polymorphism and the fixation probability under overdominant selection. *Genes Genet. Syst.*, 80:287, 2005.

[90] G. W. A. Constable and A. J. McKane. Fast-mode elimination in stochastic metapopulation models. *Phys. Rev. E*, 89:032141, 2014.

[91] G. W. A. Constable and A. J. McKane. Population genetics on islands connected by an arbitrary network. *J. Theor. Biol.*, 358:149, 2014.

[92] L. Dall'Asta and C. Castellano. Effective surface-tension in the noise-reduced voter model. *Europhys. Lett.*, 77:60005, 2007.

[93] L. Dall'Asta and T. Galla. Algebraic coarsening in voter models with intermediate states. *J. Phys. A Math. Theor.*, 41:435003, 2008.

[94] M. Kimura and G. Weiss. The stepping stone model of population structure and the decrease of genetic correlation with distance. *Genetics*, 49:561, 1964.

[95] P. L. Krapivski, S. Redner, and E. Ben-Naim. *A kinetic view of statistical physics.* Cambridge University Press, 2010.

[96] F Ritort. Single-molecule experiments in biological physics: methods and applications. *J. Phys. Cond. Matt.*, 18:R531, 2006.

[97] Marcos Sotomayor and Klaus Schulten. Single-molecule experiments in vitro and in silico. *Science*, 316:1144, 2007.

[98] Gerhard Hummer and Attila Szabo. Free energy reconstruction from nonequilibrium single-molecule pulling experiments. *P. Natl. Acad. Sci. USA*, 98:3658, 2001.

[99] Amar Nath Gupta, Abhilash Vincent, Krishna Neupane, Hao Yu, Feng Wang, and Michael T. Woodside. Experimental validation of free-energy-landscape reconstruction from non-equilibrium single-molecule force spectroscopy measurements. *Nat. Phys.*, 7:631, 2011.

[100] Nolan C. Harris, Yang Song, and Ching-Hwa Kiang. Experimental free energy surface reconstruction from single-molecule force spectroscopy using jarzynski's equality. *Phys. Rev. Lett.*, 99:068101, 2007.

[101] Gene-Wei Li and X. Sunney Xie. Central dogma at the single-molecule level in living cells. *Nature*, 475:308, 2011.

[102] Sotaro Uemura, Colin Echeverría Aitken, Jonas Korlach, Benjamin A. Flusberg, Stephen W. Turner, and Joseph D. Puglisi. Real-time trna transit on single translating ribosomes at codon resolution. *Nature*, 464:1012, 2010.

[103] Jin-Der Wen, Laura Lancaster, Courtney Hodges, Ana-Carolina Zeri, Shige H Yoshimura, Harry F Noller, Carlos Bustamante, and Ignacio Tinoco. Following translation by single ribosomes one codon at a time. *Nature*, 452:598, 2008.

[104] B. Alberts, A. Johnson, J. Lewis, M. Raff, K. Roberts, and P. Walter. *Molecular Biology of the Cell*. Garland Science, New York, 2002.

[105] Namiko Mitarai, Kim Sneppen, and Steen Pedersen. Ribosome collisions and translation efficiency: Optimization by codon usage and mrna destabilization. *J. Mol. Bio.*, 382:236, 2008.

[106] Shlomi Reuveni, Isaac Meilijson, Martin Kupiec, Eytan Ruppin, and Tamir Tuller. Genome-scale analysis of translation elongation with a ribosome flow model. *PLoS Comput. Biol.*, 7:e1002127, 2011.

[107] Philip Greulich, Luca Ciandrini, Rosalind J. Allen, and M. Carmen Romano. Mixed population of competing totally asymmetric simple exclusion processes with a shared reservoir of particles. *Phys. Rev. E*, 85:011142, 2012.

[108] Luca Ciandrini, Ian Stansfield, and M. Carmen Romano. Ribosome traffic on mrnas maps to gene ontology: Genome-wide quantification of translation initiation rates and polysome size regulation. *PLoS Comput. Biol.*, 9:e1002866, 2013.

[109] Joshua B Plotkin and Grzegorz Kudla. Synonymous but not the same: the causes and consequences of codon bias. *Nat. Rev. Genet.*, 12:32, 2011.

[110] Hila Gingold and Yitzhak Pilpel. Determinants of translation efficiency and accuracy. *Mol. Syst. Biol.*, 7:481, 2011.

[111] Edward P. O'Brien, Michele Vendruscolo, and Christopher M. Dobson. Prediction of variable translation rate effects on cotranslational protein folding. *Nat. Commun.*, 3:868, 2012.

[112] Ignacio Tinoco Jr and Jin-Der Wen. Simulation and analysis of single-ribosome translation. *Phys. Biol.*, 6:025006, 2009.

[113] Joachim Frank and Ruben L Gonzalez Jr. Structure and dynamics of a processive brownian motor: the translating ribosome. *Annu. Rev. Biochem.*, 79:381, 2010.

[114] Ajeet K Sharma and Debashish Chowdhury. Distribution of dwell times of a ribosome: effects of infidelity, kinetic proofreading and ribosome crowding. *Phys. Biol.*, 8:026005, 2011.

[115] Kimberly A Dittmar, Michael A Sörensen, Johan Elf, Må ns Ehrenberg, and Tao Pan. Selective charging of tRNA isoacceptors induced by amino-acid starvation. *EMBO Rep.*, 6:151, 2005.

[116] Chris A Brackley, M Carmen Romano, and Marco Thiel. The dynamics of supply and demand in mrna translation. *PLoS Comput. Biol.*, 7:e1002203, 2011.

[117] Sibylle E Wohlgemuth, Thomas E Gorochowski, and Johannes A Roubos. Translational sensitivity of the escherichia coli genome to fluctuating trna availability. *Nucleic Acids Res.*, 41:8021, 2013.

[118] Hengjiang Dong, Lars Nilsson, and Charles G. Kurland. Co-variation of trna abundance and codon usage inescherichia coliat different growth rates. *J. Mol. Biol.*, 260:649, 1996.

[119] Gong Zhang, Ivan Fedyunin, Oskar Miekley, Angelo Valleriani, Alessandro Moura, and Zoya Ignatova. Global and local depletion of ternary complex limits translational elongation. *Nucleic Acids Res.*, 38:4778, 2010.

[120] R K P Zia and B Schmittmann. A possible classification of nonequilibrium steady states. *J. Phys. A: Math. Gen.*, 39:L407, 2006.

[121] R K P Zia and B Schmittmann. Probability currents as principal characteristics in the statistical mechanics of non-equilibrium steady states. *J. Stat. Mech. Theor. Exp.*, 2007:P07012, 2007.

[122] T. Platini. Measure of the violation of the detailed balance criterion: A possible definition of a "distance" from equilibrium. *Phys. Rev. E*, 83:011119, 2011.

[123] T Chou, K Mallick, and R K P Zia. Non-equilibrium statistical mechanics: from a paradigmatic model to biological transport. *Rep. Prog. Phys.*, 74:116601, 2011.

[124] W. Feller. *An introduction to probability theory and its applications*. Wiley, 1968.

[125] H. Liljenström, G. Heijne, C. Blomberg, and J. Johansson. The trna cycle and its relation to the rate of protein synthesis. *Eur. Biophys. J.*, 12:115, 1985.

[126] Jun Zhu, Pawel A. Penczek, Rasmus Schröder, and Joachim Frank. Three-dimensional reconstruction with contrast transfer function correction from energy-filtered cryoelectron micrographs: Procedure and application to the 70sescherichia coliribosome. *J. Struct. Biol.*, 118:197, 1997.

[127] Geert Van Den Bogaart, Nicolaas Hermans, Victor Krasnikov, and Bert Poolman. Protein mobility and diffusive barriers in escherichia coli: consequences of osmotic stress. *Mol. Microbiol.*, 64:858, 2007.

[128] Hans Bremer, Patrick P Dennis, et al. Modulation of chemical composition and other parameters of the cell by growth rate. In Frederick Carl Neidhardt, editor, *Escherichia coli and Salmonella: cellular and molecular biology*, volume 2, pages 1553–1569. ASM press, Washington DC, 1996.

[129] Sidney Redner. *A guide to first-passage processes*. Cambridge University Press, 2001.

[130] M. Abramowitz and I. A. Stegun. *Handbook of mathematical functions*. Departmen of commerce USA, 1964.

[131] J. F. Crow and M. Kimura. *An introduction to population genetics theory*. Blackburn Press, 1970.